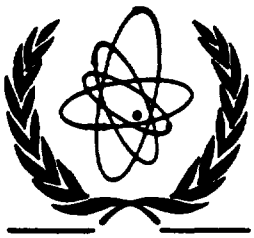

International Atomic Energy Agency

INDC(BLR)-006
Distr. G

INDC INTERNATIONAL NUCLEAR DATA COMMITTEE

EVALUATION OF NEUTRON DATA FOR AMERICIUM-243

V.M. Maslov, E.Sh. Sukhovitskij, Yu.V. Porodzinskij,
A.B. Klepatskij, G.B. Morogovskij

Radiation Physics & Chemistry Problems Institute
220109, Minsk-Sosny, Belarus

October 1996

IAEA NUCLEAR DATA SECTION, WAGRAMERSTRASSE 5, A-1400 VIENNA

Reproduced by the IAEA in Austria
October 1996

INDC(BLR)-006
Distr. G

EVALUATION OF NEUTRON DATA FOR AMERICIUM-243

V.M. Maslov, E.Sh. Sukhovitskij, Yu.V. Porodzinskij,
A.B. Klepatskij, G.B. Morogovskij

Radiation Physics & Chemistry Problems Institute
220109, Minsk-Sosny, Belarus

Abstract

The evaluation of neutron data for ^{243}Am is made in the energy region from 10^{-5} eV to 20 MeV. The results of the evaluation are compiled in the ENDF/B-VI format.

This work is performed under the Project Agreement CIS-03-95 with the International Science and Technology Center (Moscow). The Financing Party for the Project is Japan. The evaluation was requested by Y. Kikuchi (JAERI).

Date of Manuscript: September 11, 1996

Contents

1 Introduction

The advanced nuclear fuel cycle studies request the nuclear data of transplutonium isotopes.[1] The neutron data for americium isotopes are especially important in this respect. Recently we have evaluated the data for ^{243}Cm, ^{245}Cm, ^{246}Cm and ^{241}Am. In this work the evaluation of ^{243}Am neutron data is performed. The next isotope, which neutron data would be evaluated is ^{242m}Am. The curium and americium isotopes data to be evaluated were requested by the General Manager of Japan Nuclear data Center Dr. Y. Kikuchi. The quantities evaluated are resolved and unresolved resonance parameters, total, elastic and inelastic scattering, fission, capture, (n,2n) and (n,3n) reaction cross sections, angular and energy distributions of secondary neutrons, including partial (n,xn) and (n,xnf) reaction spectra, fission spectra and number of neutrons per fission. The incident neutron energy range covered is from 10^{-5} eV up to 20 MeV. The evaluated quantities are compared with ENDF/B-VI[2] , JEF[3] and JENDL-3[4] evaluations.

2 Resolved resonance region

The measured data base is similar to that of ^{241}Am at least in one respect. The extensive bomb-shot fission data of Seeger[5] should be discarded, as is the case for ^{241}Am fission data by Seeger et al.[6] However, the fission data by Knitter and Budtz-Jørgensen[7] below 100 eV are inaccessible, so the data by Seeger[6] would be renormalized using the estimate of average fission width value.

2.1 Previous evaluations of resolved resonance parameters

The evaluated resonance parameters of ENDF/B-VI and JENDL-3 are based on the resonance parameters E_r , Γ_n , Γ_γ by Simpson et al.[8] from 10^{-5} eV up to 250 eV and fission width Γ_f values due to Knitter and Budtz-Jørgensen[7] from 10^{-5} eV up to 56 eV. The number of fission resonances observed by Knitter and Budtz-Jørgensen[7] amounts only to one-half of those observed in total cross section measurement by Simpson et al.[8] The difference between the resonance parameter sets is due to adopted values of fission widths Γ_f for the missed fission resonances of Knitter and Budtz-Jørgensen[7] below 56 eV and assumed values in the region 56 eV - 250 eV. In ENDF/B-VI they adopted $\Gamma_f = 0.025$ meV up to 56 eV and $\Gamma_f = 0.16$ meV above 56 eV. In JENDL-3 evaluation they adopted $\Gamma_f = 0.12$ meV for all resonances.

Thermal total σ_t and capture σ_γ cross sections of ENDF/B-VI and JENDL-3 are compatible, while thermal fission values are discrepant. In ENDF/B-VI thermal fission cross section σ_f is based on the measured data by Wagemans et al.[9], which is compatible with data by Hulet et al.[10] and Belanova et al.[11] In JENDL-3 estimates of thermal fission cross section measurement of Ashgar et al.[12] and Gavrilov et al.[13] is taken into account.

Strength functions and resonance integrals of both evaluations are compatible (see Table 2.1).

2.2 Measured data fitting

The purpose of current resonance parameter evaluation is to extract resolved resonance parameters up to 250 eV by consistent analysis of available data on total and fission cross sections. The incident neutron energy range is divided into two intervals: 10^{-5} - 50 eV and 50 - 250 eV. The energy of 50 eV was chosen because we used the data of Knitter and Budtz-Jørgensen[7] up to this point.

The multi-level Breit-Wigner formalism is employed. The assigning of resonance spins was done as follows. Two assumptions were adopted: the number of resonances with spin J is proportional to $(2J+1)$, reduced neutron width distribution should obey that of Porter-Thomas, neutron resonance spacing distribution should obey that of Wigner.

2.2.1 Thermal cross sections

We employed the following values of thermal cross sections:

1) renormalized value by Berreth and Simpson[14] for σ_t = 84 b;

2) value for σ_f = 0.074 b by Wagemans et al.[6], estimate of $\sigma_f < 0.07$ b by Hulet et al.[10] with updated ^{239}Pu thermal value of $\sigma_f^{0.0253}$, value for σ_f = 0.1983 $\pm$ 0.0042 b by Asghar et al.[12] at incident neutron energy of 0.0021 eV. The latter value corresponds to the σ_f = 0.056 b at 0.0253 eV.

3) value for $\sigma_\gamma = 73.6 \pm 1.8$ b by Butler et al.[15], $\sigma_\gamma = 73 \pm 6$ b by Bak et al.[16] and σ_γ = 78 b by Folger et al.[17]

2.2.2 Total cross section

The total cross section data of Simpson et al.[8] and Berreth et al.[14] are available. We employed the data of Simpson et al.[8] for the thick sample in the energy region of 0.5 eV - 250 eV, for the thin sample in the energy region of 0.5 eV - 50 eV and the data of Berreth et al.[14] in the energy region of 0.008 eV - 14 eV.

2.2.3 Fission cross section

We employ the fission areas from 31 resonances of Knitter and Budtz-Jørgensen[7] up to 50 eV and for the resonance 55.87 eV and measured data of Seeger[5] in the energy region of 50 eV - 250 eV except the 55.87-eV resonance.

2.2.4 Energy region $10^{-5} \div 50$ eV

In this region resonance parameters were obtained using total cross section data of Simpson et al.[8] and Berreth et al.[14] as well as fission areas by Knitter and Budtz-Jørgensen.[7] For the fission resonances, which are unobserved by Knitter and Budtz-Jørgensen[7] we adopted value of 19 mb×eV. Fission widths of these resonances were calculated using $2g\Gamma_n^o$ and Γ_γ values, recommended by Simpson et al.[8]

When the final values J, $2g\Gamma_n^o$ and Γ_γ for the resonances up to 50 eV were obtained, the Γ_f values were updated employing the fission areas of all resonances, visible in total cross section measurement from 1 eV up to 50 eV. The fission widths of the three first resonances were fitted to the adopted thermal fission cross section value. Thermal cross section values are presented in Table 2.1.

2.2.5 Energy region $50 \div 250$ eV

In this energy region resonance parameters were obtained using total cross section data of Simpson et al.[8] and fission cross section data of Seeger.[5] Consistent analysis of total and fission cross sections data would allow to estimate a number of missed and unresolved doublets. Figure 2.1 shows total data fit around 160 eV. We assume that the resonance around 158.7 eV is actually an unresolved resonance doublet. At higher energies weak resonance should be added at 160.1 eV, this resonance is observed in fission experiment of Seeger.[5] However it was found that average fission width value $< \Gamma_f >$, obtained for Seeger[5] data is much greater than fission width one needs to fit the data by Knitter and Budtz-Jørgensen[7] in the unresolved resonance region. To reconcile resonance parameters derived from Seeger[5] data with data by Knitter and Budtz-Jørgensen[7] above 50 eV, the Γ_f values for all resonances above 50 eV, excluding the 55.87-eV resonance, were renormalised. The purpose is to obtain for them average fission width $< \Gamma_f >= 0.228$ meV. Figure 2.2 shows the comparison of measured data with present and previous evaluations. The fission widths renormalization has no appreciable influence on the calculated cross section shape.

The total number of resonances increased from 220 to 239, as compared with previous evaluations. There are six resonances with anomalously low fission width $\Gamma_f = 4 \times 10^{-7}$ eV. The contribution of these resonances into fission cross section is negligible. The resonance energies of some resonances

were slightly changed to fit the experimental data. The 251.9-eV resonance was added to fit data near 250 eV.

2.2.6 Resonance parameter analysis

We have got 239 resonance parameters up to 250 eV. The average resonance parameters, thermal cross sections and resonance integrals are presented in Table 2.1. Figures 2.3, 2.4 demonstrate the available data fit below 0.5 eV. Figure 2.5 shows the distribution of radiative capture widths for positive resonances. The resonance missing as well as reduced neutron width $\langle\Gamma_n^0\rangle$ and neutron resonance spacing $\langle D\rangle$ distributions are discussed below. Table 2.1 shows that thermal cross sections of present evaluation are fairly compatible with measured data.

Resonance integrals, calculated for various libraries, shown in Table 2.1, are compatible. The present evaluation estimate of capture resonance integral I_γ is slightly smaller than that of ENDF/B-VI and JENDL-3. It is due to the difference of the parameters of 10 strong resonances below 13.152 eV which define ~90 % of I_γ in the resolved resonance region. For these resonances I_γ of ENDF/B-VI and JENDL-3 are about 28 b higher than in present work but with present parameters we can fit measured total cross section data[8,14] better.

Table 2.1

	ENDF/B-VI	JENDL-3	This evaluation
$\langle\Gamma_n^0\rangle$, meV	0.2257	0.2259	0.1872
$\langle\Gamma_f\rangle$, meV	0.1349	0.1294	0.20596
$\langle\Gamma_\gamma\rangle$, meV	39.027	39.036	43.067
$\langle D\rangle$, eV	1.1493	1.1493	1.0623
$S_0 \times 10^4$	0.98627	0.98987	0.86401
σ_t , barn	83.688	86.101	84.233
σ_γ , barn	75.076	78.501	76.705
σ_f , barn	0.0739	0.11601	0.0638
σ_n , barn	8.5377	7.4834	7.4642
g_γ	1.01680	1.01608	1.01756
g_f	1.01512	1.00759	1.02008
I_γ , barn	1819.14	1822.62	1788.15
I_f , barn	7.6196	7.5815	7.4361

The average resonance parameters, thermal total σ_t, capture σ_γ, fission σ_f and scattering σ_n cross sections, $g_\gamma-$, and g_f-factors, as well as resonance integrals $I\gamma$ and I_f values are calculated with codes PSYCHE and INTER.[18]

In case of JENDL-3 and present evaluations the multi-level Breit-Wigner formalism was used, while for ENDF/B-VI evaluation single-level formula was employed.

3 Unresolved resonance region

3.1 Review

Unresolved resonance region of ^{243}Am is supposed to be from 0.25 keV up to 42.3751 keV. The lower energy is the end-point of resolved resonance region, the upper energy is the threshold energy of the inelastic scattering. We suppose $s-$, $p-$ and $d-$wave neutron-nucleus interactions to be effective.

3.2 The s-wave average resonance parameter evaluation

3.2.1 Estimate of resonance level missing influence on $\langle D_{obs} \rangle$ and $\langle S_0 \rangle$

The preliminary estimates of average partial widths were obtained by averaging the evaluated resolved resonance parameters. Figure 3.1 shows the cumulative number of resolved resonance levels. The average resolved resonance parameters obtained for positive resonances are given below. Note that average fission width value was obtained after experimental fission width values for resonances above 55 eV were renormalized to reproduce $\langle \Gamma_f \rangle = 0.228$. This average fission width for $s-$wave neutrons fits the data by Knitter and Budtz-Jørgensen[7] in unresolved energy region:

$$\begin{aligned} \langle \Gamma_n^0 \rangle &= 1.849 \times 10^{-4} \text{ (eV)}^{1/2} \\ \langle \Gamma_f \rangle &= 0.207 \text{ meV} \\ \langle D_{obs} \rangle &= 1.050 \text{ eV} \\ \langle \Gamma\gamma \rangle &= 43 \text{ meV} \end{aligned}$$

Note that due to missing of weak resonances these values overestimate actual reduced neutron width $\langle g\Gamma_n^0 \rangle$ and neutron resonance spacing $\langle D_{obs} \rangle$. To get a physically justified values of $\langle g\Gamma_n^0 \rangle$ and $\langle D_{obs} \rangle$ we employ a method, which is described elsewhere.[19] Both reduced neutron width and neutron resonance spacing distributions are obtained in a unified approach. We take into account the correlation of weak resonance missing and resonance missing due to poor experimental resolution. The resolution function parameters as well as $\langle g\Gamma_n^0 \rangle$ and $\langle D_{obs} \rangle$ values are obtained by maximum likelihood method. Actually we compare experimental distributions of reduced neutron width and resonance spacing with Porter-Thomas[20] and Wigner distributions. The latter distribution takes into account existence of two systems

of resonances[21] in the resolved energy region with $j = J \pm 1/2$, both are modified for the resonance missing. The latter distributions will be called expected distributions.

3.2.2 Evaluation of $\langle D_{obs} \rangle$, $\langle S_0 \rangle$, $\langle \Gamma_\gamma \rangle$ and $\langle \Gamma_f \rangle$ based on the resonance parameters

To evaluate average neutron resonance spacing $\langle D_{obs} \rangle$ and s-wave neutron strength function S_0 we apply our method to the resolved resonance data base. We suppose that data up to 150 eV should be taken into account. Figure 3.1 shows the cumulative sum of resolved resonance levels. The evaluated values are:

$$\langle S_0 \rangle = (\ 0.873 \pm 0.146) \times 10^{-4}\ (\mathrm{eV})^{-1/2}$$
$$\langle D_{obs} \rangle = (0.566 \pm 0.049)\ \mathrm{eV}$$

Figure 3.2 shows cumulative sum of reduced neutron width. Figure 3.3 shows the comparison of expected and experimental reduced neutron width distributions. Figure 3.4 shows the comparison of distributions for neutron resonance spacing. Distributions for reduced neutron width and resonance spacings without account of missing are also demonstrated. Comparison of the latter with the predicted expected distributions shown on the figures 3.3 and 3.4 demonstrate the effect of resonance missing. The resonance data shown on the figures encompass the energy interval 0-150eV, since at higher energies resonance missing exceeds the relative portion we could handle with our method.[19] The figures 3.3, 3.4 show that for energy interval 0-150 eV the expected distributions are consistent with the experimental data within statistical errors . That is the reason to consider the $\langle D_{obs} \rangle$ and S_0 estimates reliable.

3.3 The s-, p- and d-wave average resonance parameter evaluation

3.3.1 Neutron width

Average neutron width is calculated as follows

$$\langle \Gamma_n^{lJ} \rangle = S_l \langle D_J \rangle E_n^{1/2} P_l,$$

where P_l is the transmission factor for the lth partial wave, which was calculated within black nucleus model. The p-wave neutron strength function S_1

$= 2.176\times10^{-4}$ $(\mathrm{eV})^{-1/2}$ was calculated with the optical model, using the deformed optical potential, described below. According to the results of optical model calculations we assumed linear decrease of $s-$wave strength function to the value of S_0=$0.834\times10^{-4}(\mathrm{eV})^{-1/2}$ for neutron energy of 42.3751keV. The d-wave neutron strength function was taken from optical model calculations: $S_2 = 1.059\times10^{-4}$ (eV).$^{-1/2}$ Since the d-wave contribution is rather small, the impact of any reasonable approximation on calculated cross section values is negligible.

3.3.2 *Neutron resonance spacing*

Neutron resonance spacing $\langle D_J \rangle$ was calculated with the phenomenological model[22], which takes into account the shell, pairing and collective effects. The main parameter of the model $\tilde{a}$ was normalized to the observed neutron resonance spacing $\langle D_{obs} \rangle$ =0.566 eV.

3.3.3 Fission width

Fission widths are calculated within a double-humped fission barrier model. Energy and angular momentum dependence of fission width is defined by the transition state spectra at inner and outer barrier humps. We constructed transition spectra by supposing the triaxiality of inner saddle and mass asymmetry at outer saddle. They will be described below. The calculated fission widths $\langle \Gamma_f^{2-} \rangle$ and $\langle \Gamma_f^{3-} \rangle$ for $s-$wave neutrons are normalized to $\langle \Gamma_f \rangle$ =0.228 meV, which allows to describe measured fission data up to 42 keV. This value is somewhat higher than average resolved resonance fission width suggested by Knitter and Budtz-Jørgensen.[7]

3.3.4 Radiative capture width

Energy and angular momentum dependences of radiative capture width are calculated within a two-cascade γ-emission model with allowance for the (n,γf) and (n,γn) reaction competition to the (n,$\gamma\gamma$) reaction. In this energy region (n,γ) reaction appears to be a radiative capture reaction. The radiative capture width was normalized to the value of $\langle \Gamma_\gamma \rangle$ =43 meV. (For details see Chapter IV).

3.4 Cross section evaluation in the region 0.25-42.3751 keV

3.4.1 Fitting of fission cross section structure

Experimental fission cross-sections in the unresolved resonance region are measured by Knitter and Budtz-Jørgensen[7] and Wisshak and Kappeler[23] at the higher edge of the unresolved resonance energy range. Both experimental fission cross section sets are consistent in the energy region of interest

and do not expose any significant structure. So we fitted the measured data with fission width normalized to $s-$wave value of $\langle\Gamma_f\rangle = 0.228$ meV. Comparison of evaluated and experimental fission cross sections in the unresolved resonance energy region is given on Fig 3.5.

Table 3.1 Comparison of the evaluated fission and capture cross sections

Energy, keV	$\sigma\gamma, b$			σ_f, b		
	present	JENDL-3	ENDF/B-VI	present	JENDL-3	ENDF/B-VI
0.250	20.78	21.58	22.05	0.110	0.066	0.113
0.350	17.35	17.81	18.42	0.092	0.055	0.094
0.550	13.58	13.90	14.19	0.071	0.043	0.073
0.650	12.41	12.63	12.95	0.065	0.039	0.066
0.850	10.72	10.94	11.08	0.056	0.034	0.057
1.250	8.70	8.75	8.85	0.045	0.027	0.045
1.750	7.26	7.34	7.37	0.037	0.022	0.038
3.5	5.06	5.04	5.03	0.025	0.015	0.026
4.5	4.47	4.46	4.40	0.022	0.014	0.023
8.5	3.38	3.38	3.26	0.016	0.010	0.017
12.5	2.92	2.91	2.78	0.013	0.009	0.015
17.5	2.62	2.62	2.48	0.011	0.008	0.013
22.5	2.44	2.44	2.29	0.010	0.007	0.012
27.5	2.32	2.30	2.14	0.009	0.007	0.012
42.3751	2.07	1.99	1.84	0.008	0.007	0.010

3.4.2 Capture cross section energy dependence

Capture cross section in the energy region of interest is measured by Wisshak and Kappeler[23] and by Weston and Todd.[24] There is a systematic difference of ~8 % between the experimental data sets, while the shapes of the capture cross sections are consistent. In present evaluation we fitted capture cross section data of Weston and Todd[24] since with the adopted average resonance parameters we could not lower any further calculated cross section above 10 keV. Comparison of evaluated and experimental capture cross sections in unresolved resonance region is shown on Fig 3.6.

3.4.3 Comparison of current and JENDL-3 and ENDF/B-VI evaluated data

Present evaluated fission cross sections is consistent with ENDF/B-VI in the unresolved resonance region as they are based on the same data, while JENDL-3 is twice lower since they adopted $\langle\Gamma_f\rangle = 0.12$ meV. Figure 3.5 gives the comparison of fission cross sections for both evaluations. Current

evaluated capture cross section in unresolved resonance region almost coincide with JENDL-3. Capture cross section of ENDF/B-VI is higher by ~ 8 % around 150 eV and lower by ~ 8 % at the outer edge of unresolved resonance region. Fig 3.6 gives comparison of capture cross sections. Comparison of the evaluated fission and capture cross sections is given in Table 3.1.

4 Fast neutron cross sections

The measured neutron data in fast energy region, i.e. above ~42 keV are available for capture and fission cross sections. There are a lot of discrepancies in fission data in a deep subthreshold region, in a plateau region and at higher energies, specifically around 14.6 MeV. Nonetheless, the available fission and capture data fit would be used as constraint for (n, n') and $(n, 2n)$ reaction cross sections calculation. We reproduce also the average resonance fission width within double-humped fission barrier model. To fix fission channel parameters the systematic trends are used.

4.1 Optical potential

The deformed optical potential for n+^{243}Am interaction is employed. The starting values for the potential parameters were those for n+^{241}Am interaction, defined in our previous evaluation[25] by slightly varying potential parameters[26] of n+ ^{238}U interaction. They fit total cross section data by Phillips and Howe[27], available for n+ ^{241}Am interaction. The isotopic dependences of real and imaginary parts of the potential were calculated using the optical potential parameter systematics.[28] Previously we modified the original potential geometry parameters[27] to fit total cross section and differential scattering data for N-odd and even targets above 10 MeV. This procedure of parameter fitting is well tested in case of ^{233}U, ^{239}Pu, ^{235}U, ^{232}Th and ^{238}U targets. Four levels of the ground state rotational band ($5/2^-$,$7/2^-$,$9/2^-$,$11/2^-$) are coupled. The deformation parameters β_2 and β_4 are obtained by fitting S_0 value of 0.873×10^{-4} (eV)$^{-1/2}$ determined from resolved resonance parameters and S_1 having value lower than 2.00×10^{-4} (eV).$^{-1/2}$ The p-wave strength function was requested by fitting experimental capture cross section data above 10 keV energy region. The potential parameters are as follows:

$$V_R = 46.04 - 0.3E, MeV, r_R = 1.26\ fm, a_R = 0.615\ fm$$
$$W_D = \begin{cases} 3.50 + 0.4E, MeV, & E \leq 10 MeV, r_D = 1.24\ fm, a_D = 0.5\ fm \\ 7.50\ MeV, & E > 10\ MeV \end{cases}$$
$$V_{SO} = 6.2\ MeV, r_{SO} = 1.12\ fm, a_{SO} = 0.47\ fm, \beta_2 = 0.180, \beta_4 = 0.086$$

The s-, p-, and d-wave strength functions and potential scattering cross section, calculated with this potential parameters in a coupled channel approach equal at incident neutron energy of 150 eV:

$$S_0 = 0.872 \times 10^{-4}(\mathrm{eV})^{-1/2} \quad , \quad R' = 9.1187 \text{ fm} \; ;$$

and at 42.3751 keV:

$$S_0{=}0.834 \times 10^{-4}(\mathrm{eV})^{-1/2}, \quad S_1{=}2.176 \times 10^{-4}(\mathrm{eV})^{-1/2}, \quad S_2{=}1.059 \times 10^{-4}(\mathrm{eV})^{-1/2} \; .$$

The reaction cross sections, calculated with deformed optical potential and spherical optical potential, which is used in JENDL-3 evaluation, are compared on fig. 4.1. The significant differences below 1 MeV and above 10 MeV would be manifested in inelastic scattering cross section and $(n, 3n)$ cross section. The total cross section seem rather different (see figs. 4.2), especially at low energies. The differences at low energies are due to rather low value of $s-$wave strength function, adopted in present evaluation.

4.2 Fission cross section

4.2.1 Status of the experimental data

A small number of measurements are available for fission cross section, but most of them are discrepant with each other.

Fission cross section of ^{243}Am was measured by Seeger et al.[5] from 49 eV to 2.97 MeV at the bomb-shot Pommard. There is a large scatter of the data points in plateau region.

Butler et al.[29] defined fission cross section of ^{243}Am in the energy region from 0.3 MeV to 1.7 MeV. They have measured fission cross sections ratio of ^{243}Am and ^{235}U. The neutrons were produced by the ^{7}Li(p,n)^{7}Be reaction with the protons from an electrostatic generator. The fission events were detected with the gas scintillator counter. The sample weight was defined by α-counting, using $T_{\alpha_{1/2}}$ =7950 years, so their results should be renormalized to new value[30] of $T_{\alpha_{1/2}}$ =7380 years.

The fission cross section ratios were measured by Behrens and Browne[31] from 0.2 MeV to 30 MeV using ionization fission chambers and a threshold cross section method. Neutrons were produced with linac. The data are severely discrepant with previous data of Butler et al.[29] and Seeger[5], which are up to ~15% lower, however the data shapes are quite similar. About the same situation one faces in case of ^{241}Am fission cross section, when the data by Behrens and Browne[31] define the highest cross section level.

Subthreshold fission cross section was measured by Wisshak and Käppeler[23] in the energy range from 5 to 250 keV, using ^{235}U as a standard. Neutrons

were produced via ^{7}Li(p,n) (5-100 keV) and the T(p,n) (40-250 keV) reaction with Van de Graaff accelerator. Fission events were detected by a fission neutrons detector (liquid scintillator). The fission ratio was converted into absolute fission cross section using ^{235}U fission cross section of ENDF/B-VI.[3]

The energy dependence of fission cross section ratio of ^{243}Am and ^{235}U was defined by Fomushkin et al.[32] in the of incident neutron energy range from 0.3 MeV to 4 MeV. The neutrons were produced by the underground nuclear explosion. The fission events were detected with a polymer film detectors. The sample weight was defined by α-counting, using value of $T_{\alpha_{1/2}}$ =7380 years. The authors have estimated the ^{243}Am fission cross section in the plateau region, σ_f = 1.411±0.067 barns, claiming that energy dependence is well reproduced with the Bohr-Wheeler formula. The average fission cross sections of ^{243}Am and ^{235}U for neutron spectra of uranium assembly were utilized. The fission cross section at incident neutron energy ~14.8 MeV was also measured. The measurement was made relative to the ^{235}U fission cross section. The neutrons were produced by the T(d,n) reaction. The value obtained (2.275 barns) is compatible with previously measured value.[33]

The fission cross section at incident neutron energy 14.5 MeV was measured with neutrons, produced by the T(d,n) reaction by Fomushkin et al.[33] The measurement was made relative to the ^{238}U or ^{237}Np fission cross section. However, it is not stated explicitly which flux monitor was used in that particular case. The fission events were detected with mica detectors and ionization chamber in pulsed mode. The sample weight was defined by α-counting, using $T_{\alpha_{1/2}}$ =8800 years, so their results should be renormalized to new value of $T_{\alpha_{1/2}}$ =7380 years. The absolute fission cross section value for ^{243}Am was defined using the recent values of ^{238}U and ^{237}Np fission cross sections. The data are spread between 2.28 barns and 2.53 barns.

The ratio of fission cross sections of ^{243}Am and ^{239}Pu was measured in the energy range from 0.135 to 7.4 MeV by Fursov et al.[34] The neutrons were produced by the ^{7}Li(p,n)^{7}Be, T(p,n)^{3}He and D(d,n)^{3}He reactions. The energy dependence of fission ratios was defined using ionization fission chambers. The relative number of nuclei in ^{243}Am sample was defined by α-counting, using $T_{\alpha_{1/2}}$ =7380 years. The absolute values of fission cross section ratios were obtained using measurements with mica detectors. The absolute values of fission cross sections were obtained using ^{239}Pu fission cross section of ENDF/B-V. The data are compatible with data by Butler et al.[29] There is strong discrepancy with data by Behrens et al.[31] while both data shapes are consistent. The upward data trend above 4 MeV incident neutron energy seems to be incorrect, it may be due to doing measurements relative to ^{239}Pu fission cross section.

Kanda et al.[36] have measured fission cross section ratios of ^{243}Am and

^{235}U from 1.06 MeV to 6.83 MeV. The neutrons were produced via the T(p,n) (1.06-2.88 MeV), D(d,n) (4.31-6.83 MeV) reactions. The ^{243}Am fission cross section data turned out to be systematically lower than data of Fursov et al.[34] and data by Knitter and Budtz-Jørgensen.[7]

The fission cross section ratio of ^{243}Am and ^{235}U was measured by Knitter and Budtz-Jørgensen[7] in the energy range from 1 eV to 10 MeV. Fission events of ^{243}Am were registered by fragment detection using an ionization chamber. The neutrons were produced via the ^{7}Li(p,n)^{7}Be (0.33-1.14 MeV), T(p,n) (0.897-3.96 MeV), D(d,n) (3.76-9.92 MeV) reactions. Above 300 keV the measurements were executed with pulsed Van de Graaff accelerator. Neutrons of energies from 100 eV to 1.3 MeV were produced with the linac. In the neutron energy range from 100 eV to 1.4 MeV the relative fission cross section ratio was normalized to the average value of R= 1.211±0.029. The latter value was measured at the Van de Graaff , where it turned out to be almost constant in the energy range from 1.4 to 3 MeV. The 'linac' data are in good agreement with Van de Graaff' data as well as data by Wisshak and Kappeler.[23] In the neutron energy range from 1 eV to 30 keV the ^{243}Am fission cross section was measured relative to the ^{6}Li(n,t)^{4}He cross section shape. Then it was normalized to the fission integral of ^{235}U between 7.8 and 11 eV, which value was recommended by Wagemans and Deruytter.[37] Although many resonances are seen below 1 keV neutron energy, the fission areas of only 31 resonances below 56 eV were evaluated. Below 10 eV they have detected all the resonances, observed in measurement of Simpson et al.[8] except 8.77-eV resonance. Virtually, in the common incident neutron energy range between 0.1 and 30 keV both data sets are consistent within experimental errors. Quantities $2g\Gamma_f$ were calculated from the fission areas using $2g\Gamma_n^0$ and Γ_γ values due to Simpson et al.[8]

Data of Knitter and Budtz-Jørgensen[7] are compatible with data measured by Wisshak and Käppeler[23] in the energy range from 5 to 250 keV, with data measured by Butler in the energy range 0.3-1.7 MeV and with data measured by Fursov et al.[34] In latter case there is a discrepancy of data shapes in the plateau region (around 4 MeV.)

Fission cross section ratios ^{243}Am and ^{235}U above the (n,nf) reaction threshold (5 MeV - 10.5 MeV) were measured by Goverdovskij et al.[38] To obtain the absolute values of cross section ratios method of isotopic impurities was employed. The neutrons were produced via the D(d,n)^{3}He reaction. Fission events were registered using ionization chamber. The resulted fission cross section exhibits a strong bump above 7 MeV incident neutron energy. Below 7 MeV the data are compatible with data by Behrens et al.[31] while at higher energies they are discrepant.

Absolute values of the ^{243}Am measured fission cross section were obtained using ^{235}U reference fission cross section of ENDF/B-VI.[3]

The problem of consistency of ^{243}Am fission cross section looks like that. Some discrepancies occur below ~0.250 keV up. There is a scatter of data points of Wisshak et al.[23], while the data of Knitter and Budtz-Jørgensen[7] are compatible with them up to 150 keV. The data of Fursov et al.[34] tend to support the tendency to higher cross section values above 150 keV, stemming from data of Knitter and Budtz-Jorgensen.[7]

In the plateau region the data of Knitter and Budtz-Jørgensen[7], Fursov et al.[34] and Butler et al.[29] practically coincide, while the data of Behrens and Browne[31] are lying systematically (up to ~15 %) higher.

At excitation energies above emissive fission threshold the close agreement between data Knitter and Budtz-Jørgensen[7] and Behrens and Browne[31] seems to be rather strange. As regards the data of Fursov et al.[34] the systematic discrepancy with data by Behrens and Browne[31] persists, although it tends to decrease. However, this feature is characteristic for the fission cross section measurements relative to ^{239}Pu fission cross section. The data by Goverdovskij et al.[37] seem to be rather high, even as compared with data by Behrens and Browne.[31] The data of Fomushkin et al.[32] around 14.8 MeV assume rather sharp increase of fission cross section just above (n,2nf) fission reaction threshold.

4.2.2 Statistical model calculation of fission cross section

We choose to fit data of Knitter and Budtz-Jørgensen[7] in describing measured data base. That means the lower cross section level in the first plateau region as compared with data by Behrens et al.[31] From 250 keV up to 2 MeV the measured data are virtually consistent. From 2 MeV up to emissive fission threshold the data of Knitter and Budtz-Jørgensen[7] exhibit a rather strong fluctuation with incident neutron energy. The most peculiar feature of data by Knitter and Budtz-Jørgensen[7] is the strong dip around 4 MeV. We will follow the trend of data by Knitter and Budtz-Jørgensen[7] and Fursov et al.[34] up to 3 MeV and the trend of latter data at higher energies. The comparison of calculated fission cross section with measured data is shown in figs. 4.4, 4.5, 4.6 and 4.7. The statistical theory calculation of fission cross section was accomplished within the double-humped fission barrier model. The approach employed in code STAT is described in more details elsewhere.[39,40,41] The procedure of calculating fission transmission coefficients is briefly described below.

4.2.3 Fission transmission coefficient, level density and transition state spectrum

The intrinsic two-quasiparticle state spectrum of odd-odd nuclide ^{244}Am at equilibrium deformation are modelled by Sood and Singh.[42] Using these

intrinsic states as the bandhead energies we build the rotational bands, i.e. transition state spectra of fissioning nuclide ^{244}Am . The discrete transition spectra, as well as continuous level contribution to the fission transmission coefficient are dependent upon the order of symmetry for ^{244}Am fissioning nucleus at inner and outer saddles. Due to the axial asymmetry at the inner saddle[43] we additionally assume $(2J + 1)$ rotational levels for each J value. The rotational band levels of positive parity at outer saddle are assumed to be doubly degenerate due to mass asymmetry.[43] With transition state spectra defined in the first 0.1 MeV excitation energy range (see Table 4.1) the fission barrier parameters (see table 4.2) are obtained by fitting fission data (see figs.4.4-4.6). The fission width $\Gamma_f^{2^-} = 0.2$ meV calculated at incident neutron energy of 0.15 keV is consistent with average fission width obtained from unresolved resonance region. The fission cross section in deep subthreshold region is rather sensitive to the positions of transition states of negative (for $s-$wave neutrons) and positive (for $p-$wave neutrons) parity. With transition spectra thus generated the fission cross section data could be described up to ~0.9 MeV incident neutron energy. For higher incident neutron energies, especially in the range 0.9 - 1.4 MeV, the inner barrier transition states are fully open and the cross section value is sensitive to the number of transition states. We suppose that the level density approach gives more accurate estimate of the number of transition states. To calculate fission cross section for incident neutron energies above 0.9 MeV the level density modelling[40] was employed.

The discrete character of few-quasiparticle excitations is virtually unimportant in case of odd-odd ^{244}Am fissioning nuclide. We will model the level density above 0.1 MeV in the following approximate way. The level density of axially symmetric fissioning nucleus is calculated in constant temperature approximation, i.e. $\rho(U) = T_f^{-1} \exp((U - U_o)/T_f)$. The respective parameters, nuclear temperature T_f and excitation energy shift U_o are defined at the matching energy U_c =2.4 MeV. At excitation energies above U_c the continuum part of the transition state spectrum is represented with the phenomenological model[22], which takes into account pairing, shell and collective effects at saddle deformations. The asymptotic value of the main parameter of the level density for fissioning nucleus ^{244}Am is assumed to be the same, as that of ^{244}Am compound nuclide. After that the effects of non-axiality and mass asymmetry are included. The detailed procedure of calculating fission transmission coefficient is described elsewhere.[39,40] The respective parameters: shell correction at saddles δW, pairing correlation function Δ, quadrupole deformation ε, and momentum of inertia at zero temperature $F_0/\hbar^2$ are given in Table 4.3.

Above ~2 MeV incident neutron energy fission cross section data were fitted (see fig. 4.6) by slight increase of pairing correlation function Δ value.

Table 4.1

Transition spectra band-heads of ^{244}Am

inner saddle		outer saddle	
K^π	E_{K^π}, MeV	K^π	E_{K^π}, MeV
1^-	0.020	1^-	0.020
0^-	0.030	0^-	0.030
6^-	0.000	6^-	0.000
1^+	0.210	1^+	0.210
6^+	0.240	1^-	0.210
		6^+	0.240
		6^-	0.240

Table 4.2

Fission barrier parameters

Nucleus	Barrier	Barrier height, MeV	Curvature, MeV
^{244}Am	inner	6.25	0.7
^{244}Am	outer	5.9	0.525
^{243}Am	inner	6.4	1.0
^{243}Am	outer	5.05	0.5
^{242}Am	inner	6.315	0.6
^{242}Am	outer	5.775	0.4
^{241}Am	inner	6.000	0.8
^{241}Am	outer	5.350	0.5
^{240}Am	inner	6.100	0.6
^{240}Am	outer	6.000	0.4
^{239}Am	inner	6.000	0.8
^{239}Am	outer	5.400	0.6

Table 4.3

Level density parameters of ^{244}Am fissioning nucleus and residual nucleus ^{243}Am

Parameter	inner saddle	outer saddle	neutron channel
δW, MeV	2.5	0.6	-2.128
$\triangle$, MeV	$\triangle_0$ +0.04	$\triangle_0$ +0.04	$\triangle_0$
ε	0.6	0.8	0.24
$F_0/\hbar^2$, MeV^{-1}	100	200	73

The parameters used for calculation of residual nuclide ^{243}Am level density for neutron emission competition are described below.

Below incident neutron energy of 0.267 MeV the neutron cross sections are calculated within Hauser-Feshbach approach with a width fluctuation correction taken into account. For width fluctuation correction calculation only Porter-Thomas fluctuations are taken into account. Effective number of degrees of freedom for fission channel is defined at the higher (inner) saddle as $\nu_f^{J\pi} = T_f^{J\pi}/T_{f\,\mathbf{max}}^{J\pi}$, where $T_{f\,\mathbf{max}}^{J\pi}$ is the maximum value of the fission transmission coefficient $T_f^{J\pi}$. Above incident neutron energy of 0.267 MeV the Tepel et al.[44] approach is employed. The calculations are made with code STAT.[45]

4.2.4 Fission cross section above emissive fission threshold

The first chance fission cross section of ^{243}Am(n,f) reaction above the emissive fission threshold is fixed with the level density and fission barrier parameters systematics[40] (see Tables 4.2, 4.3) and secondary neutron spectra parameterization (see fig. 4.7). A consistent description of a complete set of measured data on (n,f), (n,2n) and (n,3n) for ^{238}U and ^{235}U targets was accomplished with the secondary neutron spectra parameterization[46], which is used here.

The fission cross section is calculated with the statistical code STAPRE.[47] The fission barrier parameters of ^{243}Am, fissioning in (n,nf) reaction are defined by fitting ^{242m}Am fission data in the first plateau region (see Fig. 4.8). The resulted fission barrier parameters of ^{243}Am allow fitting ^{243}Am(n,f) data by Fursov et al.[34] above emissive fission threshold. The calculated fission cross section around (n,2nf) reaction threshold neutron energy is lower than data by Fomushkin et al.[32] However, this discrepancy is unavoidable, since the fission barrier parameters of ^{242}Am fissioning nuclide are also fixed by ^{241}Am(n,f) cross section data analysis.[25] The first-chance fission cross section could be increased by softening the first emitted neutron spectra. However, we do not think this procedure justified in this particular case.

The calculated fission cross section is different from JENDL-3 and ENDF/B-VI evaluated curves around (n,nf) reaction threshold (see fig. 4.9). Calculated fission cross section shape is similar to that of JEF-2 evaluation, which is inferred from data by Behrens and Browne.[31]

4.3 Inelastic scattering cross section

The inelastic scattering cross section is calculated with the statistical codes STAT[45] and STAPRE.[47] The discrete level excitation (compound and di-

rect), continuum excitation and pre-equilibrium emission contribute to the inelastic scattering cross section.

4.3.1 Levels of ^{243}Am

The low-lying levels of scheme of Nuclear Data Sheets[48] appears incomplete at rather low excitation energy (see fig. 4.10). Previous evaluations take this into account.

4.3.2 ^{243}Am level density

The continuum level density below excitation energy U_c = 3.6 MeV is calculated with the constant temperature model

$$\rho(U) = T^{-1} \exp((U - U_o)/T),$$

here, energy shift U_0 = -0.98278 MeV, nuclear temperature T = 0.39984 MeV are the constant temperature model parameters, . The cumulative number of observed levels is compared with constant temperature approximation on fig.4.10. At higher excitation energies the phenomenological model[22] is used. The main model parameter $\tilde{a}$ for ^{243}Am residual nucleus is obtained by fitting the evaluated neutron resonance spacing of ^{242m}Am target nuclide $\langle D_{obs} \rangle$ = 0.272 eV.

4.3.3 Compound inelastic scattering

The residual nucleus ^{243}Am level density modelling, adopted in present work changes the inelastic scattering cross section below 5 MeV as compared with JENDL-3 evaluation (see figs. 4.11 - 4.19). Above ~1.5 MeV incident neutron energy the discrepancy is due to direct excitation of the ground state band levels. Above 1 MeV incident neutron energy inelastic scattering to the continuum gives a major contribution to the total inelastic scattering cross section (see fig. 4.12). Above 5 MeV incident neutron energy pre-equilibrium emission and direct inelastic scattering are the two reaction mechanisms which define inelastic scattering cross section (see fig. 4.11). The pre-equilibrium model parameters were tested by the statistical model description of ^{238}U+n interaction secondary neutron spectra and consistent description of fission and (n,xn) reaction data for major actinides.[46] Steep decrease of inelastic scattering cross section of JENDL-3 above 5 MeV (see fig. 4.12) is due to missing of pre-equilibrium emission of neutrons.

4.3.4 Direct inelastic scattering

The direct inelastic scattering changes the shape of ground band levels excitation cross sections above 1 MeV incident neutron energy (see figs. 4.13, 4.15). This mechanism defines partly the hard-energy tail in total inelastic scattering cross section (see fig. 4.11). The calculations were accomplished with the code COUPLE.[28]

Table 4.4
Level scheme of ^{243}Am

$E^J_{K^\pi}$, MeV	J	π	K	band
0.0000	5/2	-	5/2	A
0.0422	7/2	-	5/2	A
0.0840	5/2	+	5/2	B
0.0964	9/2	-	5/2	A
0.1092	7/2	+	5/2	B
0.1435	9/2	+	5/2	B
0.1623*	11/2	-	5/2	A
0.1893	11/2	+	3/2	B
0.2380	13/2	-	5/2	A
0.2440	13/2	+	5/2	B
0.2660	3/2	-	5/2	C

*)added

4.3.5 ^{244}Am level density

The level density of odd-odd compound nuclide ^{244}Am one needs to calculate radiative capture width and (n,γn') reaction contribution to the compound inelastic scattering cross section. The continuum level density below excitation energy U_c = 2.4 MeV is calculated with the constant temperature model, the constant temperature model parameters are: energy shift U_0 = -1.6413 MeV, nuclear temperature T = 0.3891 MeV. The cumulative number of observed levels is compared with constant temperature approximation on fig. 4.20. At higher excitation energies the phenomenological model[22] is used. The main model parameter $\tilde{a}$ for ^{244}Am residual nucleus is obtained by fitting the evaluated neutron resonance spacing of ^{243}Am target nuclide $\langle D_{obs} \rangle$ = 0.566 eV.

4.4 Radiative capture cross section

Capture cross section was measured by Wisshak and Käppeler[23] in the energy range from 5 to 250 keV, using ^{197}Au as a standard. Capture events

were detected by Moxon-Rae system. The data have been converted to absolute values using the ^{197}Au(n,γ) cross section of ENDF/B-VI. We will fit the capture cross section data of Wisshak and Käppeler.[23]

Weston and Todd[24] have measured capture cross section in the range of incident neutron energy from 258 eV to 92 keV using large liquid scintillator. The cross section was normalized at the thermal energy to the value of 74.8 barns. There is a systematic difference between data of Wisshak and Käppeler[23] and that of Weston and Todd[24] of up to 10% below 100 keV.

The radiative capture cross section is calculated within a statistical approach up to 5 MeV. Radiative capture strength function equals $S_{\gamma 0}$ = 759.72. At higher incident neutron energies we assume radiative capture cross section to be 1 mbarn. The radiative capture width was calculated with (n,γf) and (n,γn') reactions competition against "true" capture reaction (n,$\gamma\gamma$). Due to high fission threshold for ^{244}Am compound nuclide the competition of (n,γn') reaction is stronger than that of (n,γf) reaction. The influence of (n,γn') and (n,γf) reaction competition on radiative capture cross section is illustrated on fig. 4.21 by sharp decrease of capture cross section above 1 MeV incident neutron energy, as compared with (n,γx) reaction cross section.

4.5 Cross sections of (n,2n) and (n,3n) reactions

The current and JENDL-3 evaluated (n,2n) and (n,3n) cross sections are rather different. The magnitude of (n,2n) cross section below the (n,2nf) reaction threshold is defined by (n,nf) and (n,2n) reaction competition. To calculate the (n,2n) reaction cross section we use an approach, developed for description of the ^{238}U(n,2n) reaction cross section.[46] The present and previous evaluated fission cross sections are rather different, as well as reaction cross sections above 10 MeV incident neutron energy (see fig. 4.1). The present and previous evaluations are compared in fig. 4.22. There is no hard-energy tail in (n,2n) reaction cross sections of ENDF/B-VI, JENDL-3 and JEF-2 evaluations. In case of (n,3n) reaction the difference in reaction cross section above 11 MeV (see fig. 4.1) contributes essentially to the discrepancy with JENDL-3 evaluation, shown on fig. 4.23.

5 Energy distributions of secondary neutrons

There is no measured data on secondary neutron spectra. To calculate neutron energy distributions of (n,xnγ) and (n,xnf), x=1, 2, 3 reactions we use a simple Weisscopf-Ewing evaporation model[52] taking into account fission and gamma competition to neutron emission. The pre-equilibrium emission of first neutron is included.

5.1 Model calculations of (n,nx) reaction spectra

The first neutron spectra for the (n,nx) reaction is the sum of evaporated and pre-equilibrium emitted neutron contributions. The pre-equilibrium emission contribution is calculated with a parameter systematics tested in case of n+^{238}U and n+^{235}U interactions.[46] We have calculated the 1st, 2nd and 3d neutron spectra for the (n,nγ), (n,2n) and (n,3n), where applicable. According to the ENDF/B-VI format we included the secondary neutron spectra in the following way. The calculated spectra were summed up and tabular spectra for the (n,nγ), (n,2n) and (n,3n) reactions were obtained. To clarify the competition of neutron, γ-emission emission and fission in case of (n,nx) and (n,2nx) reactions we have chosen the following presentation of spectra. Figure 5.1 shows the spectrum of 1st neutron of the reaction (n,nx) and its partial contributions for (n,nγ), (n,2n), (n,nf) (n,2nf) and (n,3n) reactions. Figure 5.2 shows the spectrum of 2nd neutron of the reaction (n,2nx) and its partial contributions for (n,2n), (n,3n) and (n,2nf) reactions. The spectra of 1st and 2nd neutrons are normalized to unity. The partial neutron spectra shown on figs. 5.1, 5.2 are normalized to the contributions of appropriate cross sections to the (n,nx) and (n,2nx) reaction cross sections, respectively.

Table 5.1 Average energies of secondary neutron spectra

E_n, MeV	1st neutron average energy, MeV									
	(n, n')			(n, 2n)			(n, n'f)	(n, 3n)		(n, 2n'f)
	pres.	B - 6	J - 3	pres.	B-6	J - 3	pres.	pres.	J - 3	pres.
2.0	0.53	0.60	0.61							
8.0	3.81	1.23	0.94	0.79	0.57	1.09	1.10			
15.0	11.00	1.63	1.51	3.91	1.23	1.50	3.00	1.05	1.50	0.91
20.0	16.00	1.86	1.74	9.39	1.52	1.74	3.90	2.80	1.74	2.62

E_n, MeV	2nd neutron average energy, MeV						3d neutron	
	(n, 2n)			(n, 3n)		(n, 2n'f)		
	pres.	B-6	J - 3	pres.	J - 3	pres.	pres.	J - 3
8.0	0.27	1.23	0.69					
15.0	0.91	1.62	1.09	0.76	1.09	0.68	0,28	0.70
20.0	0.82	1.85	1.38	1.16	1.38	1.16	0.68	0.87

The inclusion of pre-equilibrium emission changes significantly the average energies of emitted neutron spectra. That is shown in Table 5.1, where the average secondary neutron energies for current and JENDL-3 and ENDF/B-VI evaluations are compared. The most significant is the change

of neutron spectra of (n,nγ) reaction. Figs 5.3-5.7 demonstrate the discrepancies of secondary neutron spectra in current, JENDL-3 and ENDF/B-VI evaluations. Spectra of our evaluation taking into account the possibility of pre-equilibrium emission are much harder than those in JENDL-3 and ENDF/B-VI.

The 1st neutron spectra of (n,nf) and (n,2nf) reactions also becomes harder and that influences prompt fission neutron spectra. On the other hand, the spectra of 2nd and 3d neutrons become softer.

5.2 Prompt fission neutron spectra

Prompt fission neutron spectra were calculated within the framework of Madland-Nix model.[53]

5.2.1 Model calculations of prompt fission neutron spectra

The model parameters, which should be defined are the following.

5.2.1.1 Fragment masses. The fragment masses are defined as $A_L = 103$ and $A_H = 141$, in accordance with the data of Asghar et al.[54] Fragment charges are defined using the ratios of

$$\langle A_{L,H} \rangle / (Z_{L,H} \mp 0.5) = A_F / Z_F.$$

The average fragments adopted are ^{103}Nb and ^{141}Xe.

5.2.1.2 Energy parameters. Average total fission energies $\langle E_R \rangle$ and average fission-fragment separation energies are calculated as in Madland-Nix model using mass tables of Audi and Wapstra.[55] The values of $\langle TKE \rangle$ for fissioning nuclei ^{244}Am and ^{243}Am had been defined to fit experimental data on $\nu_p(E)$ from thermal to 5 MeV energy. The resulted $\langle TKE \rangle = 180.9 - 0.12E_n$ for ^{244}Am fissioning nucleus and $\langle TKE \rangle = 182.2 - 0.08E_n$ for ^{243}Am fissioning nucleus. The value of $\langle TKE \rangle = 183.02 - 0.08E_n$ for ^{242}Am fissioning nucleus had been defined according to systematics of Viola et al.[56]

5.2.2 Other parameters.

The level density parameter of the fermi-gas model is calculated as $a = A_{L,H}/10.2$, MeV^{-1}. Becchetti-Greenlees[57] spherical optical potential parameters are employed to calculate compound cross section.

5.2.3 Prompt fission neutron spectra evaluation

Below emissive fission threshold prompt fission neutron spectra are calculated with the parameters given in Table 5.2. Figure 5.8 shows the comparison of calculated thermal prompt fission neutron spectrum with maxwellian spectra of JENDL-3 ($T = 1.377$ MeV) and ENDF/B-VI ($T = 1.33$ MeV). Average energy of fission spectrum equals 2.13 MeV, it is compatible with evaluated value of JENDL-3, however the spectra shapes are significantly different. Figures 5.9, 5.10 demonstrate the discrepancy of our calculation with JENDL-3 and ENDF/B-VI evaluations. The discrepancy is due to incident neutron energy independent maxwellian fission spectrum presentation in JENDL-3 and ENDF/B-VI as well as emissive fission contribution in present evaluation.

Above emissive fission threshold the fission neutron spectra $N(E)$ is the superposition of emissive fission spectra, i.e.

$$N(E) = (\frac{\sigma_{nf}}{\sigma_{nF}}\nu_1 N_1(E) + \frac{\sigma_{nn'f}}{\sigma_{nF}}\left[\Phi_{nn'f}(E) + \nu_2 N_2(E)\right]$$
$$+\frac{\sigma_{n2nf}}{\sigma_{nF}}\left[\Phi^1_{n2nf}(E) + \Phi^2_{n2nf}(E) + \nu_3 N_3(E)\right])/$$
$$\left[\frac{\sigma_{nf}}{\sigma_{nF}}\nu_1 + \frac{\sigma_{nn'f}}{\sigma_{nF}}(1+\nu_2) + \frac{\sigma_{n2nf}}{\sigma_{nF}}(2+\nu_3)\right],$$

where σ_{nF}, σ_{nf}, $\sigma_{nn'f}$, σ_{n2nf} are the total and i-th chance fission cross sections (i = 1,2,3); $\Phi_{nn'f}$, Φ^1_{n2nf}, and Φ^2_{n2nf} are emitted neutron spectra: for (n,nf) reaction, 1st and 2nd neutrons of (n,2nf) reaction, respectively; ν_i and N_i are multiplicity and prompt neutron spectra for the i-th fissioning nucleus. The pre-equilibrium emission of the first neutron is included, the $\Phi^i_{n,xnf}$ spectra for the emissive fission are calculated with Weisscopf-Ewing evaporation model.[52]

Table 5.2

Parameters of the Madland-Nix model

Fissioning nucleus	A_L fragm.	A_H fragm.	$\langle E_R \rangle$, MeV	$\langle TKE \rangle$, MeV	B_n, MeV
^{244}Am	^{103}Nb	^{141}Xe	203.645	180.90-0.12E_n	5.538
^{243}Am	^{103}Nb	^{140}Xe	204.651	182.20-0.08E_n	6.641
^{242}Am	^{102}Nb	^{140}Xe	204.963	183.02-0.08E_n	5.538

The influence of pre-equilibrium pre-fission neutrons on prompt fission neutron multiplicity ν_i and prompt neutron spectra N_i predictions as well as $N(E)$ and $\nu(E)$, is illustrated in Table 5.3 and Fig. 5.11. In Table 5.3 $\langle E_i \rangle$ denotes average prompt fission neutron energy of i-th fissioning nucleus, $\langle E \rangle$ is the average fission neutron energy, $\langle E_{n'f} \rangle$, $\langle E_{2nf} \rangle^1$and $\langle E_{2nf} \rangle^2$are the average energies of neutrons, emitted in (n,nf) and 1st and 2nd neutrons emitted in (n,2nf) reactions, respectively. The Figs. 5.12-5.14 show the partial contributions of i-th chance fission to the total fission neutron spectrum at incident neutron energies of 8, 15 and 20 MeV.

6 Number of neutrons per fission

The number of prompt fission neutrons $\nu_p(E)$ was measured by Frehaut et al.[58] in energy range 6-15 MeV and by Khokhlov et al.[59] from 0.5 to 12 MeV. Numerical data are unaccessible and only linear energy dependences $\nu_p(E)$=3.28+0.139E$_n$ (Frehaut et al.) and $\nu_p(E)$=3.20+0.154E$_n$ (Khokhlov et al.[56], renormalized to ν_p of ^{252}Cf = 3.757) fitted to experimental data are provided. The present evaluation of $\nu_p(E)$ is based on calculation within Madland-Nix model, fitted to the energy dependence $\nu_p(E)$=3.20+0.154E$_n$ in the energy range up to 5 MeV, proposed by Khokhlov et al.[56] The calculated number of prompt fission neutrons is consistent with both the data of Khokhlov et al.[56] and of Frehaut et al.[55] The comparison of $\nu_p(E)$ with measured data, JENDL-3 and ENDF/B-VI evaluations is shown on fig. 6.1.

Table 5.3 Comparison of Madland-Nix and present approach

	E_n = 8 MeV		E_n = 15 MeV	
Quantity	M-N model[53]	Present	M-N model[53]	Present
$\langle E_1 \rangle$	2.329	2.329	2.483	2.483
ν_1	4.418	4.418	5.441	5.441
$\langle E_{n'f} \rangle$	1.173	1.104	1.590	3.001
$\langle E_2 \rangle$	2.180	2.182	2.337	2.304
ν_2	3.407	3.417	4.360	4.159
$\langle E_{2nf} \rangle^1$	-	-	1.590	0.906
$\langle E_{2nf} \rangle^2$	-	-	1.104	0.677
$\langle E_3 \rangle$	-	-	2.167	2.195
ν_3	-	-	3.182	3.342
$\langle E \rangle$	2.202	2.197	2.328	2.439
ν	4.414	4.417	5.394	5.301

E_n = 20 MeV	
M-N model[50]	Present
2.585	2.585
6.151	6.151
1.829	3.902
2.440	2.396
5.030	4.740
1.829	2.618
1.420	1.160
2.277	2.264
3.815	3.741
2.411	2.590
6.059	5.894

The Madland-Nix model calculations predict non-linear decrease of $\nu_p(E)$ above emissive threshold. The influence of pre-equilibrium pre-fission neutrons manifests in additional appreciable decrease of $d\nu/dE$ above 12 MeV. The delayed number of neutrons per fission ν_d and the decay constants for six groups of delayed neutrons are taken from Brady et al.[60,61] Specifically, $\nu_d = 0.00795$ for incident neutron energies up to 4 MeV and $\nu_d = 0.00477$ for $E_n \geq 7$ MeV.

7 Angular distributions of secondary neutrons

The angular distributions of elastically scattered neutrons and those for neutrons, scattered on three levels of ground state band are calculated with the coupled channel method. The isotropic compound scattering contribution is taken into account by renormalizing l-th Legendre polynomial coefficients A_l^{cc}, calculated with coupled channels:

$$A_l = A_l^{cc}\sigma_{dir}/(\sigma_{dir}+\sigma_{comp}),$$

where σ_{dir} and σ_{comp} are the scattering cross section direct and compound contributions, respectively. For the other contributing reactions angular distributions of secondary neutrons are assumed isotropic.

8 Conclusions

The evaluated neutron data file for ^{243}Am is compiled in ENDF/B-VI format and sent to the International Science and Technology Center (Moscow) and Japan Nuclear Data Center at Japan Atomic Energy Research Institute.

Numerous discrepancies of experimental data coupled with possibility of some new data becoming available (for example, ^{243}Am(n,f) data of Baba et al. (Tohoku University, Japan) may urge some revision of data file. Present version of ^{243}Am data file may be revised before March of 1998, the expiration date of Project CIS-03-95.

9 References

1. Nakagawa T., Kikuchi Y., Proc. of the Int. Conf. on Nuclear Data and Technology, Gatlinburg, Tenn., USA, 9-13 May, 1994, Dickens J.K. (Editor), 709, ANS Inc., 1994.
2. C.L. Dunford, Nuclear Data for Science and Technology, Proc. Int. Conf. Julich, 1991,788.Springer-Verlag,1992, Berlin
3. Nordborg C. and Salvatores M. Nuclear Data for Science and Technology, Proc. of the Int. Conf., Gatlinburg, Tennessee, USA, May 9-13, 1994, v. 2, p. 680.
4. Japanese Evaluated Data Library, Version 3, JAERI 1319, 1990.
5. Seeger P.A. LA-4420, 1970, p. 138.
6. Seeger P.A., Hemmendinger A., Diven B.C. Nucl. Phys. A96, 605 (1967)
7. Knitter H.-H., Budtz-Jorgensen C. Nucl. Sci. Engng. 99, 1 (1988).
8. Simpson O.D., Simpson F.B., Harvey J.A. et al., Nucl. Sci. Engng. 55, 273 (1974).
9. Wagemans C., Schillebeeckx P., Bocquet J.P., Private communication.
10. Hulet E.K., Hoff R.W., Bowman H.R., Mochel M.C. Phys. Rev. 107, 1294 (1957)
11. Belanova T.S. et al. Preprint SIIAR, P-156, 1972.
12. Asghar M., Caitucoli F., Perrin P. et al. Ann. Nucl. Energy, 6, 561 (1979)
13. Gavrilov V.D., Goncharov V.A., Ivanenko V.V. et al. Atomnaya Energiya, 41, 185 (1975)
14. Berreth J.R., Simpson F.B. Report IN-1407, 1970, p.66.
15. Butler J.P., Lounsbury M., Merrit J.S. Can. Journ. of Phys., 35, 147 (1957)
16. Bak M.M., Krivokhatskiy, Petrzhak K.A. et al. Atomnaya Energiya, 23, 316 (1967)
17. Folger R.L., Smith J.A., L.C. Browne et al. Nuclear Cross Sections and Technology, Proc. Conf., Washington DC, March 4-7, 1968, v.2, p.1279, NBS Special Publication 299 (1968)
18. Dunford C.L.: "ENDF Utility Codes Release 6.9", IAEA-NDS-29 (1993)
19. Porodzinskij Yu.V., Sukhovitskij E.Sh., Nuclear Constants, 4, p.27, 1987 (in Russian)
20. Porter C.E., Thomas R.G., Phys. Rev., 104, 483, (1956)
21. Jaynes F.J., Trans. Systems Sci. and Cybern., 4, 227, (1968)
22. Ignatjuk A.V., Istekov K.K., Smirenkin G.N. Sov. J. Nucl. Phys. 29, 450 (1979)
23. Wisshak K., Kappeler Nucl. Sci. Eng. 85, 251 (1983)
24. Weston L.W. and Todd J.H. Nucl. Sci. Eng., 91, 444 (1985)
25. Maslov V.M., Porodzinskij Yu.V., Sukhovitskij E.Sh., Klepatskij A.B.,

Morogovskij G.B., to be published as INDC(BLR)-4, 1996.
26. Haouat, Lachkar J., Lagrange Ch., et al., Nucl.Sci. Engng. 81, 491 (1982).
27. Phillips T.W. and Howe R.E., Nucl. Sci. Engng., 69, 375 (1979).
28. Klepatskij A.B., Sukhovitskij E.Sh., private communication.
29. Butler D.K. and Sjoblom R.K. Phys. Rev. 124, 1129 (1961).
30. Lorenz A., INDC(NDS)-149/NE, 1983.
31. Behrens J.W., Browne J.C. Nucl. Sci. Engng. 77, 444 (1981)
32. Fomushkin E.F., Novoselov G.F., Vinogradov Yu.I. et al. Yadernye Konstanty 57(3), 17 (1984).
33. Fomushkin E.F., Gutnikova E.K., Zamyatnin Yu.S. et al. Yadernaya Fyzika, 5, 966 (1967).
34. Fursov B.I., Baranov E.Yu., Klemyshev M.P. et al. Sov. J. At. Energy 59, 899 (1985)
35. Fursov B.I., Kupriyanov V.M., Ivanov V.I., Smirenkin G.N. Sov. J. At. Energy 43, 894 (1978).
36. Kanda K., Imaruoka H., Terayama H. et al., Journal of Nucl. Sci. Tech., 24, 423 (1987).
37. Wagemans C. and Deruytter A.J., Proc. IAEA Advisory Group Meeting "Nuclear Standards Reference Data", Geel, Belgium, November, 1984, IAEA-TECDOC-335, p.156, IAEA, Vienna (1985).
38. Goverdovskij A.A., Gordyushin A.K., Kuzminov B.D. et al. Sov. J. At. Energy 67, 524 (1990).
39. Ignatjuk A.V., Maslov V.M., Proc. Int. Symp. Nuclear Data Evaluation Methodology, Brookhaven,USA, October 12-16, 1992, p.440, World Scientific, 1993.
40. Maslov V.M. and Y. Kikuchi JAERI-Research, 1996.
41. Maslov V.M. Sov. J. At. Energy 64, 478 (1988).
42. Sood P.C., Singh R.N. Nucl. Phys. A373, 519 (1982).
43. Howard W.M., Moller P. Atomic Data and Nuclear Data Tables,25, 219 (1980)
44. Tepel J.W., Hoffman H.M., Weidenmuller H.A. Phys. Lett. 49, 1 (1974).
45. Klepatskij A.B., Maslov V.M., Sukhovitskij E.Sh., private communication.
46. Ignatjuk A.V., Maslov V.M., Pashchenko A.B. Sov. J. Nucl. Phys. 47, 224 (1988).
47. Uhl M. and Strohmaier B., Report IRK - 76/10 (Vienna,1976).
48. Dabbs J.W. , Bemis C.E., Raman S., et al., Nucl. Sci. Engng. 84, 1 (1983).
49. Browne J.C., White R.M., Howe R.E. et al. Phys. Rev. 29, 2188 (1984).
50. Fursov B.I., Samylin B.F., Smirenkin G.N., Polynov V.N., Nuclear Data for Science and Technology, Proc. of the Int. Conf., Gatlinburg, Tennessee,

USA, May 9-13, 1994, v.I, p. 269.
51. ENSDF, 1995.
52. Maslov V.M., Porodzinskij Yu.V.,Sukhovitskij E.Sh., Proc. Int. Conf. on Neutron Physics, 14-18 Sept., Kiev, USSR, V.1, p.413, 1988.
53. Madland D.G., Nix J.R., Nucl. Sci. Engng. 81, 213 (1982).
54. Asghar M. et al., Nuclear Physics A, 334, 327 (1980).
55. Audi G., Wapstra A.H., Nuclear Physics A, 565, 1 (1980).
56. Viola V.E., Kwiatkowski K., Walker M., Phys. Rev., 31, 1550 (1985).
57. Becchetti F.D., Greenlees G.W., Phys. Rev. 182, 1190 (1969).
58. Frehaut J. et al., Progress Report CEA-N-2396, 1984, p. 69.
59. Khokhlov Yu.A. et al., Nuclear Data for Science and Technology, Proc. of the Int. Conf., Gatlinburg, Tennessee, USA, May 9-13, 1994, v.I, p. 272.
60. Brady M.C.and England T.R., Nucl.Sci. Engng. 103, 129 (1989)
61. Brady M.C., Wright R.Q., England T.R., Report ORNL/CSD/TM-226(1991), IAEA-NDS-102, 1992.

10 Figure captions

Fig. 2.1 Total cross section of ^{243}Am around 160 eV.
Fig. 2.2 Fission cross section of ^{243}Am in the energy region below 195 eV.
Fig. 2.3 Total cross section of ^{243}Am in the energy region below 0.1 eV.
Fig. 2.4 Total cross section of ^{243}Am in the energy region below 0.5 eV.
Fig. 2.5 Distribution of radiative capture widths for ^{243}Am.
Fig. 3.1 Cumulative sum of neutron resonance levels of ^{243}Am.
Fig. 3.2 Cumulative sum of reduced neutron widths of ^{243}Am.
Fig. 3.3 Distribution of reduced neutron widths for ^{243}Am.
Fig. 3.4 Neutron resonance spacing distribution for ^{243}Am.
Fig. 3.5 Fission cross section of ^{243}Am in unresolved resonance region.
Fig. 3.6 Capture cross section of ^{243}Am in unresolved resonance region.
Fig. 4.1 Compound reaction cross section of ^{243}Am.
Fig. 4.2 Total cross section of ^{243}Am.
Fig. 4.3 Elastic scattering cross section of ^{243}Am.
Fig. 4.4 Fission cross section of ^{243}Am.
Fig. 4.5 Fission cross section of ^{243}Am.
Fig. 4.6 Fission cross section of ^{243}Am.
Fig. 4.7 Fission cross section of ^{243}Am.
Fig. 4.8 Fission cross section of ^{242m}Am.
Fig. 4.9 Fission cross section of ^{243}Am.
Fig. 4.10 Cumulative number of levels of ^{243}Am.
Fig. 4.11 Inelastic scattering cross section of ^{243}Am.
Fig. 4.12 Continuum inelastic scattering cross section of ^{243}Am.
Fig. 4.13 Cross section of ^{243}Am: 0.0422 MeV, $7/2^-$ level excitation.
Fig. 4.14 Cross section of ^{243}Am: 0.084 MeV, $5/2^+$ level excitation.
Fig. 4.15 Cross section of ^{243}Am: 0.0964 MeV, $9/2^-$ level excitation.
Fig. 4.16 Cross section of ^{243}Am: 0.1092 MeV, $7/2^+$ level excitation.
Fig. 4.17 Cross section of ^{243}Am: 0.1435 MeV, $9/2^+$ level excitation.
Fig. 4.18 Cross section of ^{243}Am: 0.1893 MeV, $11/2^-$ level excitation.
Fig. 4.19 Cross section of ^{243}Am: 0.266 MeV, $3/2^-$ level excitation.
Fig. 4.20 Cumulative number of levels of ^{244}Am.
Fig. 4.21 Radiative capture cross section of ^{243}Am.
Fig. 4.22 ^{243}Am(n,2n) reaction cross section.
Fig. 4.23 ^{243}Am(n,3n) reaction cross section.
Fig. 5.1 Components of first neutron spectrum of ^{243}Am for incident neutron energy 15 MeV.
Fig. 5.2 Components of second neutron spectrum of ^{243}Am for incident neutron energy 15 MeV.

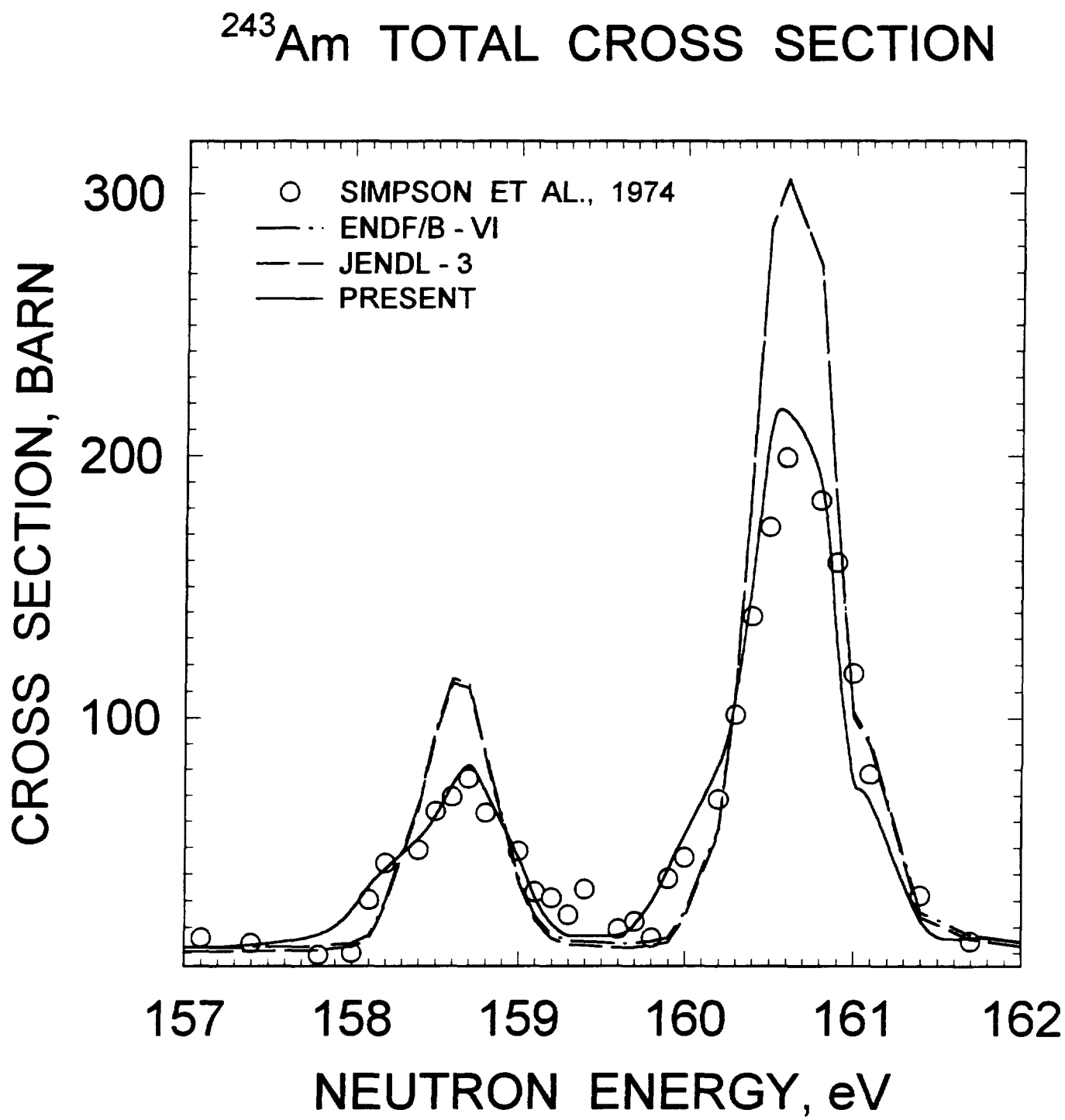
^{243}Am TOTAL CROSS SECTION
SIMPSON ET AL., 1974
ENDF/B - VI
JENDL - 3
PRESENT
CROSS SECTION, BARN
300
200
100
157
158
159
160
161
162
NEUTRON ENERGY, eV

FIG.2.1

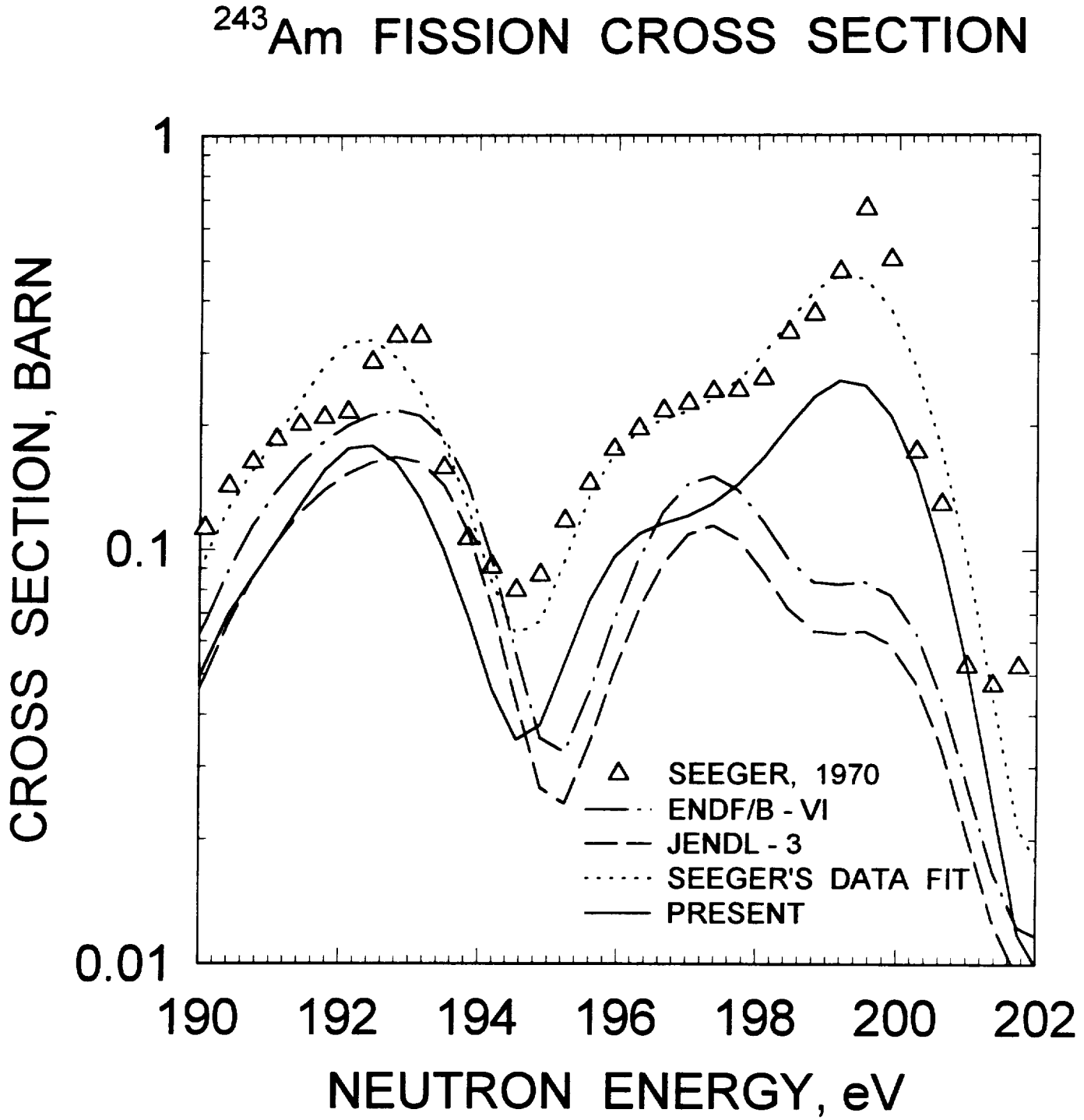
^{243}Am FISSION CROSS SECTION
CROSS SECTION, BARN
1
0.1
0.01
190
192
194
196
198
200
202
NEUTRON ENERGY, eV
SEEGER, 1970
ENDF/B - VI
JENDL - 3
SEEGER'S DATA FIT
PRESENT

FIG.2.2

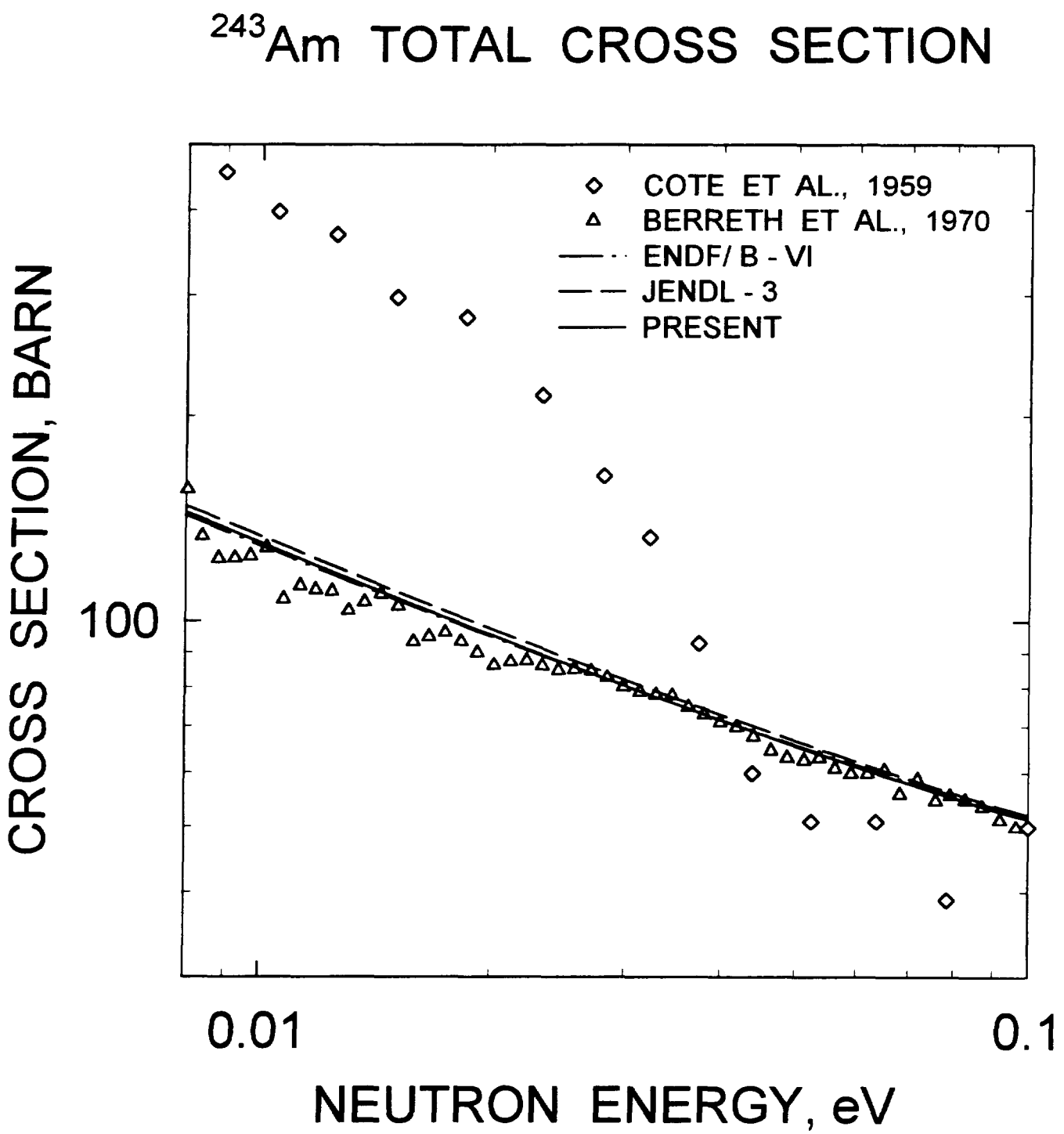
^{243}Am TOTAL CROSS SECTION
COTE ET AL., 1959
BERRETH ET AL., 1970
ENDF/ B - VI
JENDL - 3
PRESENT
CROSS SECTION, BARN
100
0.01
0.1
NEUTRON ENERGY, eV

FIG.2.3

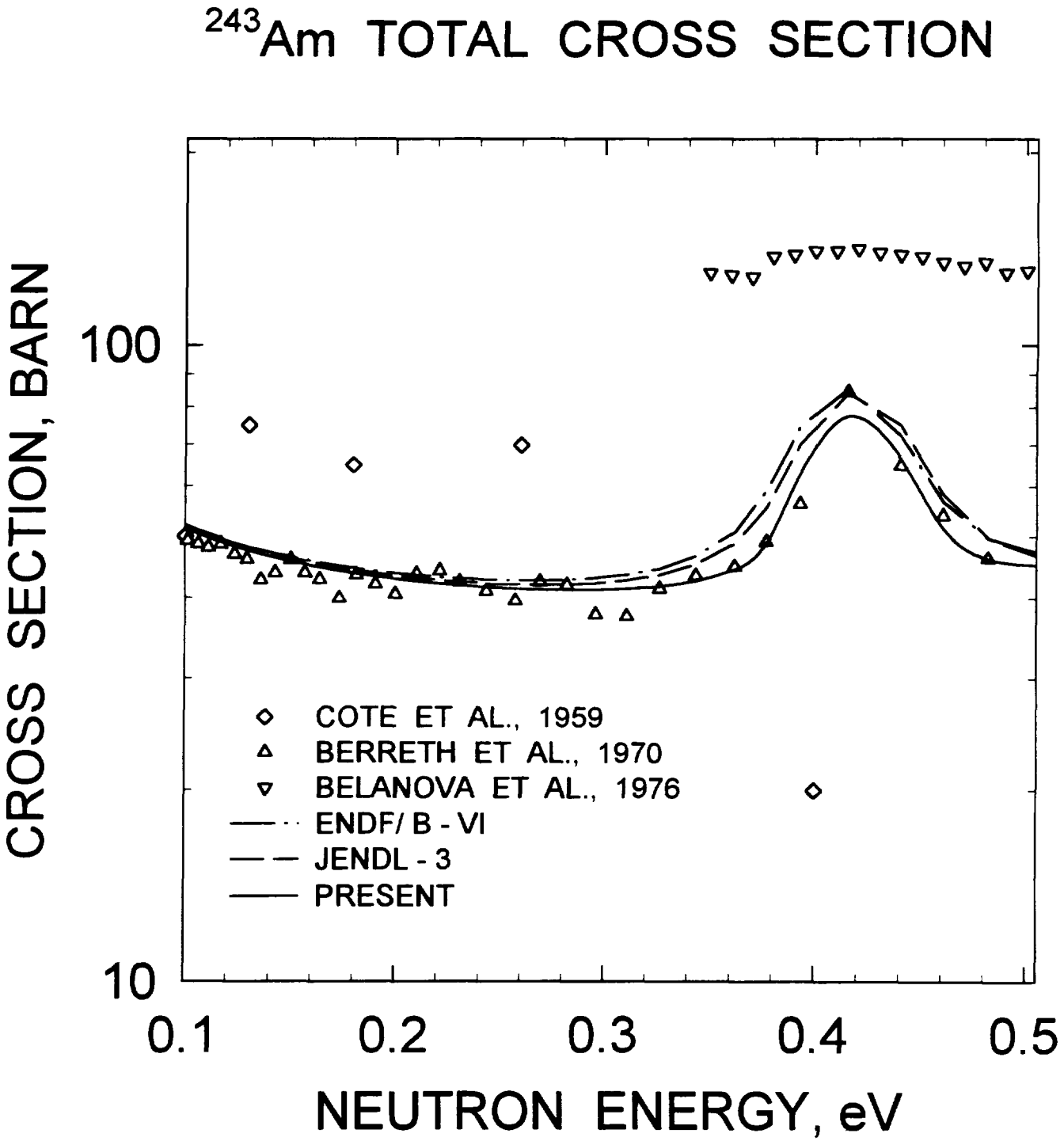
^{243}Am TOTAL CROSS SECTION
CROSS SECTION, BARN
100
10
0.1
0.2
0.3
0.4
0.5
NEUTRON ENERGY, eV
COTE ET AL., 1959
BERRETH ET AL., 1970
BELANOVA ET AL., 1976
ENDF/ B - VI
JENDL - 3
PRESENT

FIG.2.4

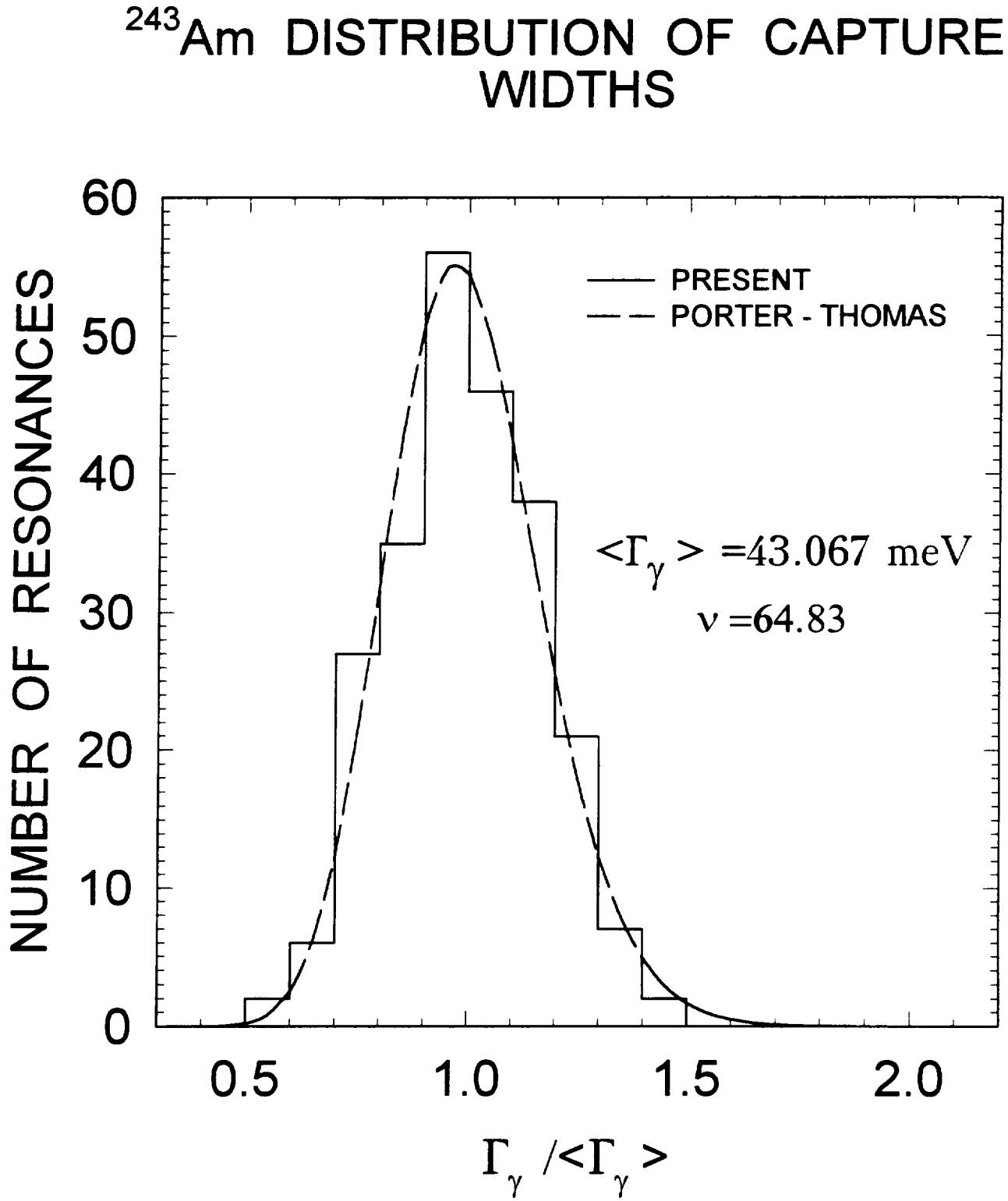
^{243}Am DISTRIBUTION OF CAPTURE WIDTHS
NUMBER OF RESONANCES
60
50
40
30
20
10
0
PRESENT
PORTER - THOMAS
$<\Gamma_\gamma>$ =43.067 meV
ν =64.83
0.5
1.0
1.5
2.0
$\Gamma_\gamma / <\Gamma_\gamma>$

FIG.2.5

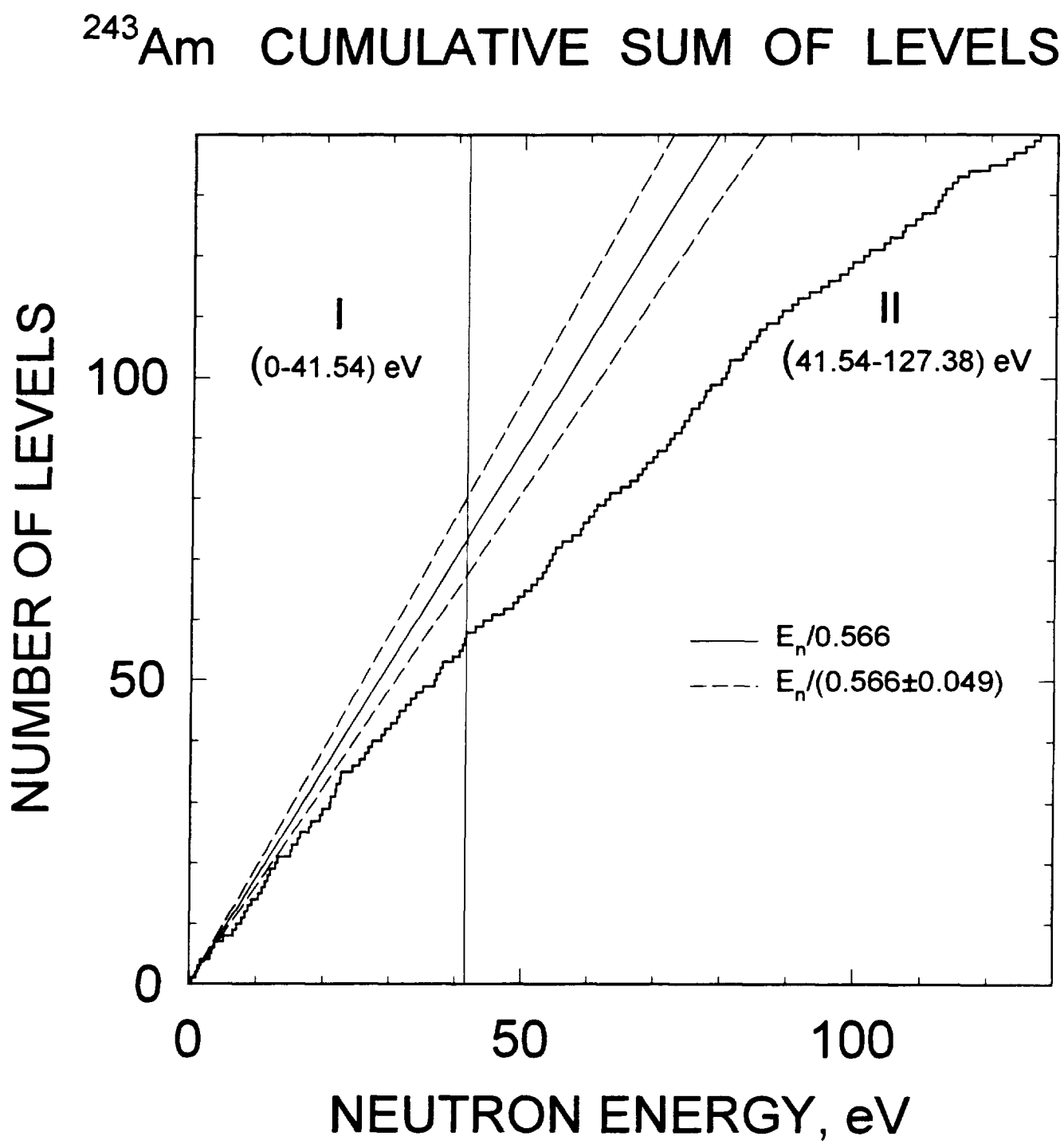
^{243}Am CUMULATIVE SUM OF LEVELS
NUMBER OF LEVELS
100
50
0
I
(0-41.54) eV
II
(41.54-127.38) eV
E_n/0.566
E_n/(0.566±0.049)
0
50
100
NEUTRON ENERGY, eV

FIG.3.1

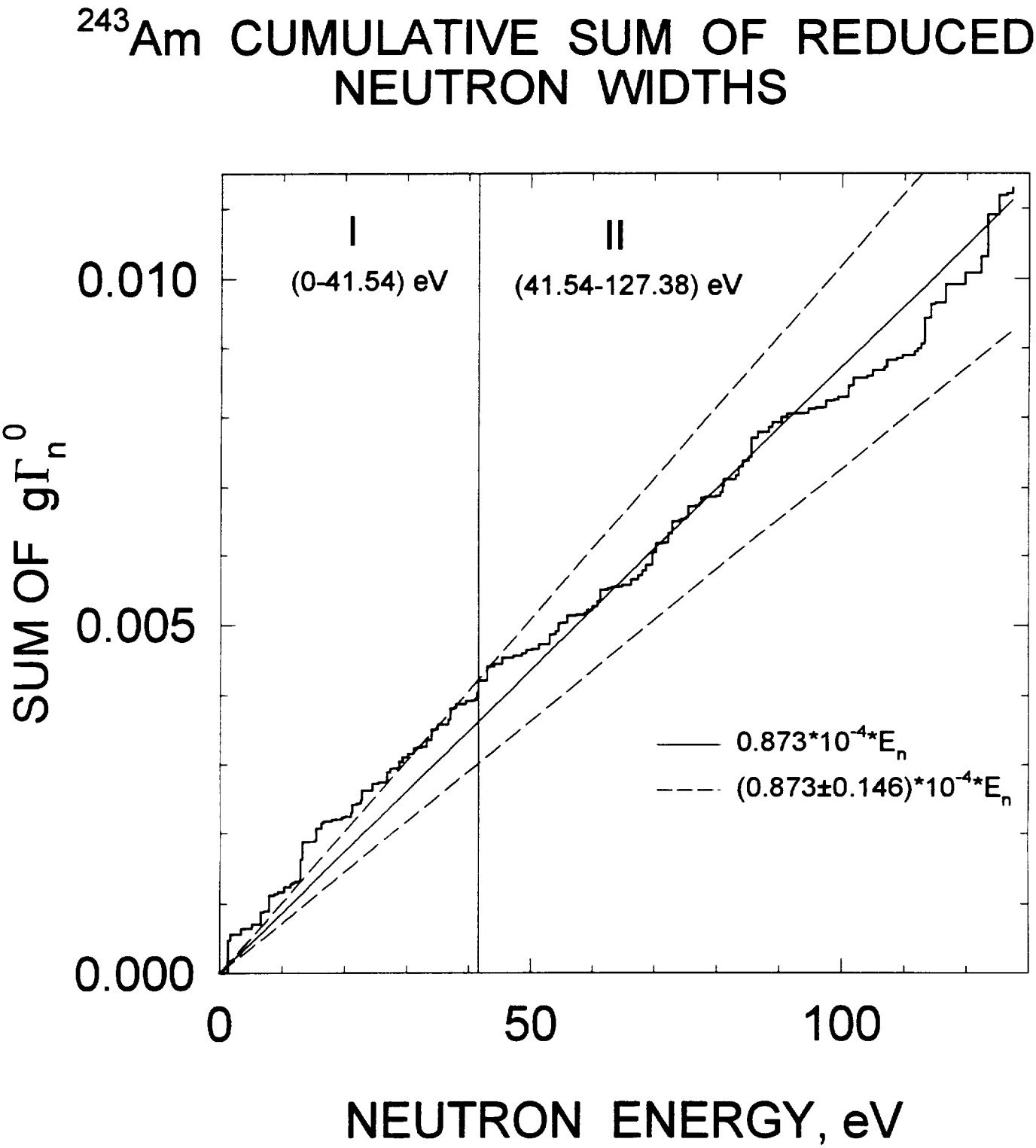
^{243}Am CUMULATIVE SUM OF REDUCED NEUTRON WIDTHS
I
(0-41.54) eV
II
(41.54-127.38) eV
0.010
0.005
0.000
SUM OF $g\Gamma_n^0$
0
50
100
NEUTRON ENERGY, eV
$0.873*10^{-4}*E_n$
$(0.873\pm0.146)*10^{-4}*E_n$

FIG.3.2

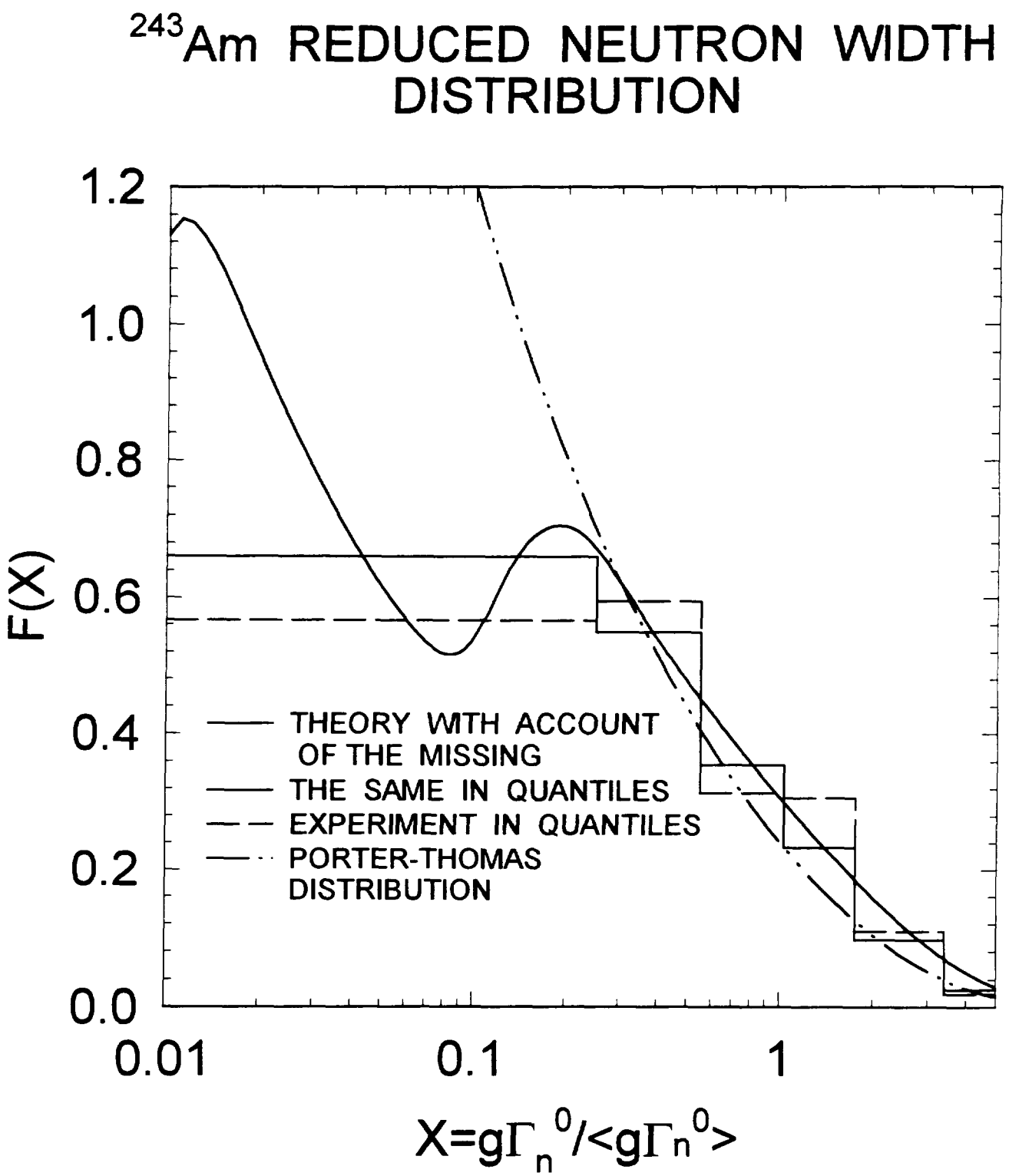
^{243}Am REDUCED NEUTRON WIDTH DISTRIBUTION
1.2
1.0
0.8
0.6
0.4
0.2
0.0
F(X)
0.01
0.1
1
THEORY WITH ACCOUNT OF THE MISSING
THE SAME IN QUANTILES
EXPERIMENT IN QUANTILES
PORTER-THOMAS DISTRIBUTION
X=gΓn0/<gΓn0>

FIG.3.3

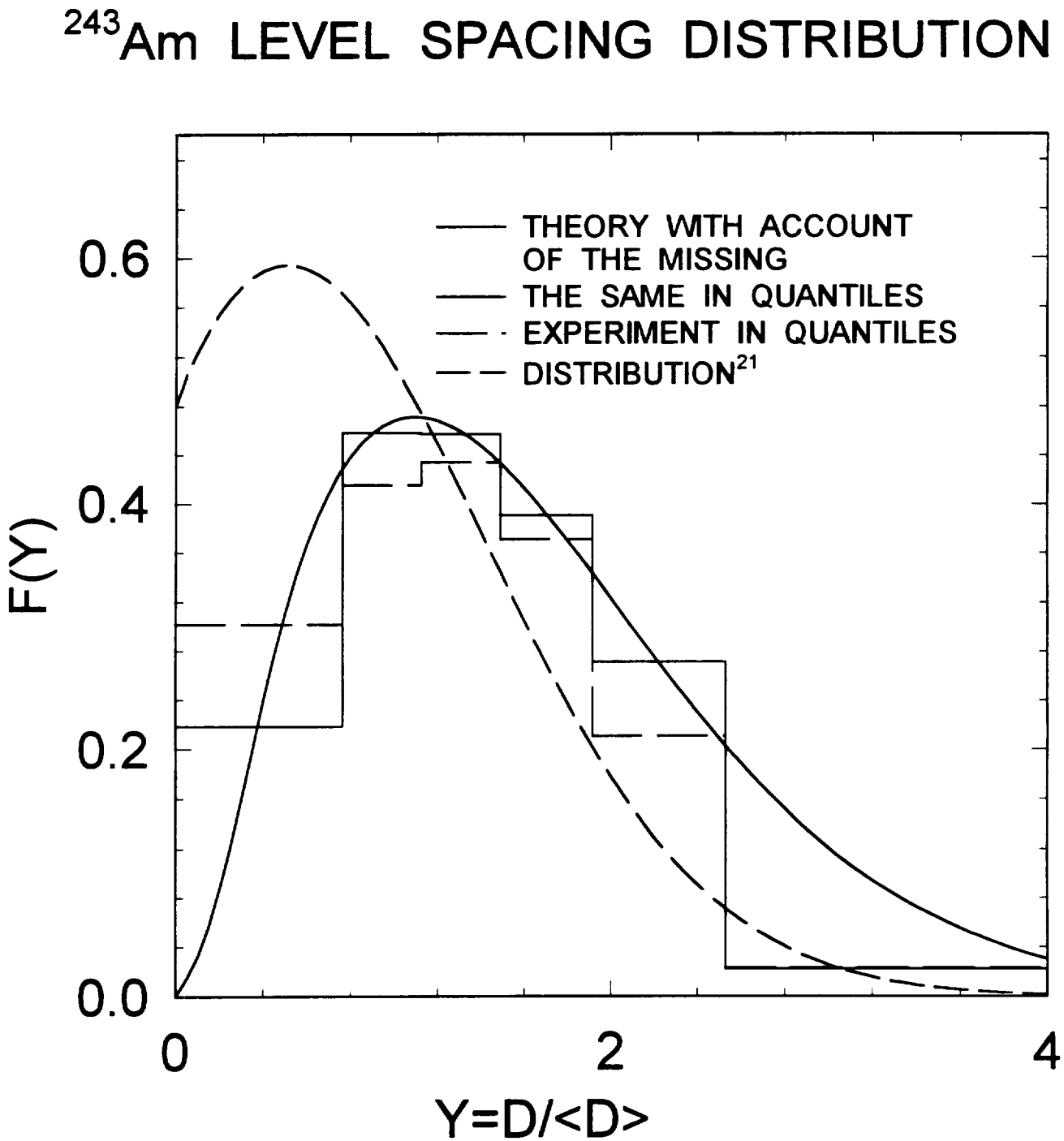
^{243}Am LEVEL SPACING DISTRIBUTION
THEORY WITH ACCOUNT OF THE MISSING
THE SAME IN QUANTILES
EXPERIMENT IN QUANTILES
DISTRIBUTION[21]
F(Y)
0.0
0.2
0.4
0.6
0
2
4
Y=D/<D>

FIG.3.4

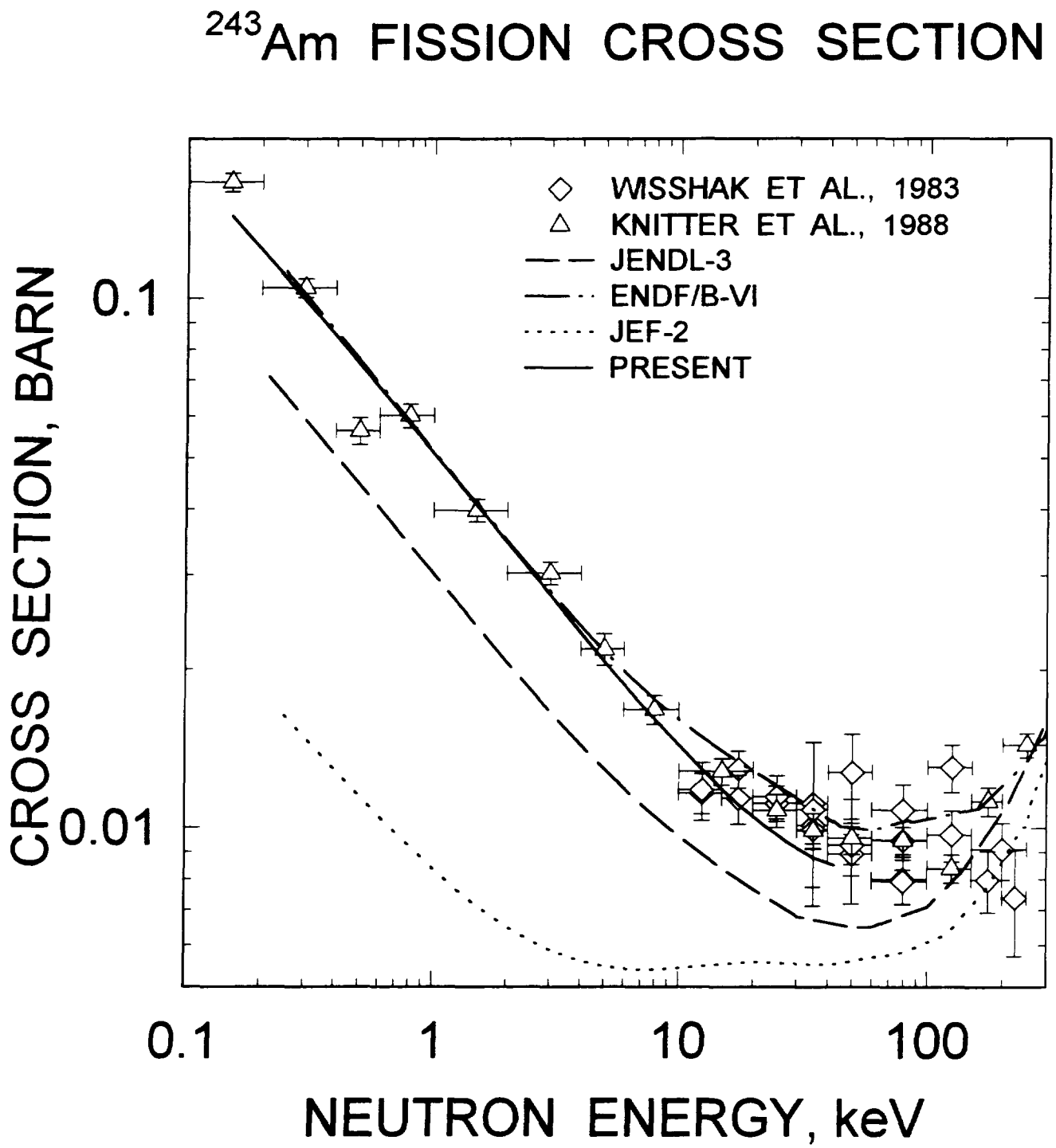
^{243}Am FISSION CROSS SECTION
WISSHAK ET AL., 1983
KNITTER ET AL., 1988
JENDL-3
ENDF/B-VI
JEF-2
PRESENT
CROSS SECTION, BARN
0.1
0.01
0.1
1
10
100
NEUTRON ENERGY, keV

FIG.3.5

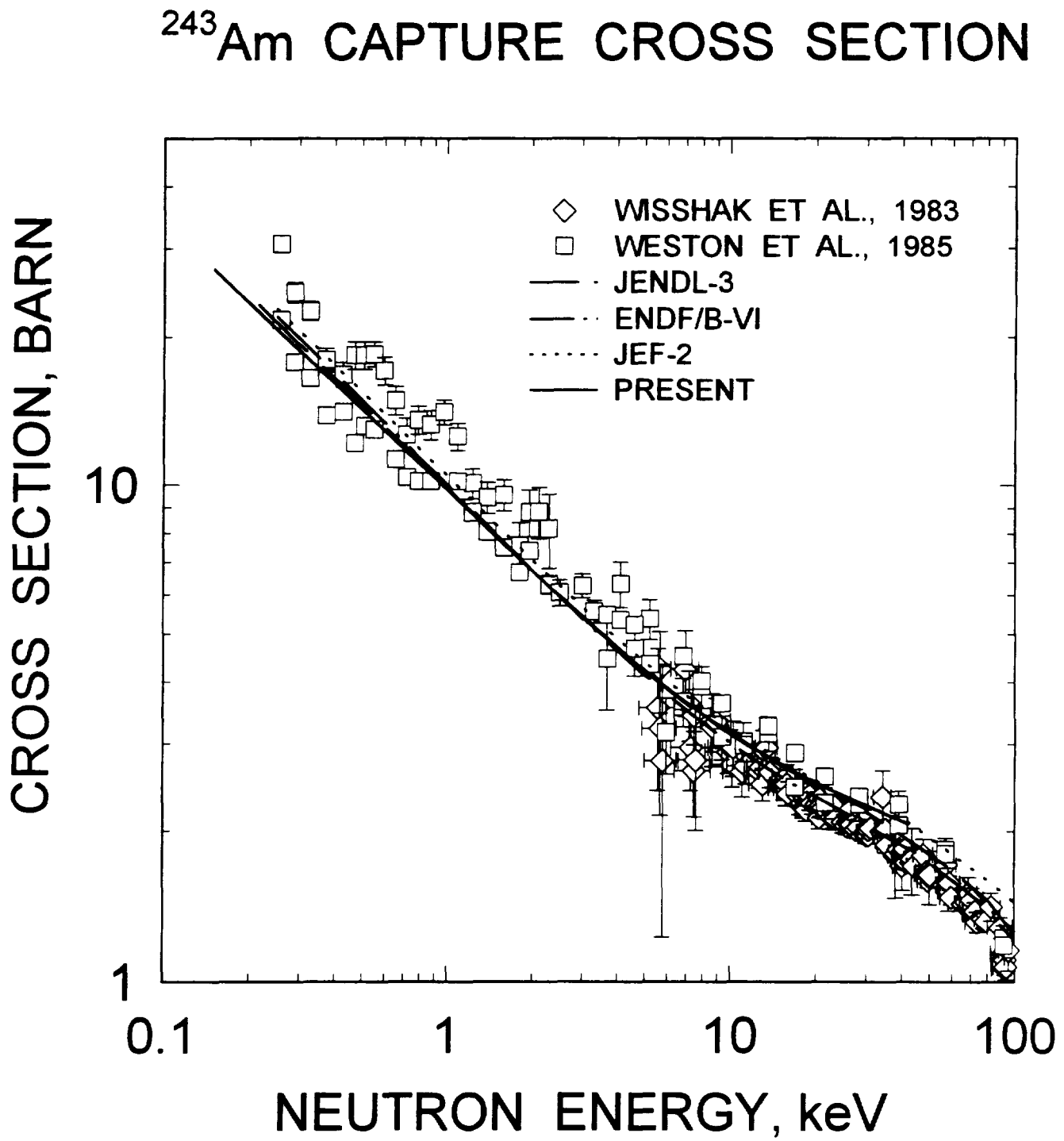
^{243}Am CAPTURE CROSS SECTION
WISSHAK ET AL., 1983
WESTON ET AL., 1985
JENDL-3
ENDF/B-VI
JEF-2
PRESENT
CROSS SECTION, BARN
10
1
0.1
1
10
100
NEUTRON ENERGY, keV

FIG.3.6

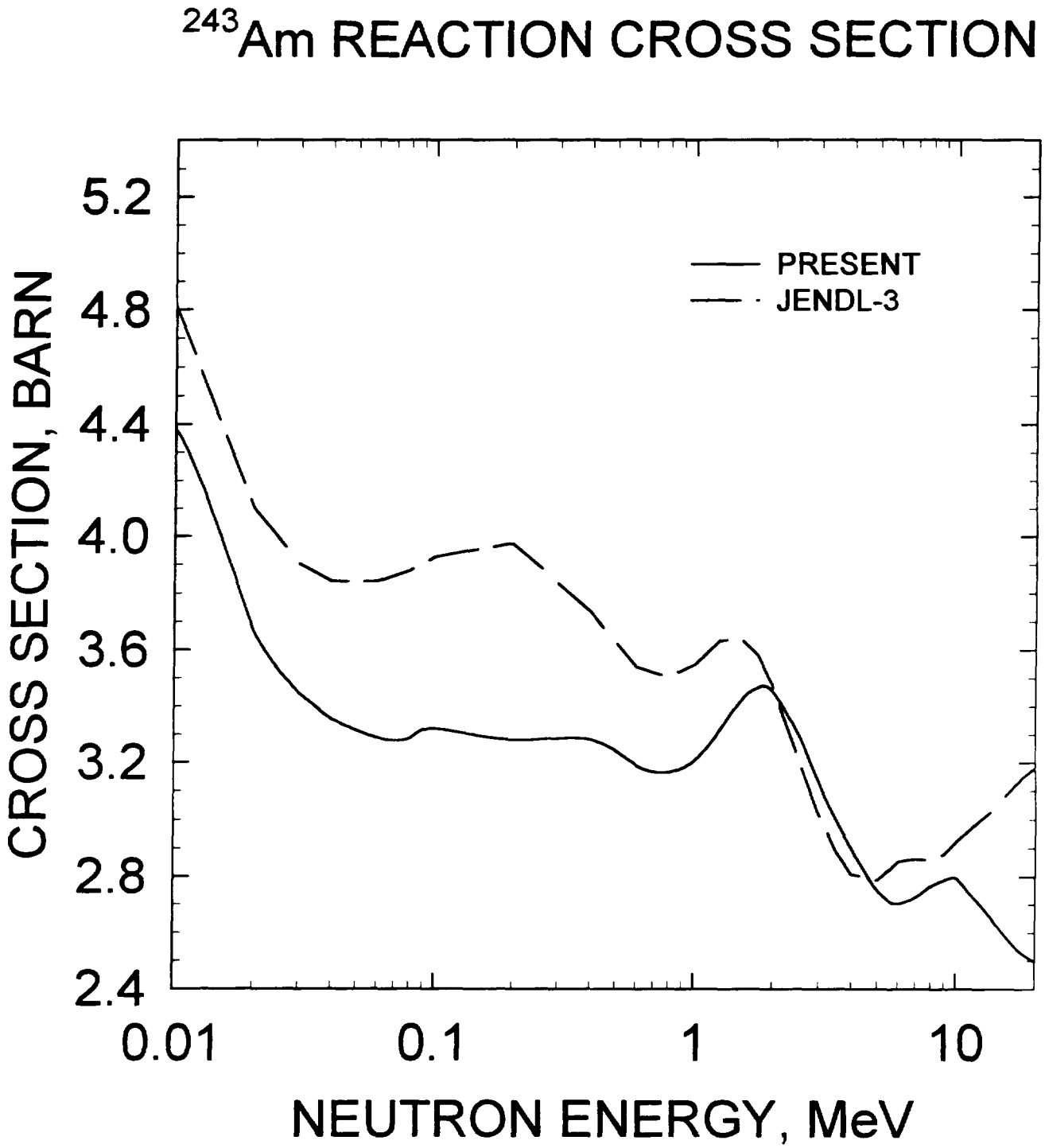
^{243}Am REACTION CROSS SECTION
CROSS SECTION, BARN
5.2
4.8
4.4
4.0
3.6
3.2
2.8
2.4
0.01
0.1
1
10
NEUTRON ENERGY, MeV
PRESENT
JENDL-3

FIG.4.1

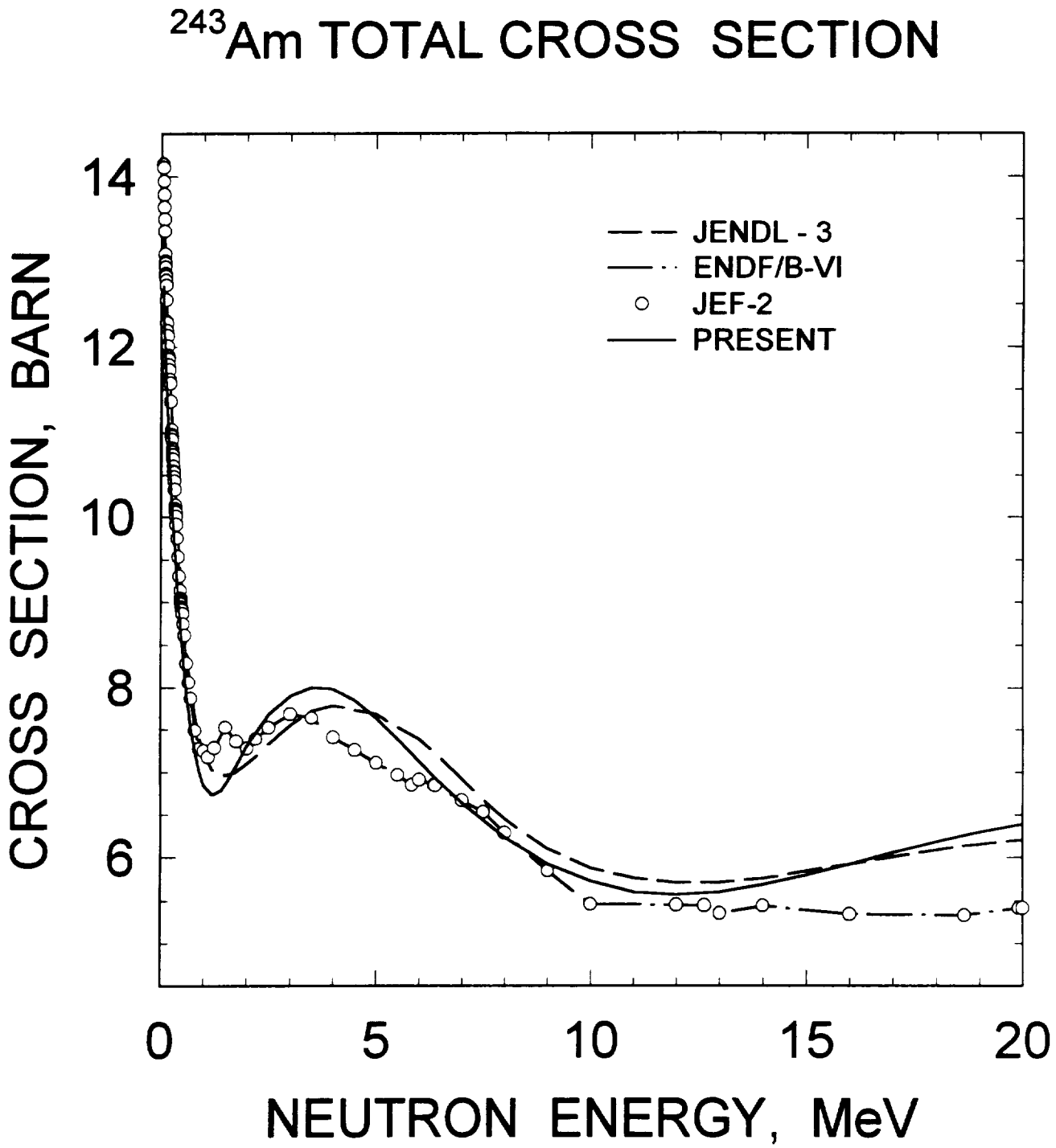
^{243}Am TOTAL CROSS SECTION
CROSS SECTION, BARN
14
12
10
8
6
0
5
10
15
20
NEUTRON ENERGY, MeV
JENDL - 3
ENDF/B-VI
JEF-2
PRESENT

FIG. 4.2

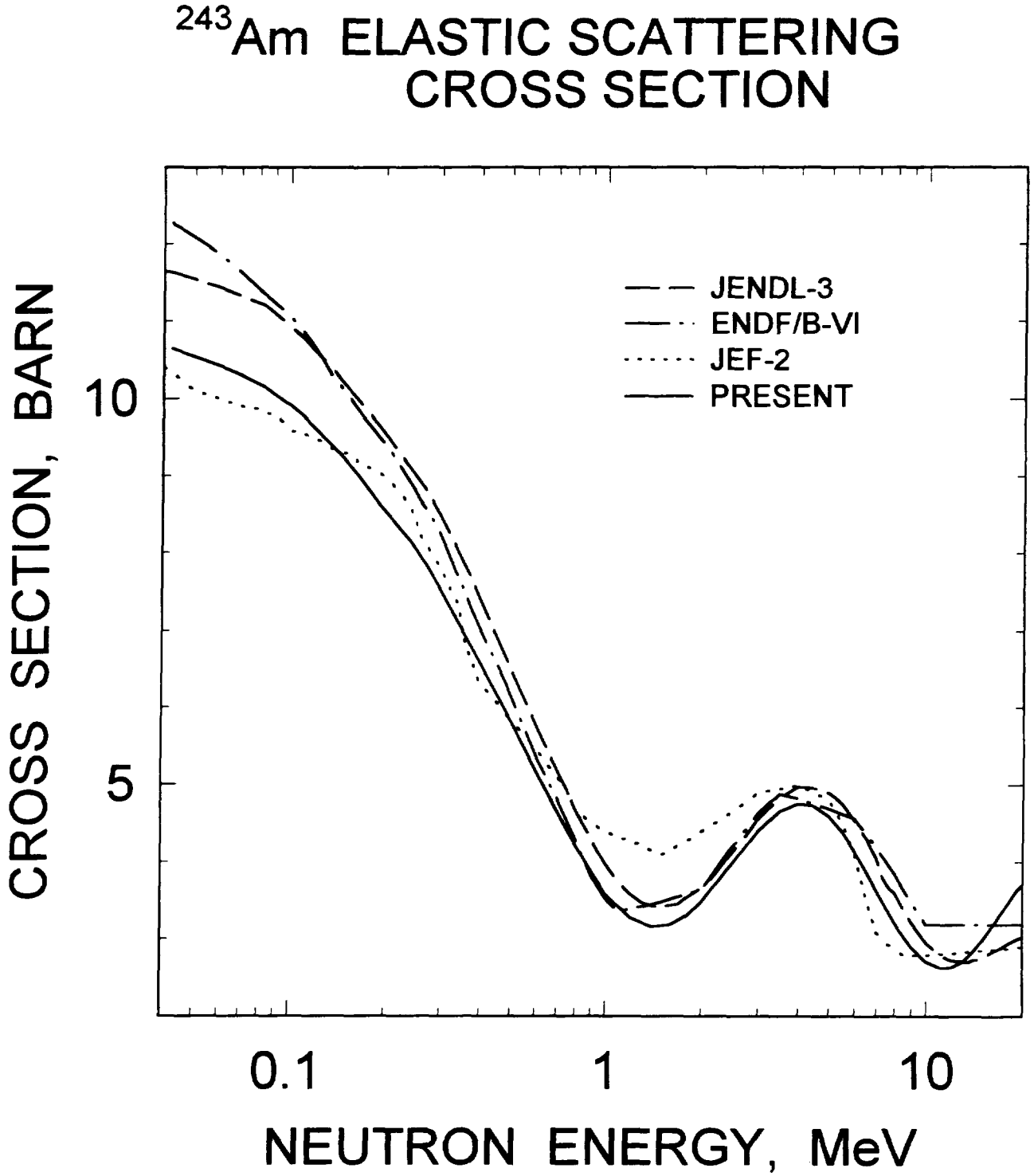
^{243}Am ELASTIC SCATTERING CROSS SECTION
JENDL-3
ENDF/B-VI
JEF-2
PRESENT
CROSS SECTION, BARN
10
5
0.1
1
10
NEUTRON ENERGY, MeV

FIG. 4.3

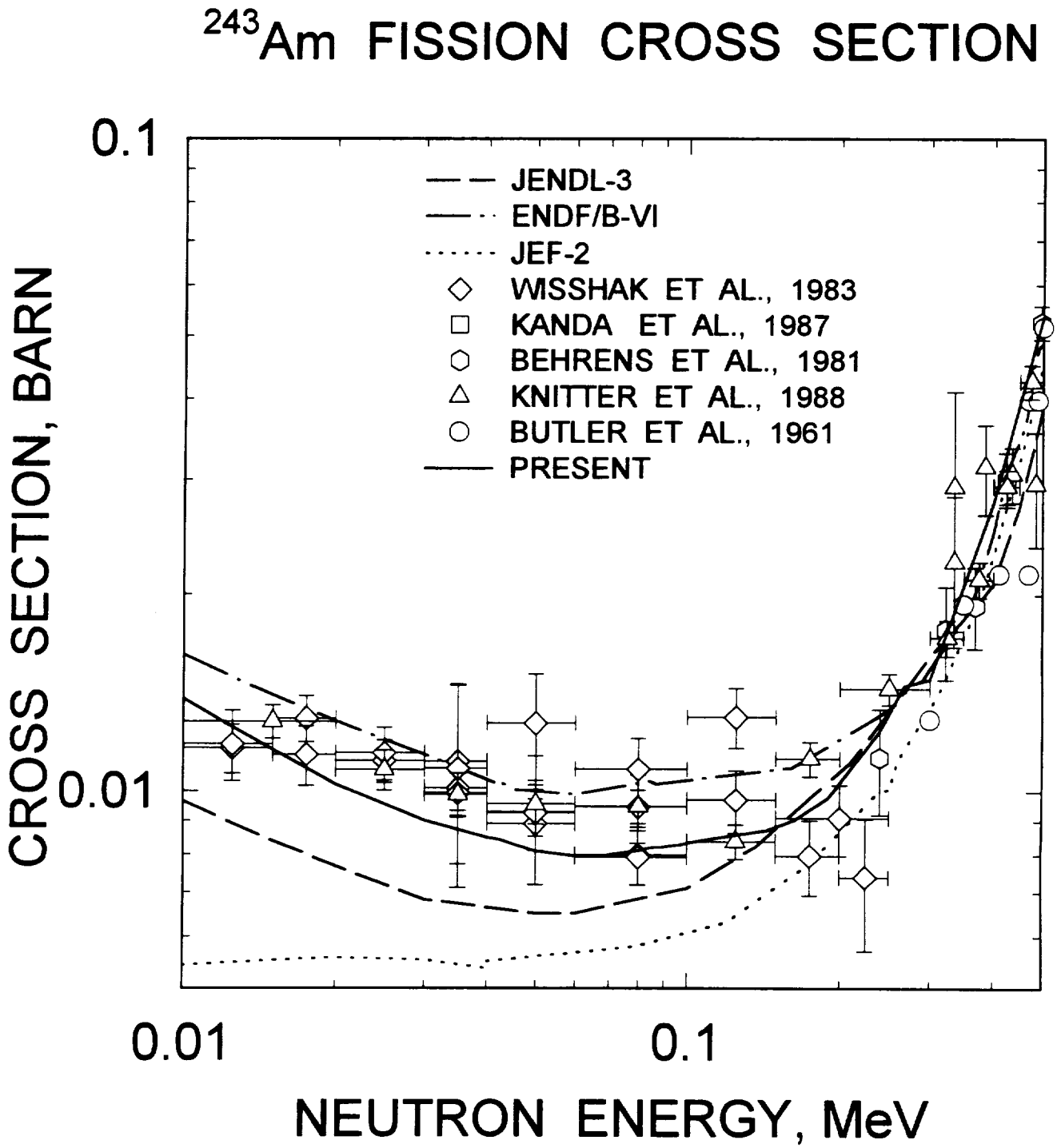
^{243}Am FISSION CROSS SECTION
0.1
0.01
CROSS SECTION, BARN
JENDL-3
ENDF/B-VI
JEF-2
WISSHAK ET AL., 1983
KANDA ET AL., 1987
BEHRENS ET AL., 1981
KNITTER ET AL., 1988
BUTLER ET AL., 1961
PRESENT
0.01
0.1
NEUTRON ENERGY, MeV

FIG.4.4

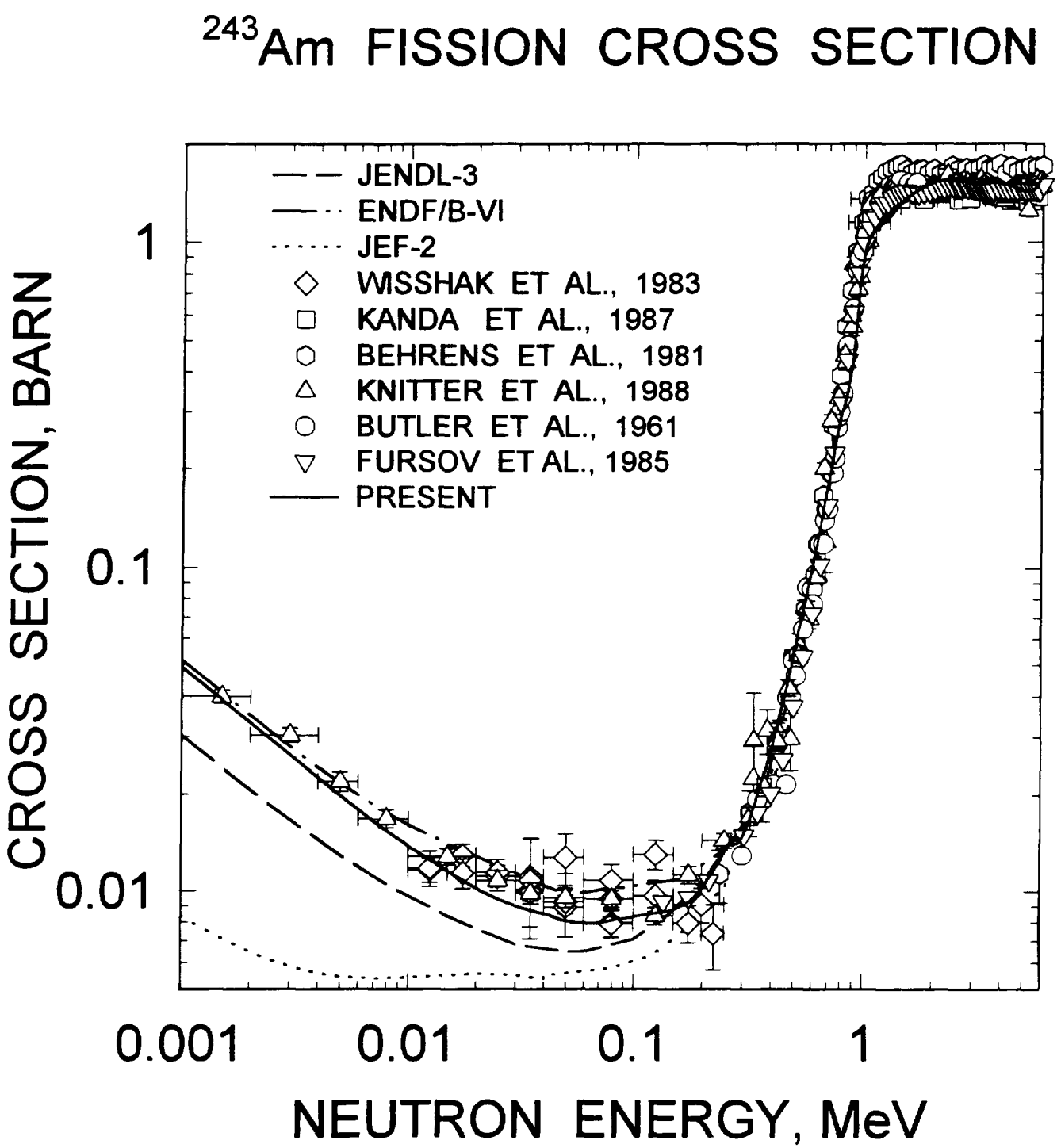
^{243}Am FISSION CROSS SECTION
JENDL-3
ENDF/B-VI
JEF-2
WISSHAK ET AL., 1983
KANDA ET AL., 1987
BEHRENS ET AL., 1981
KNITTER ET AL., 1988
BUTLER ET AL., 1961
FURSOV ET AL., 1985
PRESENT
CROSS SECTION, BARN
1
0.1
0.01
0.001
0.01
0.1
1
NEUTRON ENERGY, MeV

FIG.4.5

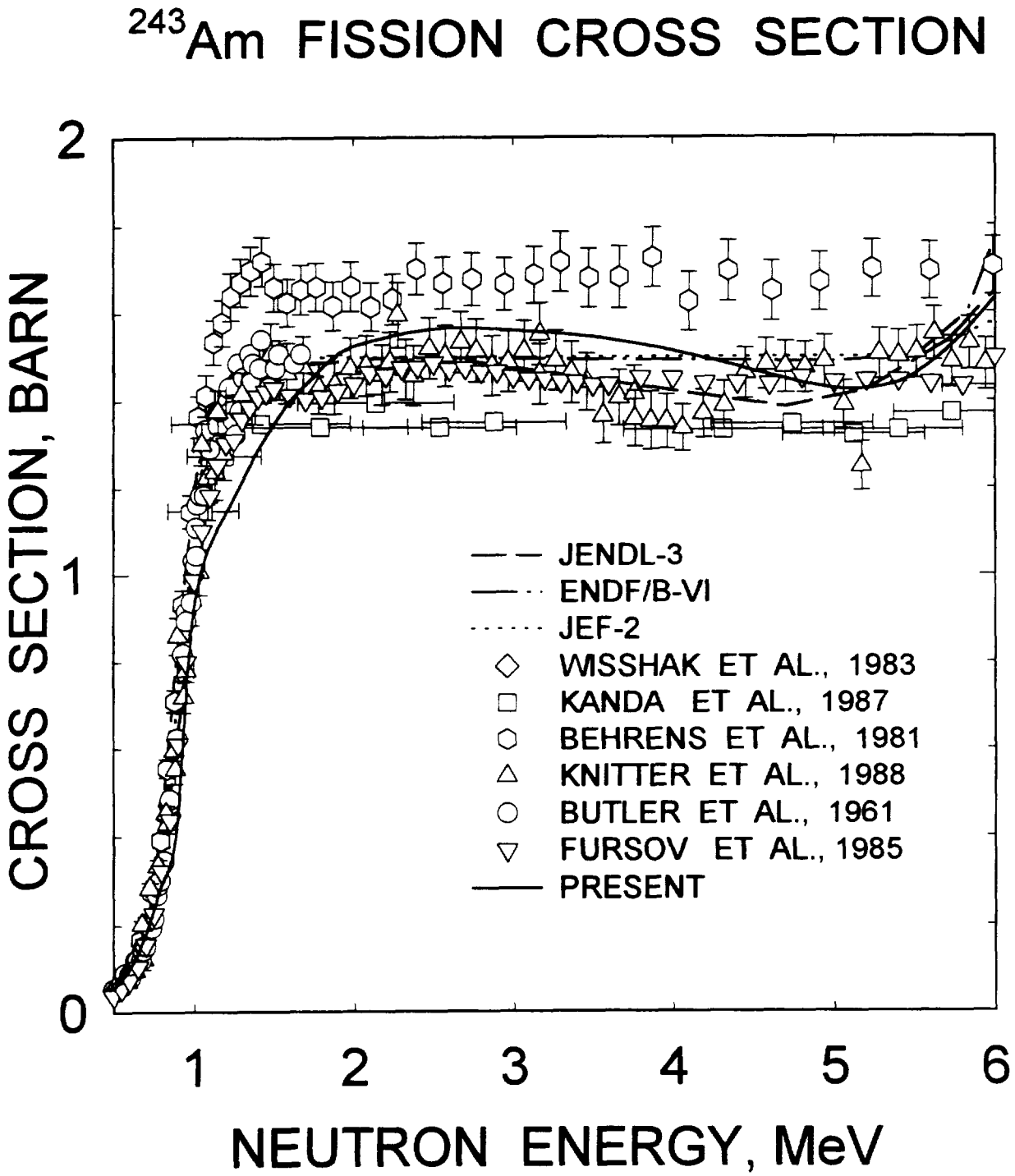
^{243}Am FISSION CROSS SECTION
CROSS SECTION, BARN
NEUTRON ENERGY, MeV
0
1
2
1
2
3
4
5
6
JENDL-3
ENDF/B-VI
JEF-2
WISSHAK ET AL., 1983
KANDA ET AL., 1987
BEHRENS ET AL., 1981
KNITTER ET AL., 1988
BUTLER ET AL., 1961
FURSOV ET AL., 1985
PRESENT

FIG.4.6

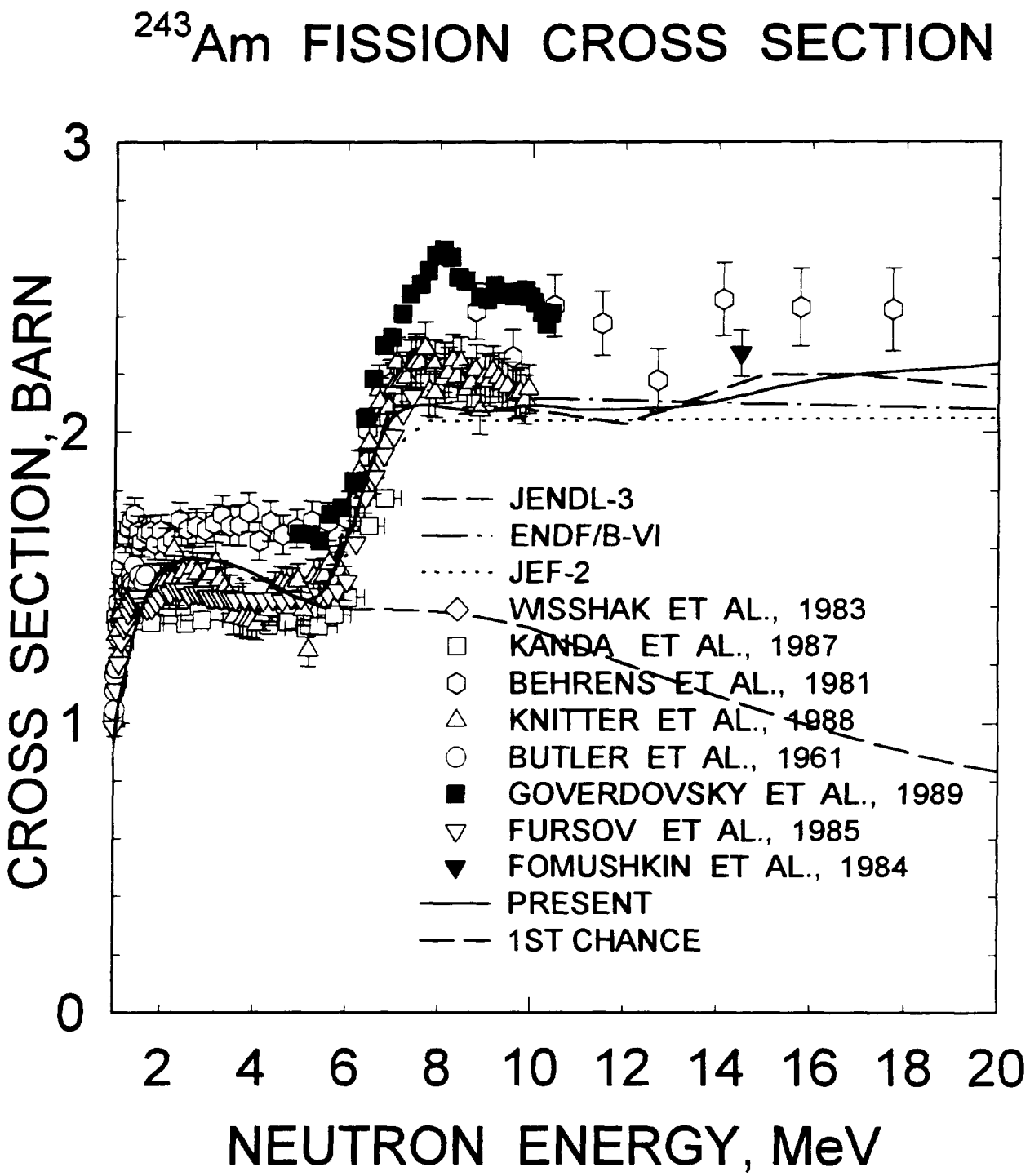
^{243}Am FISSION CROSS SECTION
CROSS SECTION, BARN
NEUTRON ENERGY, MeV
0
1
2
3
2
4
6
8
10
12
14
16
18
20
JENDL-3
ENDF/B-VI
JEF-2
WISSHAK ET AL., 1983
KANDA ET AL., 1987
BEHRENS ET AL., 1981
KNITTER ET AL., 1988
BUTLER ET AL., 1961
GOVERDOVSKY ET AL., 1989
FURSOV ET AL., 1985
FOMUSHKIN ET AL., 1984
PRESENT
1ST CHANCE

FIG.4.7

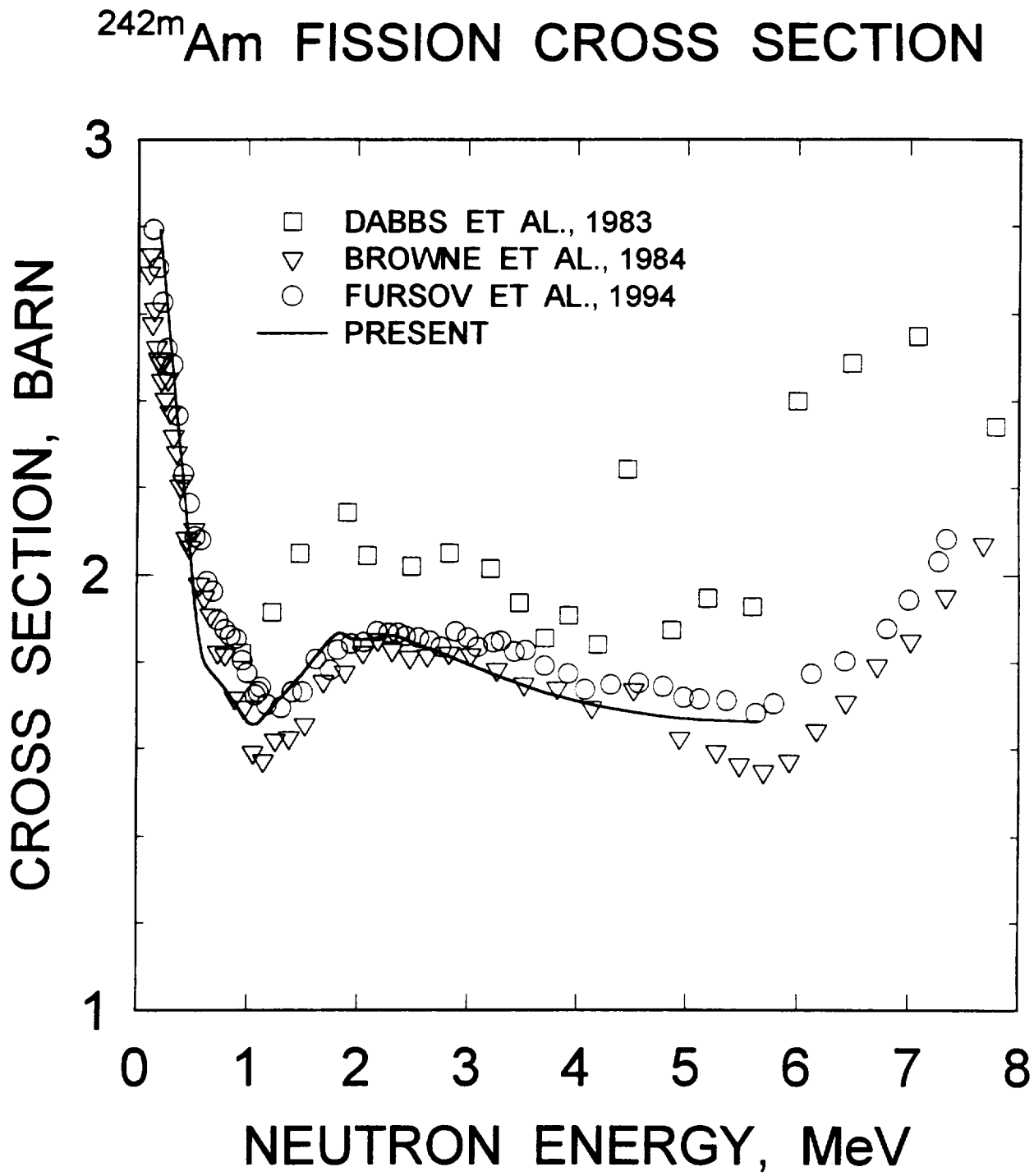
242mAm FISSION CROSS SECTION
CROSS SECTION, BARN
NEUTRON ENERGY, MeV
DABBS ET AL., 1983
BROWNE ET AL., 1984
FURSOV ET AL., 1994
PRESENT
1
2
3
0
1
2
3
4
5
6
7
8

FIG. 4.8

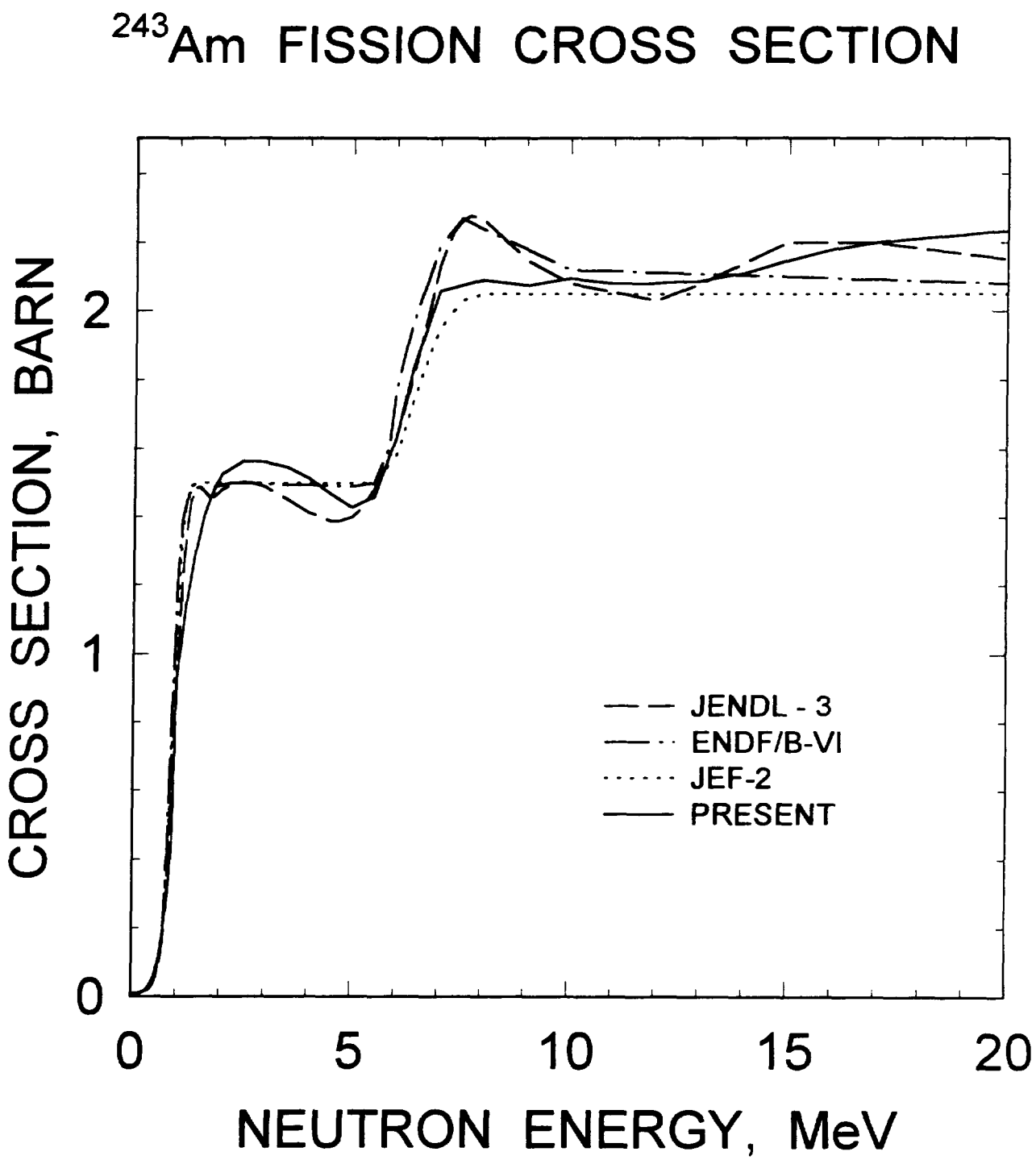
^{243}Am FISSION CROSS SECTION
CROSS SECTION, BARN
0
1
2
0
5
10
15
20
NEUTRON ENERGY, MeV
JENDL - 3
ENDF/B-VI
JEF-2
PRESENT

FIG. 4.9

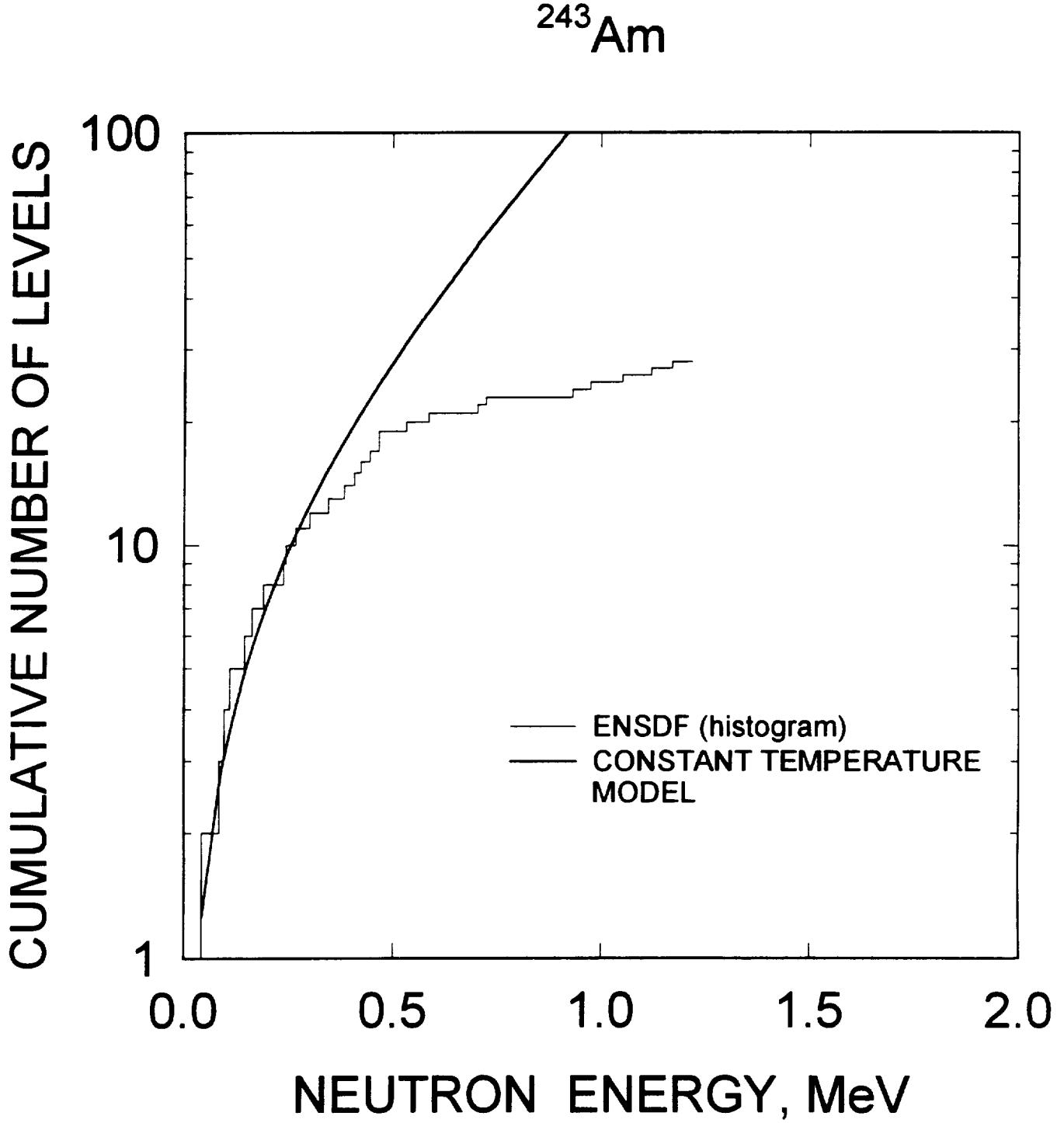
^{243}Am
CUMULATIVE NUMBER OF LEVELS
100
10
1
0.0
0.5
1.0
1.5
2.0
NEUTRON ENERGY, MeV
ENSDF (histogram)
CONSTANT TEMPERATURE MODEL

FIG.4.10

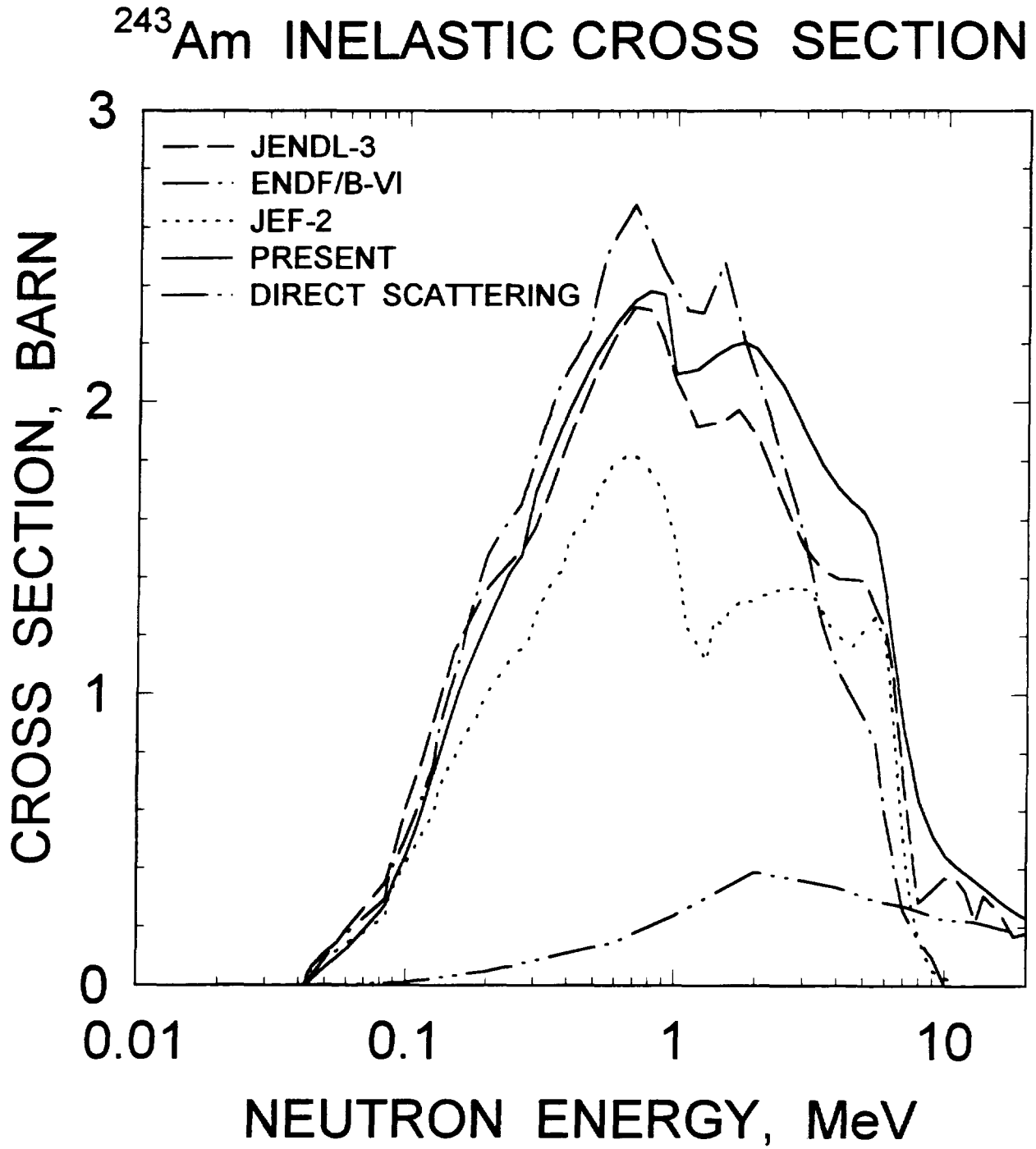
^{243}Am INELASTIC CROSS SECTION
JENDL-3
ENDF/B-VI
JEF-2
PRESENT
DIRECT SCATTERING
CROSS SECTION, BARN
0
1
2
3
0.01
0.1
1
10
NEUTRON ENERGY, MeV

FIG. 4.11

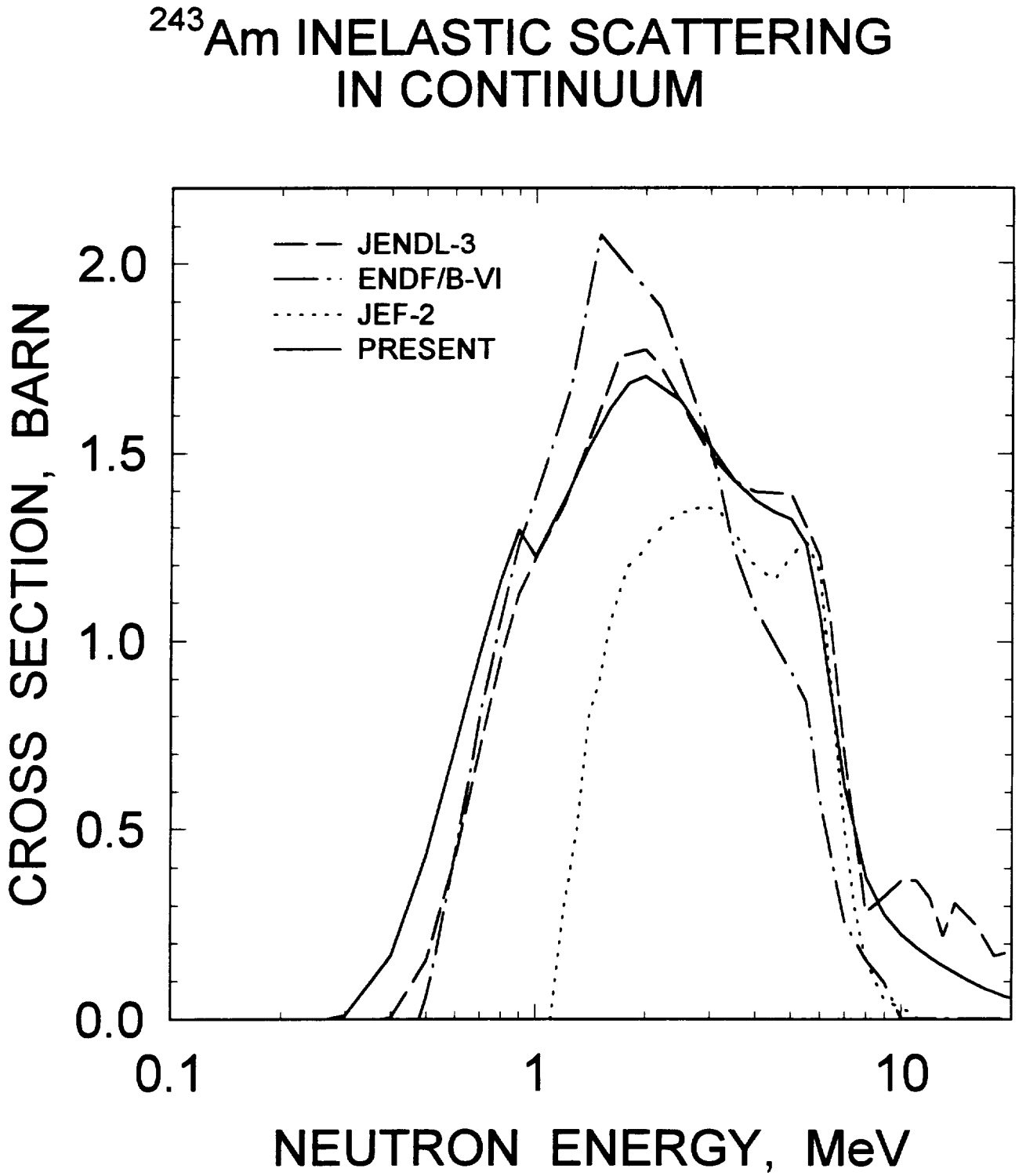
^{243}Am INELASTIC SCATTERING
IN CONTINUUM
JENDL-3
ENDF/B-VI
JEF-2
PRESENT
CROSS SECTION, BARN
2.0
1.5
1.0
0.5
0.0
0.1
1
10
NEUTRON ENERGY, MeV

FIG. 4.12

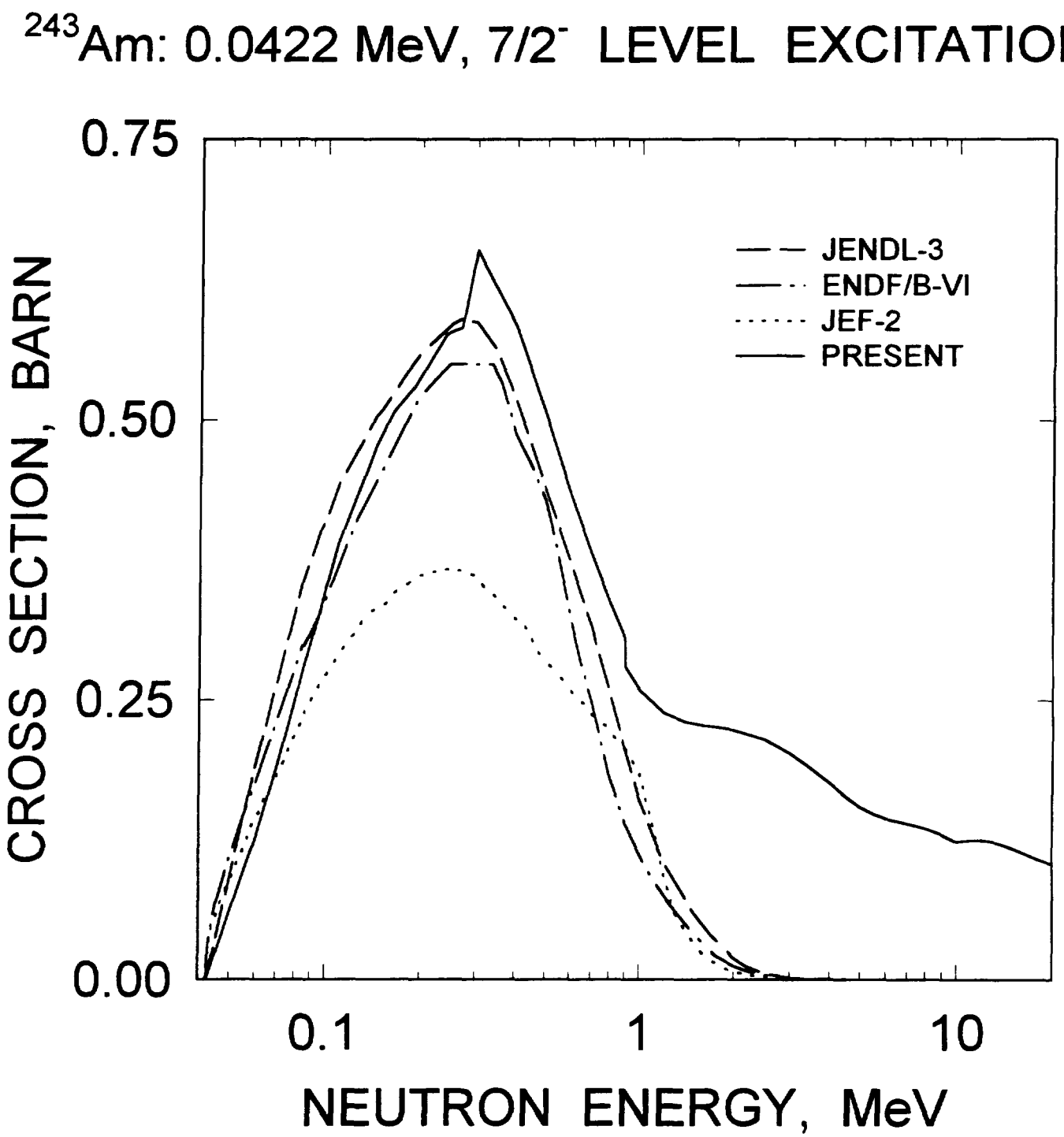
^{243}Am: 0.0422 MeV, 7/2$^-$ LEVEL EXCITATION
0.75
0.50
0.25
0.00
CROSS SECTION, BARN
JENDL-3
ENDF/B-VI
JEF-2
PRESENT
0.1
1
10
NEUTRON ENERGY, MeV

FIG. 4.13

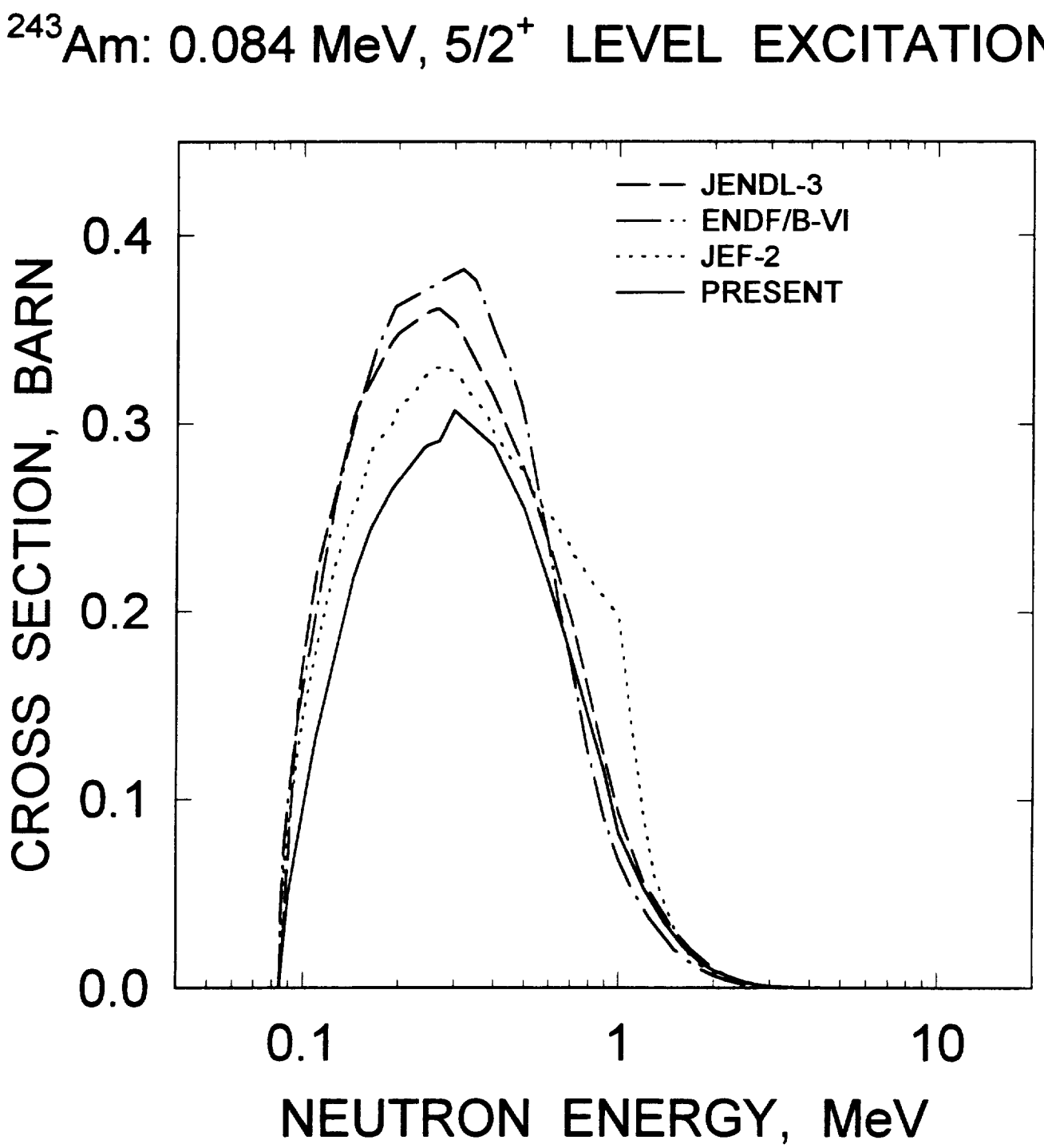
^{243}Am: 0.084 MeV, 5/2^{+} LEVEL EXCITATION
JENDL-3
ENDF/B-VI
JEF-2
PRESENT
CROSS SECTION, BARN
0.0
0.1
0.2
0.3
0.4
0.1
1
10
NEUTRON ENERGY, MeV

FIG. 4.14

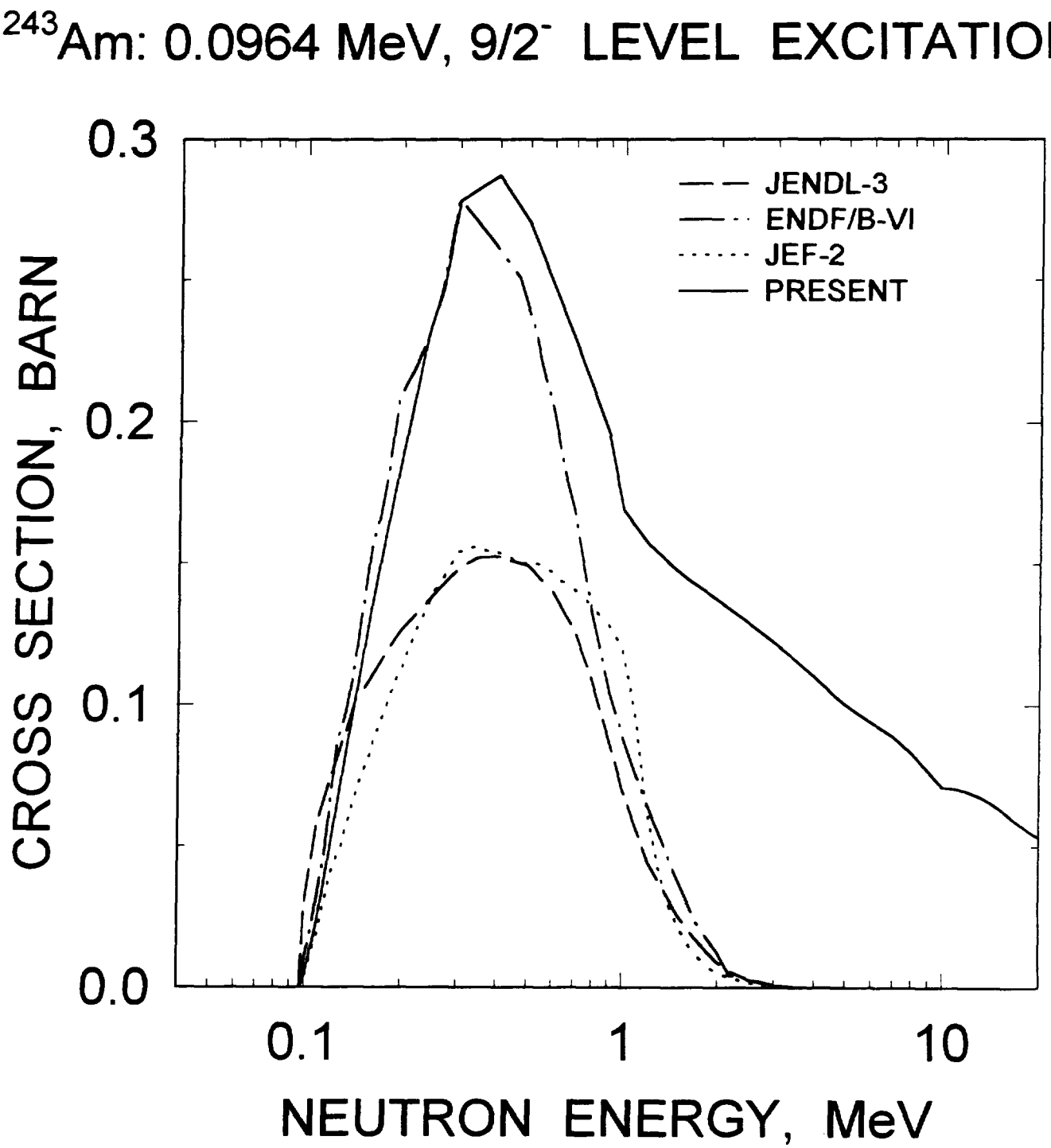
^{243}Am: 0.0964 MeV, 9/2$^-$ LEVEL EXCITATION
0.3
0.2
0.1
0.0
CROSS SECTION, BARN
JENDL-3
ENDF/B-VI
JEF-2
PRESENT
0.1
1
10
NEUTRON ENERGY, MeV

FIG. 4.15

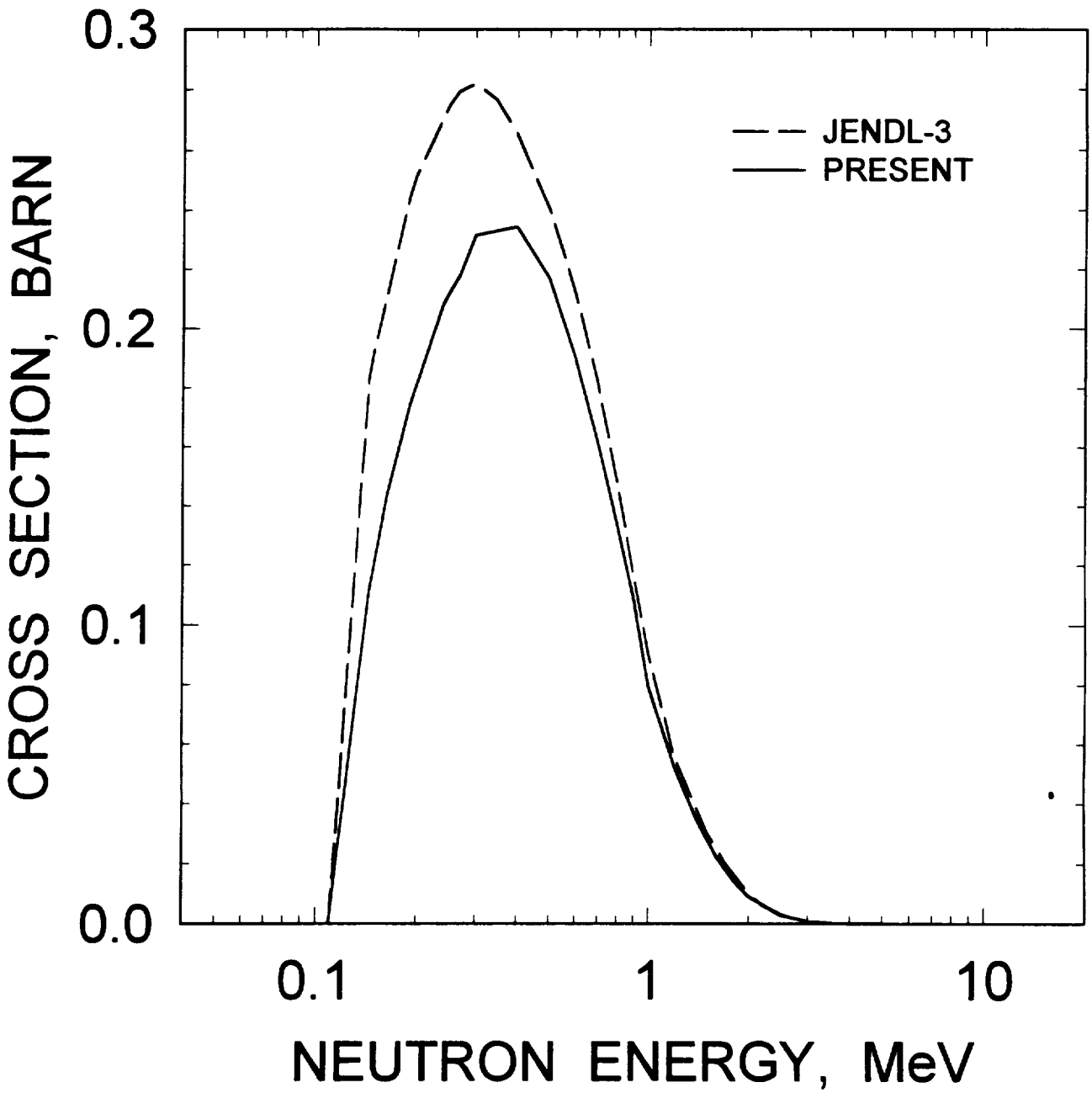
^{243}Am: 0.1092 MeV, 7/2^{+} LEVEL EXCITATION
0.3
0.2
0.1
0.0
CROSS SECTION, BARN
JENDL-3
PRESENT
0.1
1
10
NEUTRON ENERGY, MeV

FIG. 4.16

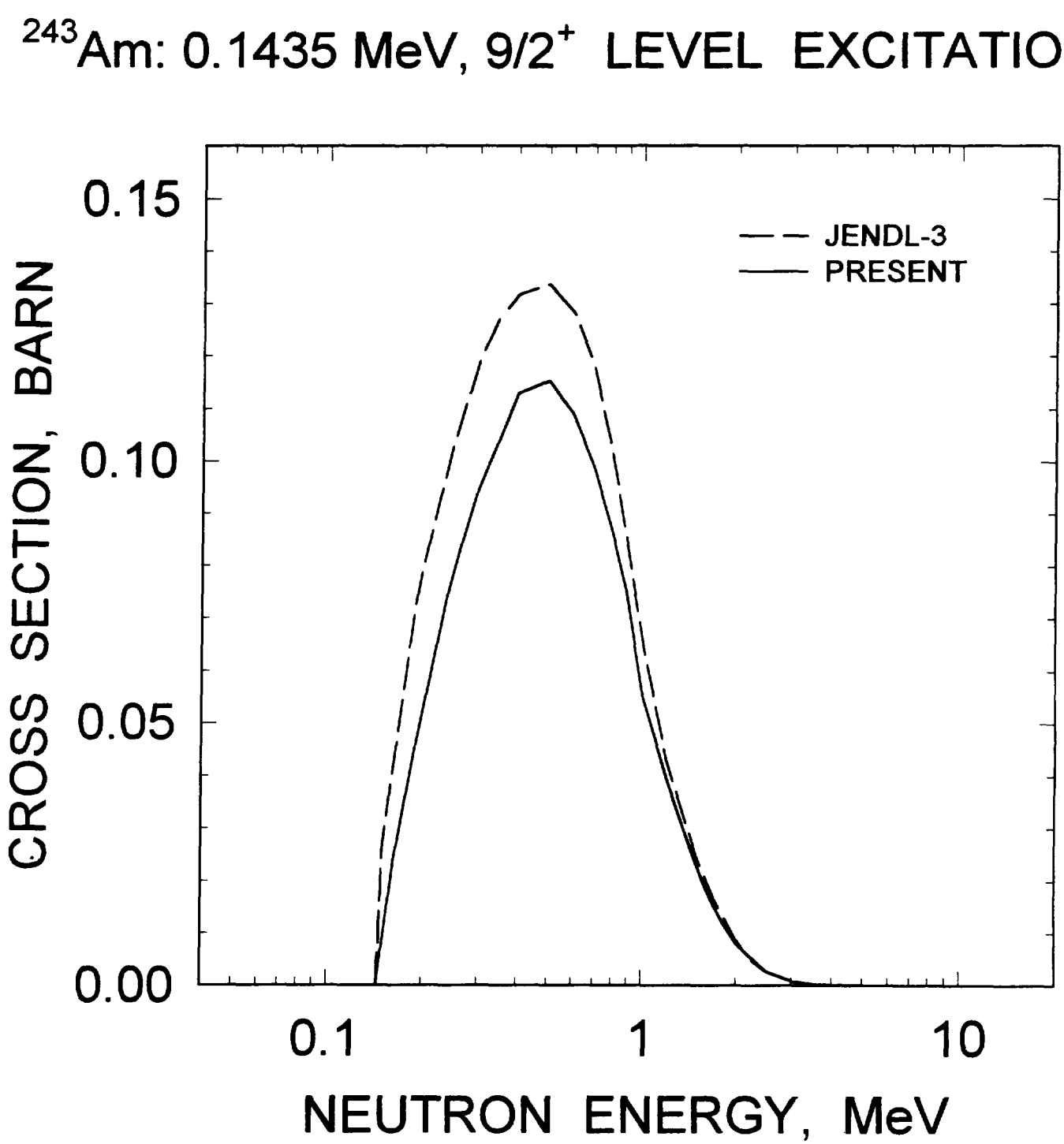
^{243}Am: 0.1435 MeV, 9/2^{+} LEVEL EXCITATION
CROSS SECTION, BARN
0.15
0.10
0.05
0.00
JENDL-3
PRESENT
0.1
1
10
NEUTRON ENERGY, MeV

FIG. 4.17

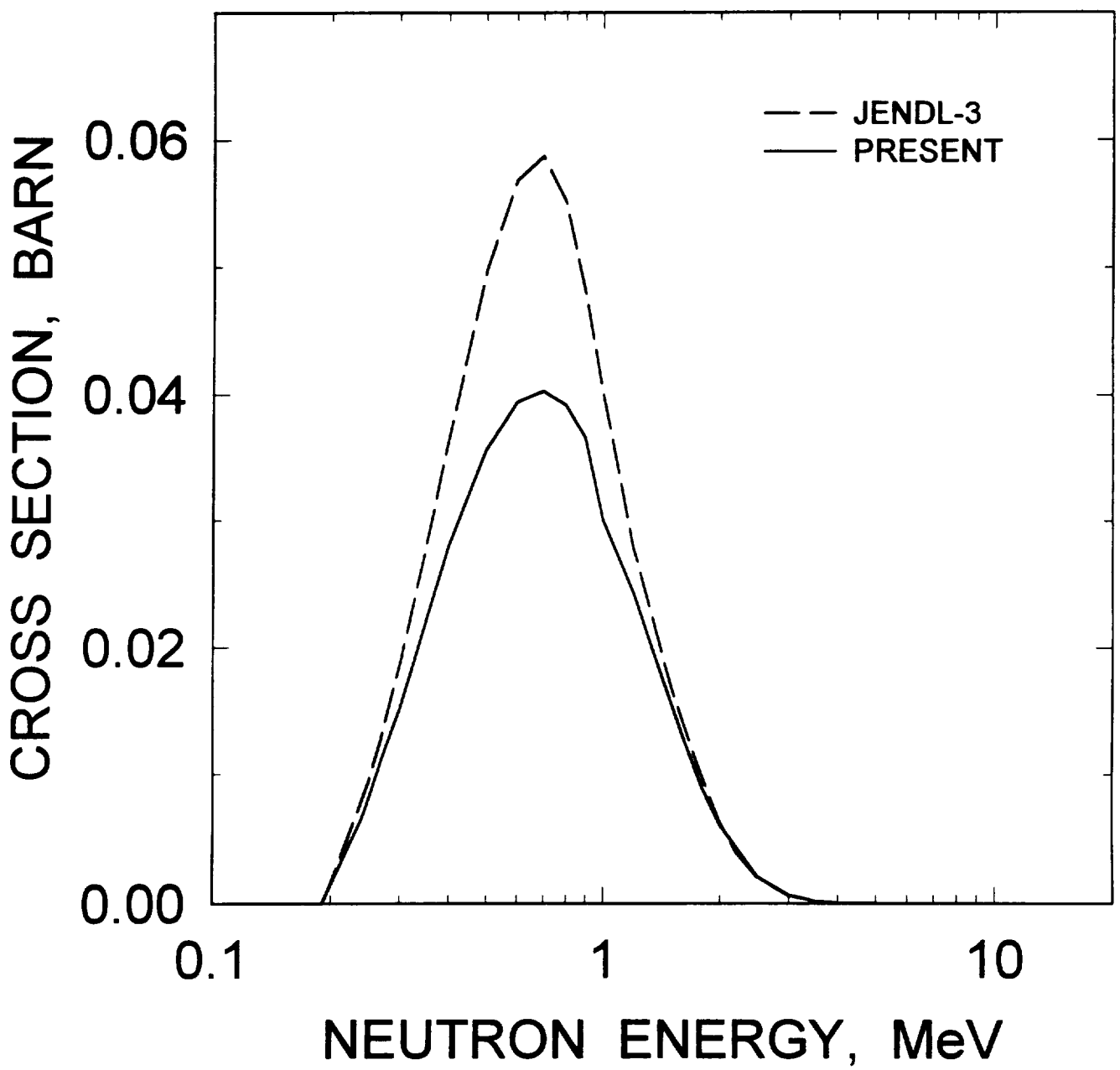
^{243}Am: 0.1893 MeV, 11/2$^-$ LEVEL EXCITATION
JENDL-3
PRESENT
CROSS SECTION, BARN
0.06
0.04
0.02
0.00
0.1
1
10
NEUTRON ENERGY, MeV

FIG. 4.18

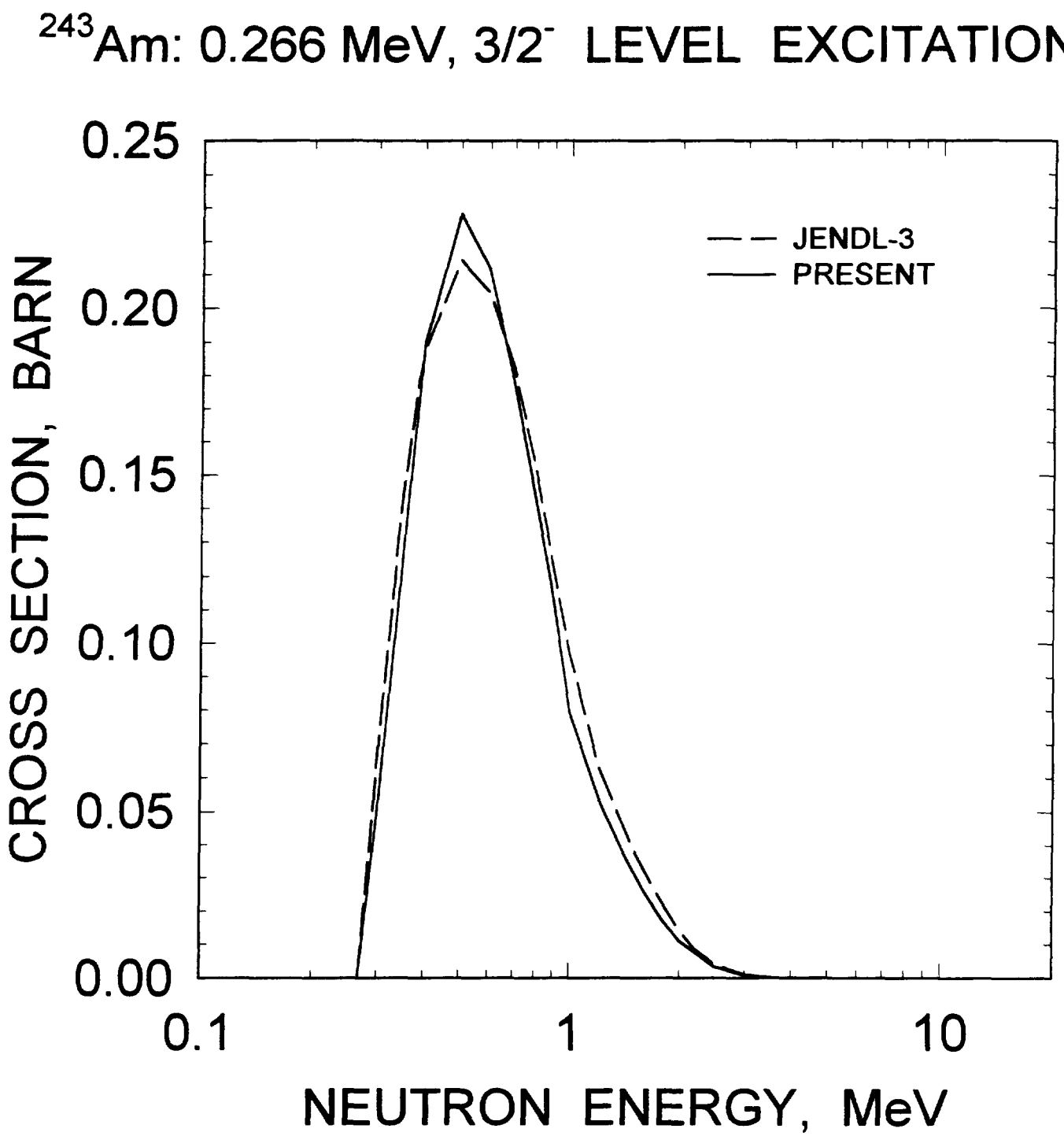
^{243}Am: 0.266 MeV, 3/2$^-$ LEVEL EXCITATION
0.25
0.20
0.15
0.10
0.05
0.00
CROSS SECTION, BARN
JENDL-3
PRESENT
0.1
1
10
NEUTRON ENERGY, MeV

FIG. 4.19

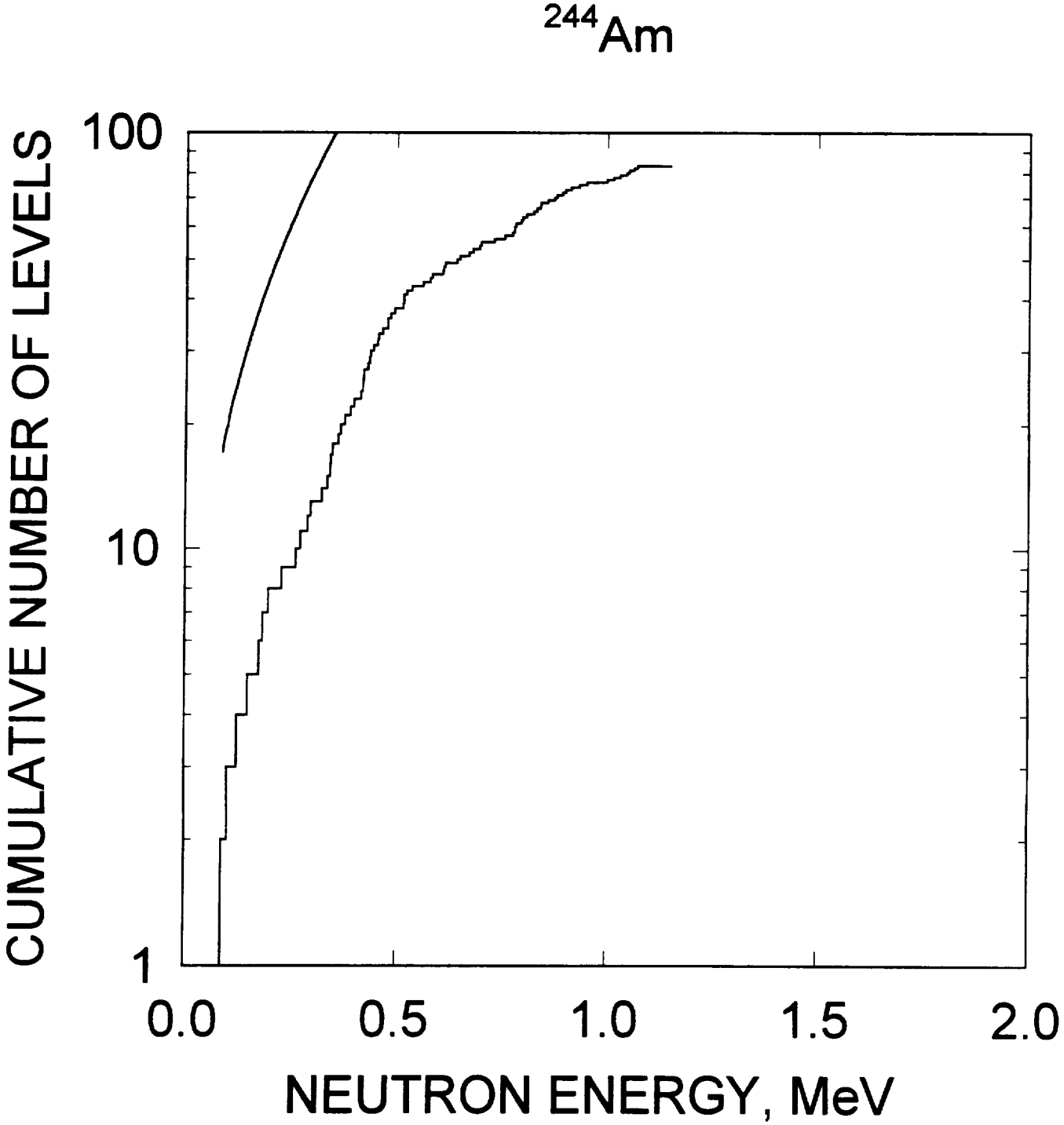
^{244}Am
CUMULATIVE NUMBER OF LEVELS
100
10
1
0.0
0.5
1.0
1.5
2.0
NEUTRON ENERGY, MeV

FIG.4.20

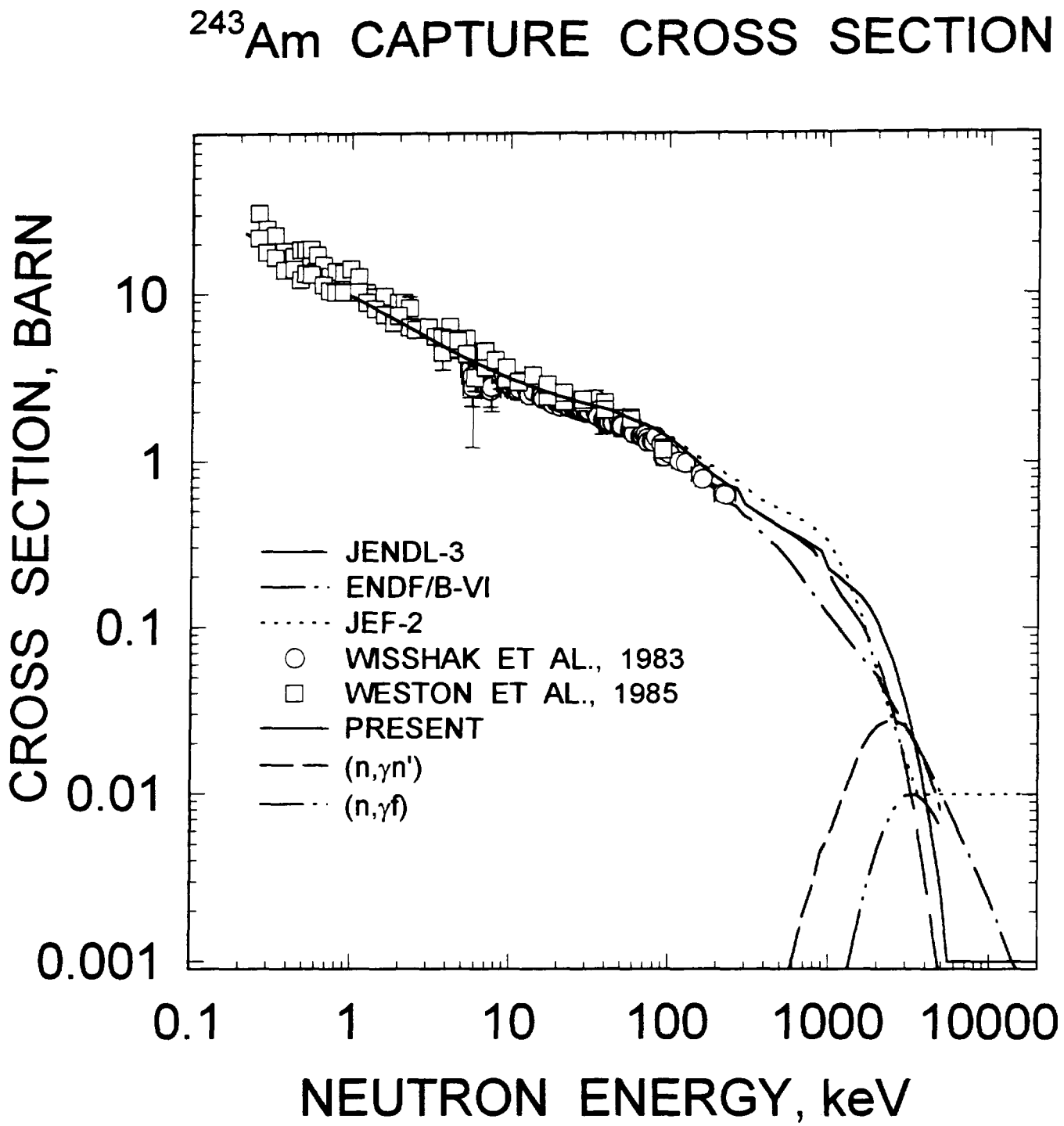
^{243}Am CAPTURE CROSS SECTION
CROSS SECTION, BARN
10
1
0.1
0.01
0.001
JENDL-3
ENDF/B-VI
JEF-2
WISSHAK ET AL., 1983
WESTON ET AL., 1985
PRESENT
(n,γn')
(n,γf)
0.1
1
10
100
1000
10000
NEUTRON ENERGY, keV

FIG.4.21

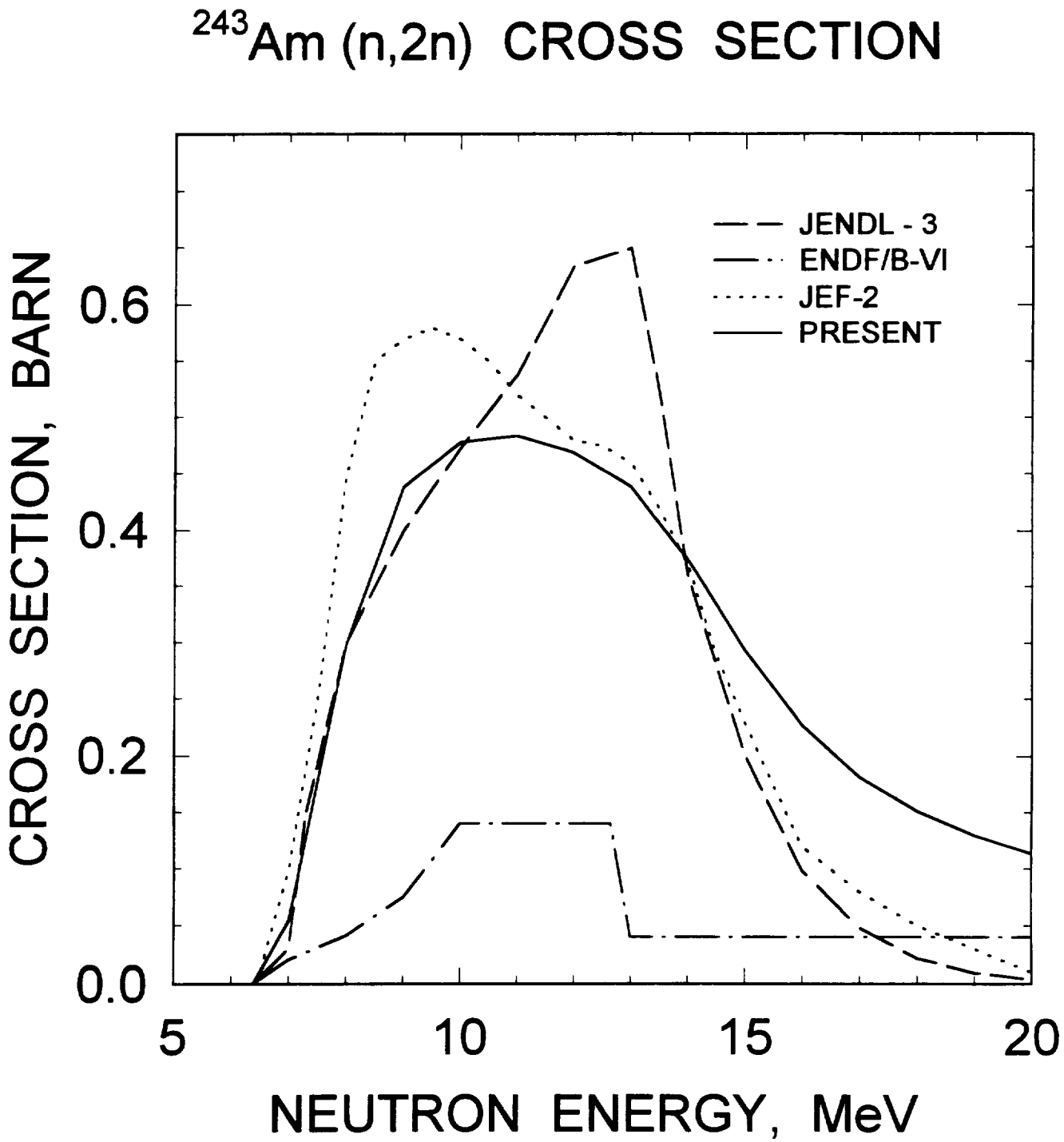
^{243}Am (n,2n) CROSS SECTION
JENDL - 3
ENDF/B-VI
JEF-2
PRESENT
CROSS SECTION, BARN
0.0
0.2
0.4
0.6
5
10
15
20
NEUTRON ENERGY, MeV

FIG. 4.22

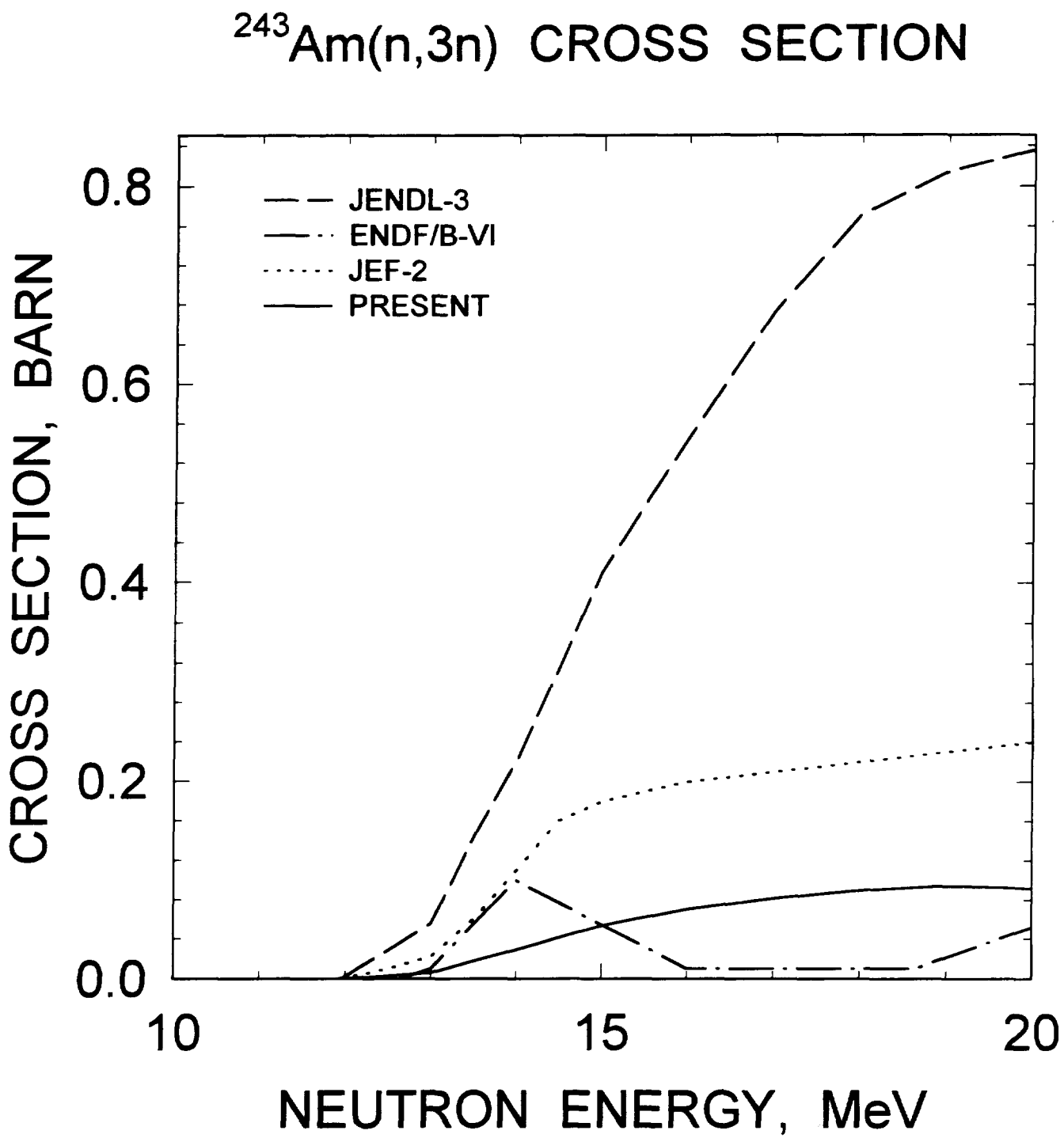
^{243}Am(n,3n) CROSS SECTION
JENDL-3
ENDF/B-VI
JEF-2
PRESENT
CROSS SECTION, BARN
0.0
0.2
0.4
0.6
0.8
10
15
20
NEUTRON ENERGY, MeV

FIG. 4.23

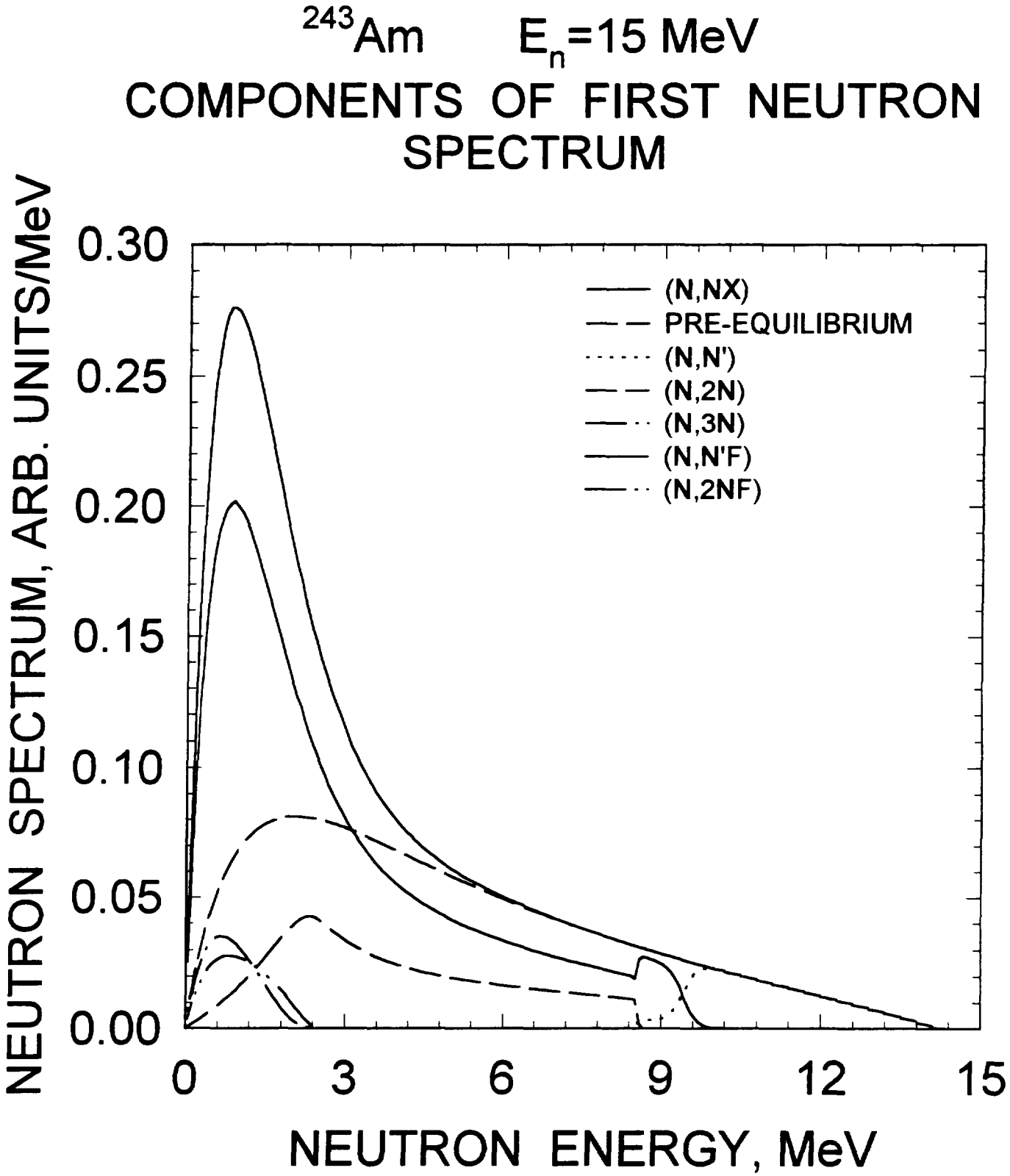
^{243}Am E_n=15 MeV
COMPONENTS OF FIRST NEUTRON SPECTRUM
NEUTRON SPECTRUM, ARB. UNITS/MeV
0.30
0.25
0.20
0.15
0.10
0.05
0.00
0
3
6
9
12
15
NEUTRON ENERGY, MeV
(N,NX)
PRE-EQUILIBRIUM
(N,N')
(N,2N)
(N,3N)
(N,N'F)
(N,2NF)

FIG.5.1

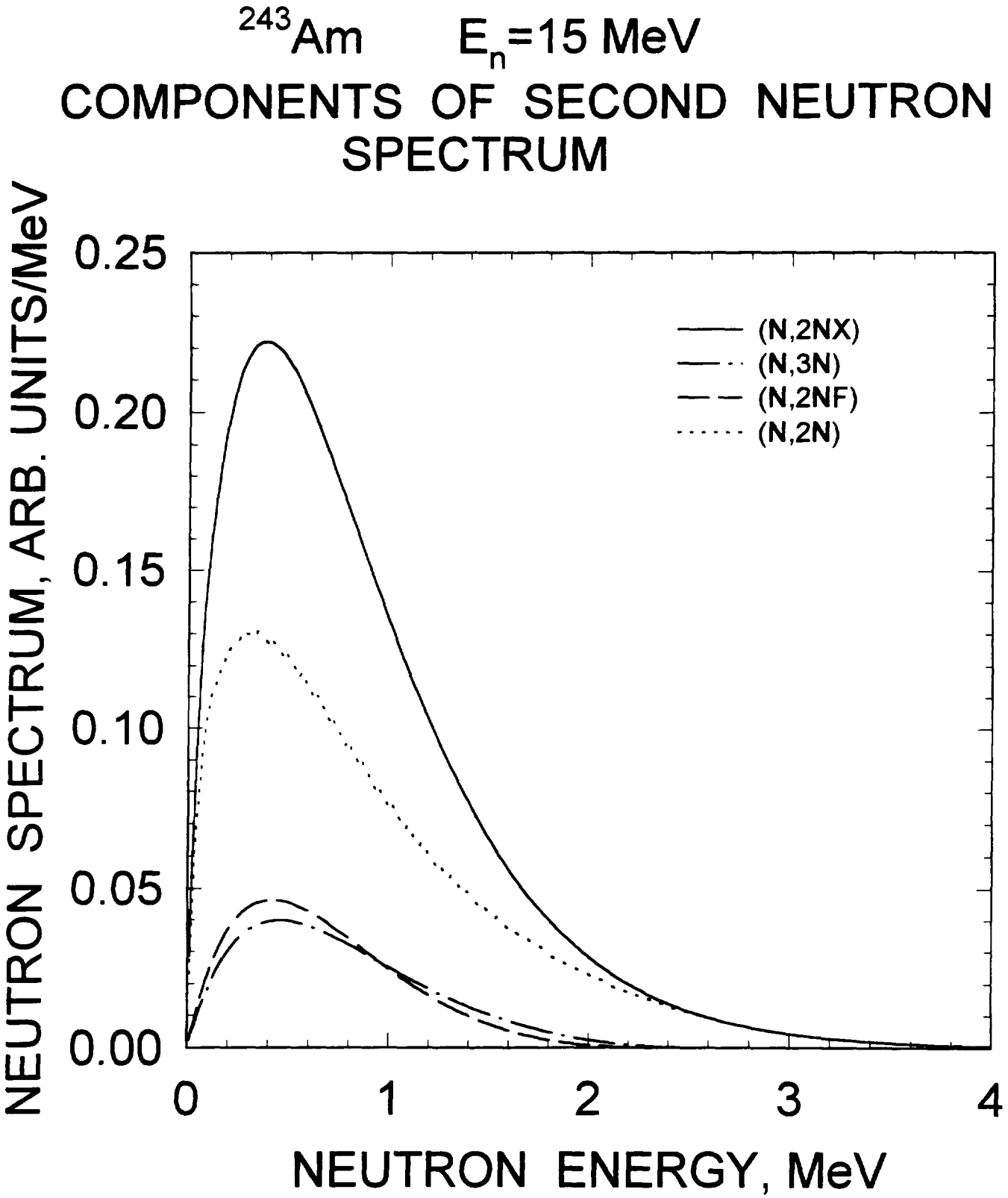
^{243}Am E_n=15 MeV
COMPONENTS OF SECOND NEUTRON SPECTRUM
NEUTRON SPECTRUM, ARB. UNITS/MeV
0.25
0.20
0.15
0.10
0.05
0.00
0
1
2
3
4
NEUTRON ENERGY, MeV
(N,2NX)
(N,3N)
(N,2NF)
(N,2N)

FIG.5.2

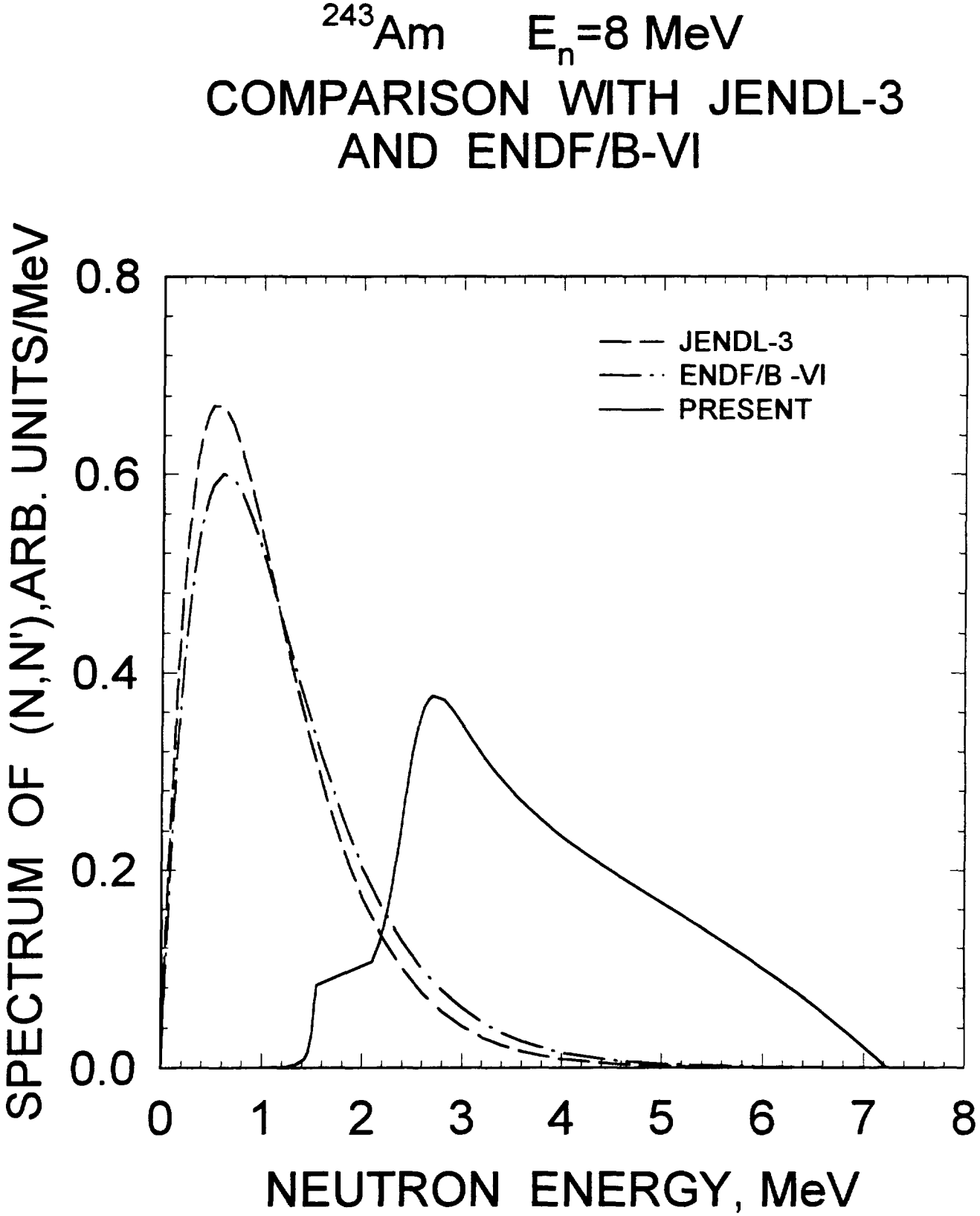
^{243}Am E_n=8 MeV
COMPARISON WITH JENDL-3
AND ENDF/B-VI
SPECTRUM OF (N,N'),ARB. UNITS/MeV
0.0
0.2
0.4
0.6
0.8
0
1
2
3
4
5
6
7
8
NEUTRON ENERGY, MeV
JENDL-3
ENDF/B -VI
PRESENT

FIG.5.3

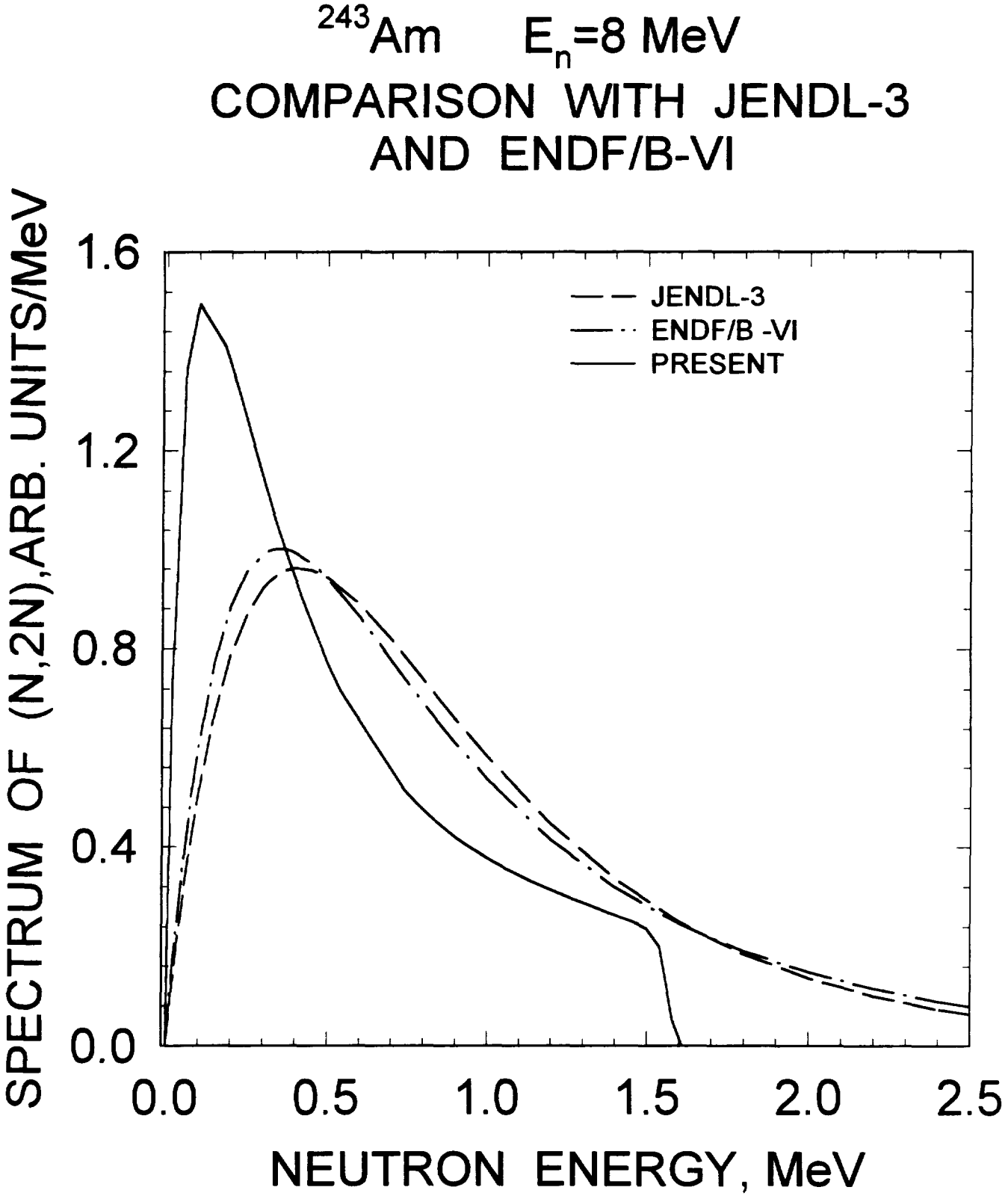
^{243}Am E_n=8 MeV
COMPARISON WITH JENDL-3
AND ENDF/B-VI
SPECTRUM OF (N,2N),ARB. UNITS/MeV
1.6
1.2
0.8
0.4
0.0
0.0
0.5
1.0
1.5
2.0
2.5
NEUTRON ENERGY, MeV
JENDL-3
ENDF/B -VI
PRESENT

FIG.5.4

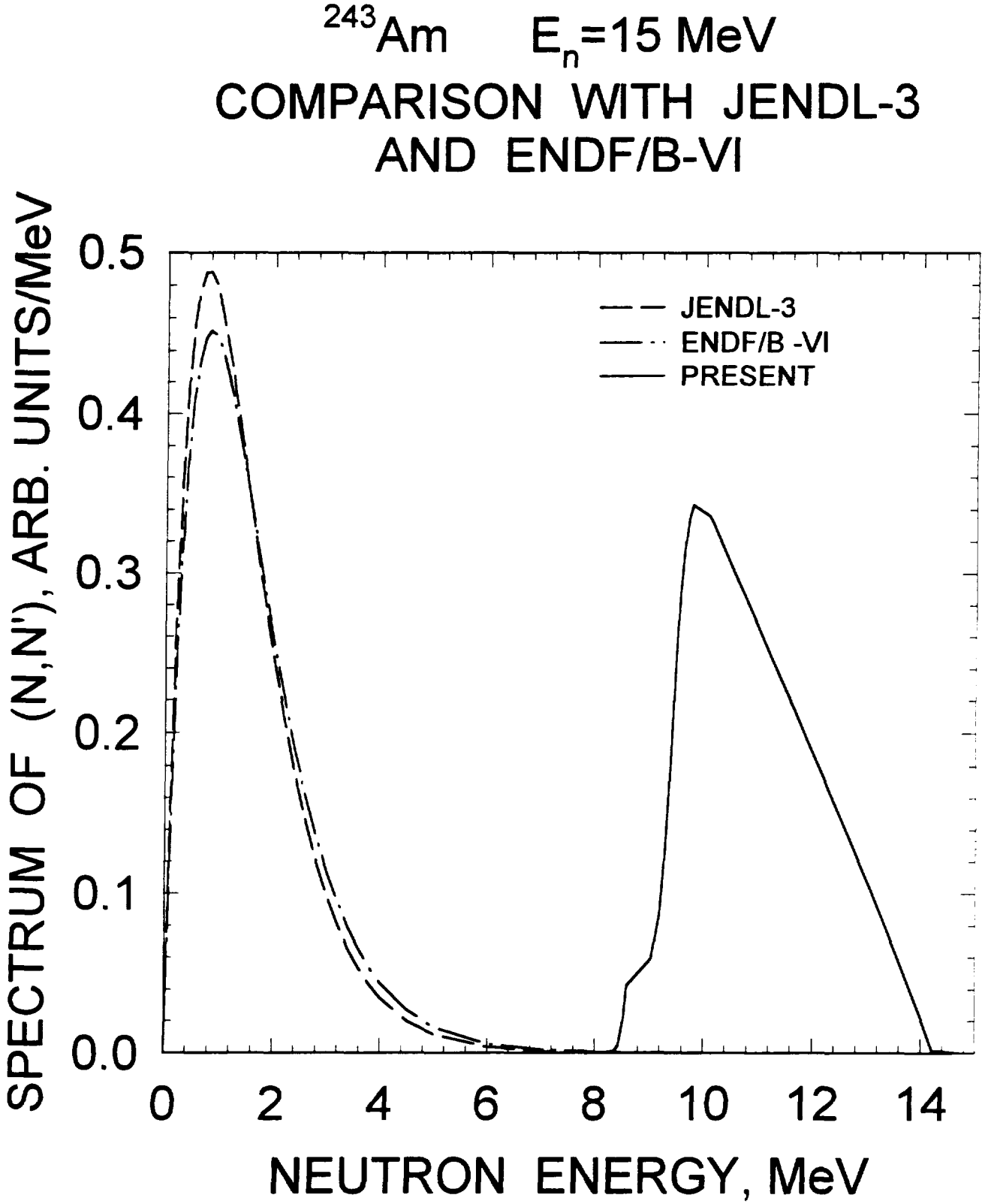
^{243}Am E_n=15 MeV
COMPARISON WITH JENDL-3
AND ENDF/B-VI
SPECTRUM OF (N,N'), ARB. UNITS/MeV
0.0
0.1
0.2
0.3
0.4
0.5
0
2
4
6
8
10
12
14
NEUTRON ENERGY, MeV
JENDL-3
ENDF/B -VI
PRESENT

FIG.5.5

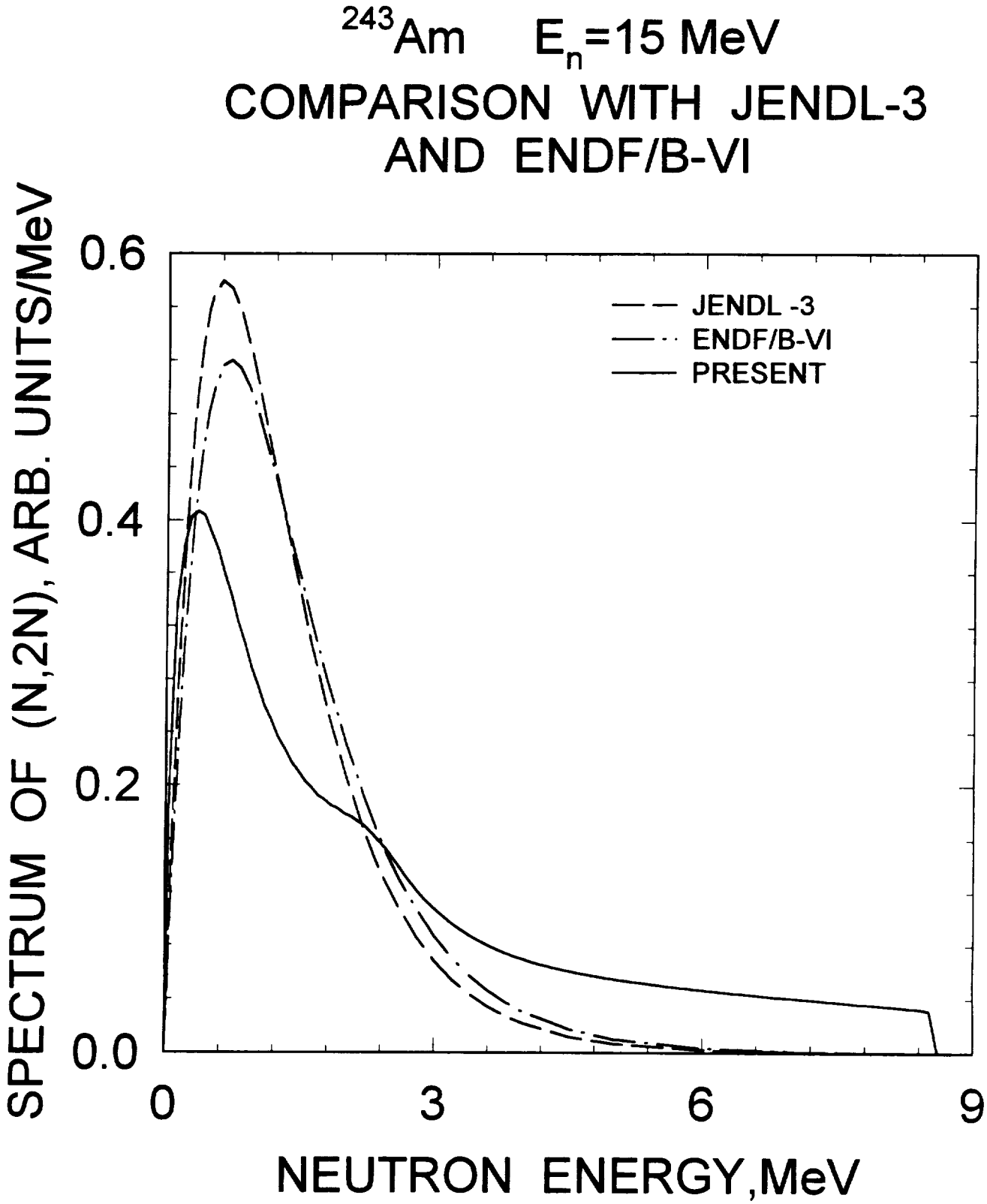
^{243}Am E_n=15 MeV
COMPARISON WITH JENDL-3
AND ENDF/B-VI
SPECTRUM OF (N,2N), ARB. UNITS/MeV
0.6
0.4
0.2
0.0
0
3
6
9
NEUTRON ENERGY,MeV
JENDL -3
ENDF/B-VI
PRESENT

FIG.5.6

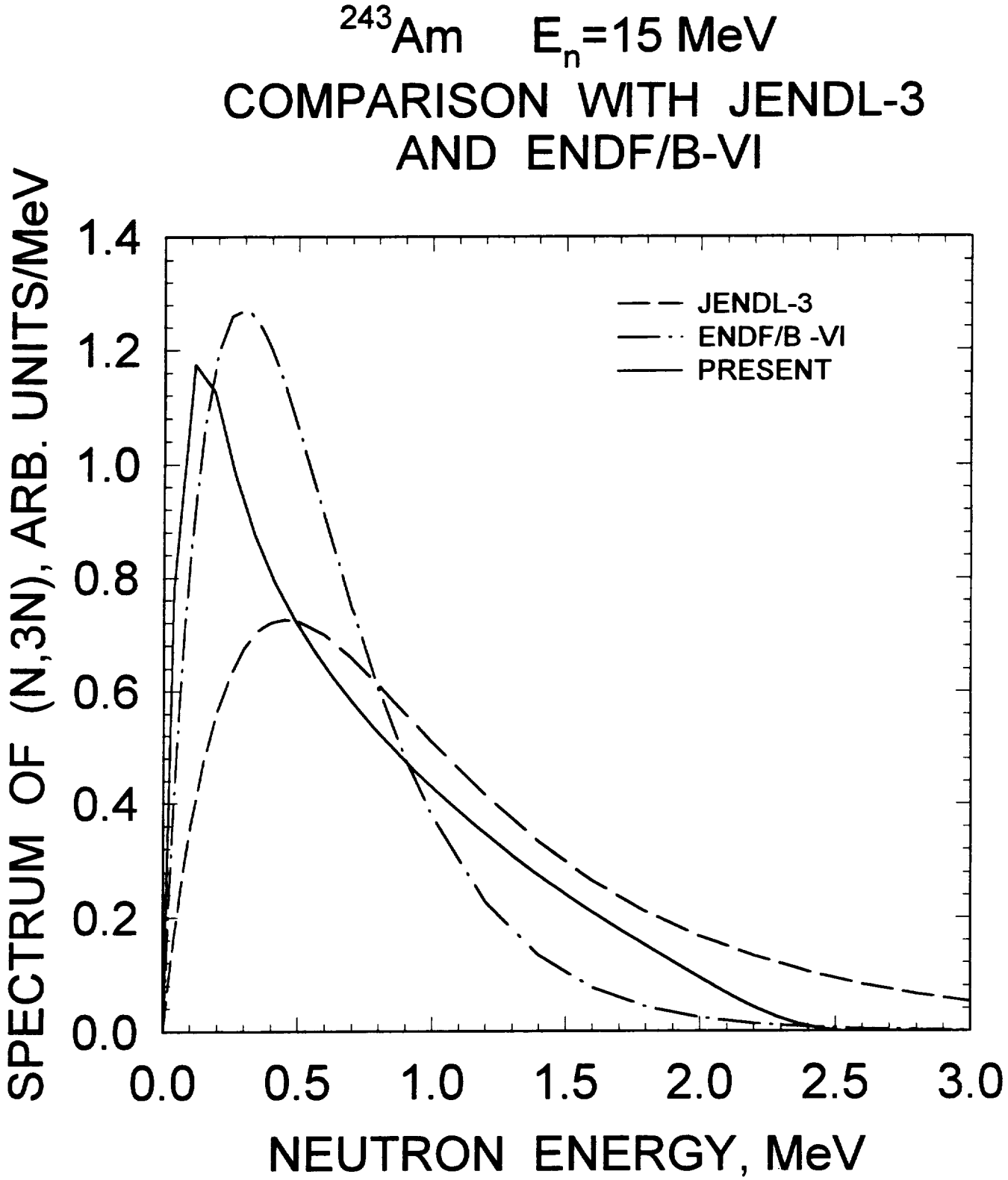
^{243}Am E_n=15 MeV
COMPARISON WITH JENDL-3
AND ENDF/B-VI
SPECTRUM OF (N,3N), ARB. UNITS/MeV
NEUTRON ENERGY, MeV
JENDL-3
ENDF/B -VI
PRESENT
0.0
0.2
0.4
0.6
0.8
1.0
1.2
1.4
0.0
0.5
1.0
1.5
2.0
2.5
3.0

FIG.5.7

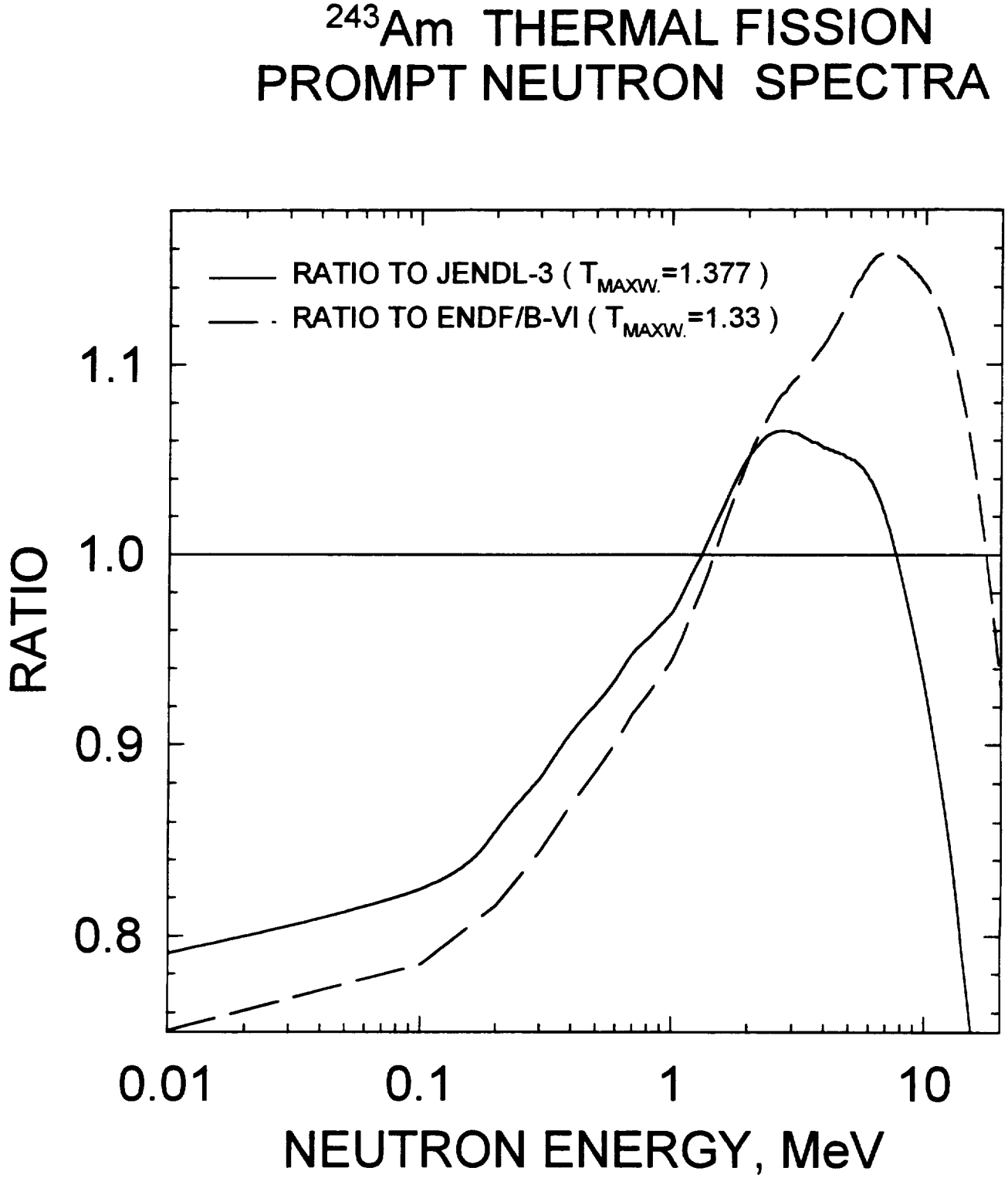
^{243}Am THERMAL FISSION
PROMPT NEUTRON SPECTRA
RATIO TO JENDL-3 ($T_{MAXW.}$=1.377)
RATIO TO ENDF/B-VI ($T_{MAXW.}$=1.33)
RATIO
1.1
1.0
0.9
0.8
0.01
0.1
1
10
NEUTRON ENERGY, MeV

FIG.5.8

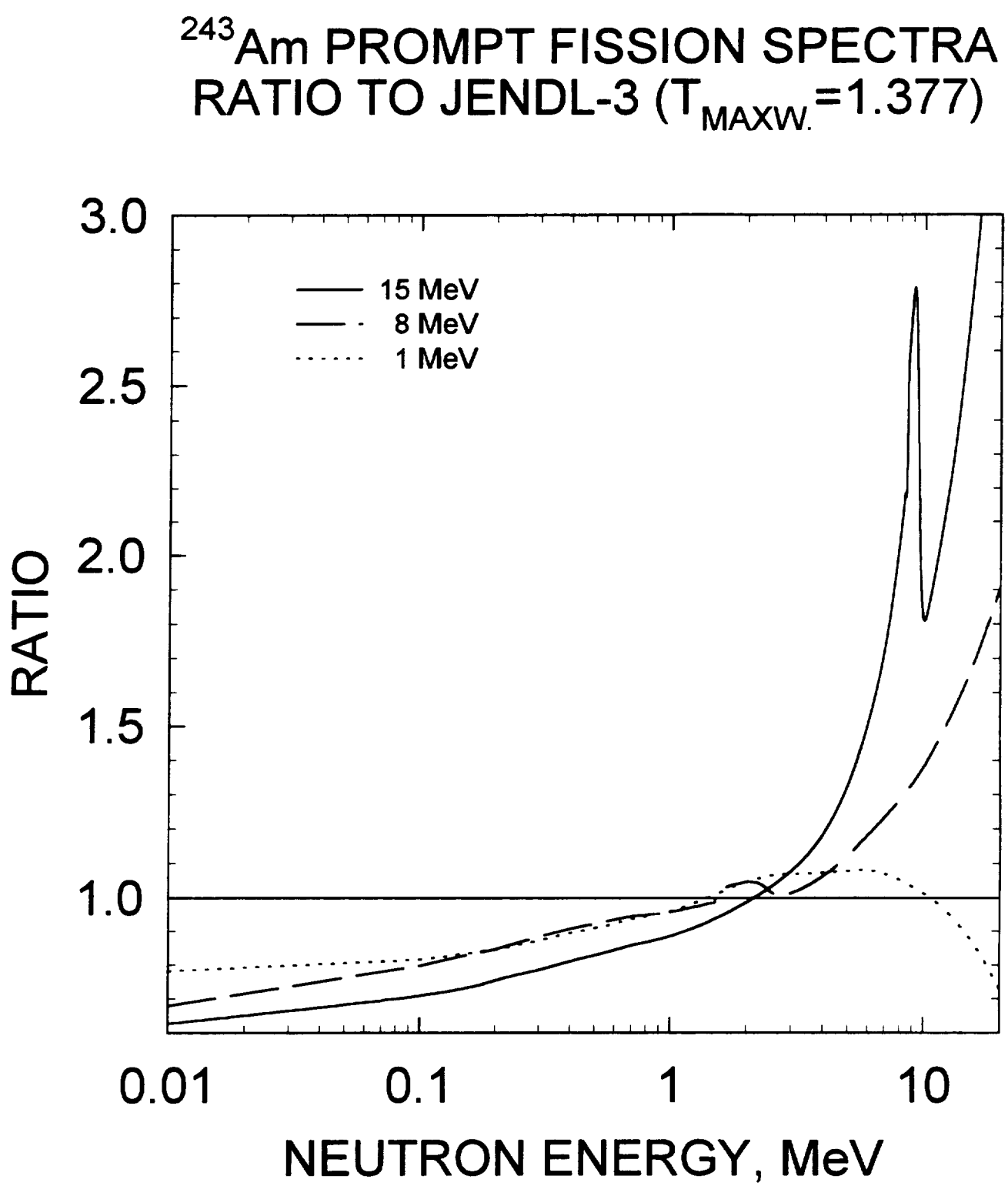
^{243}Am PROMPT FISSION SPECTRA
RATIO TO JENDL-3 ($T_{MAXW.}$=1.377)
15 MeV
8 MeV
1 MeV
RATIO
3.0
2.5
2.0
1.5
1.0
0.01
0.1
1
10
NEUTRON ENERGY, MeV

FIG. 5.9

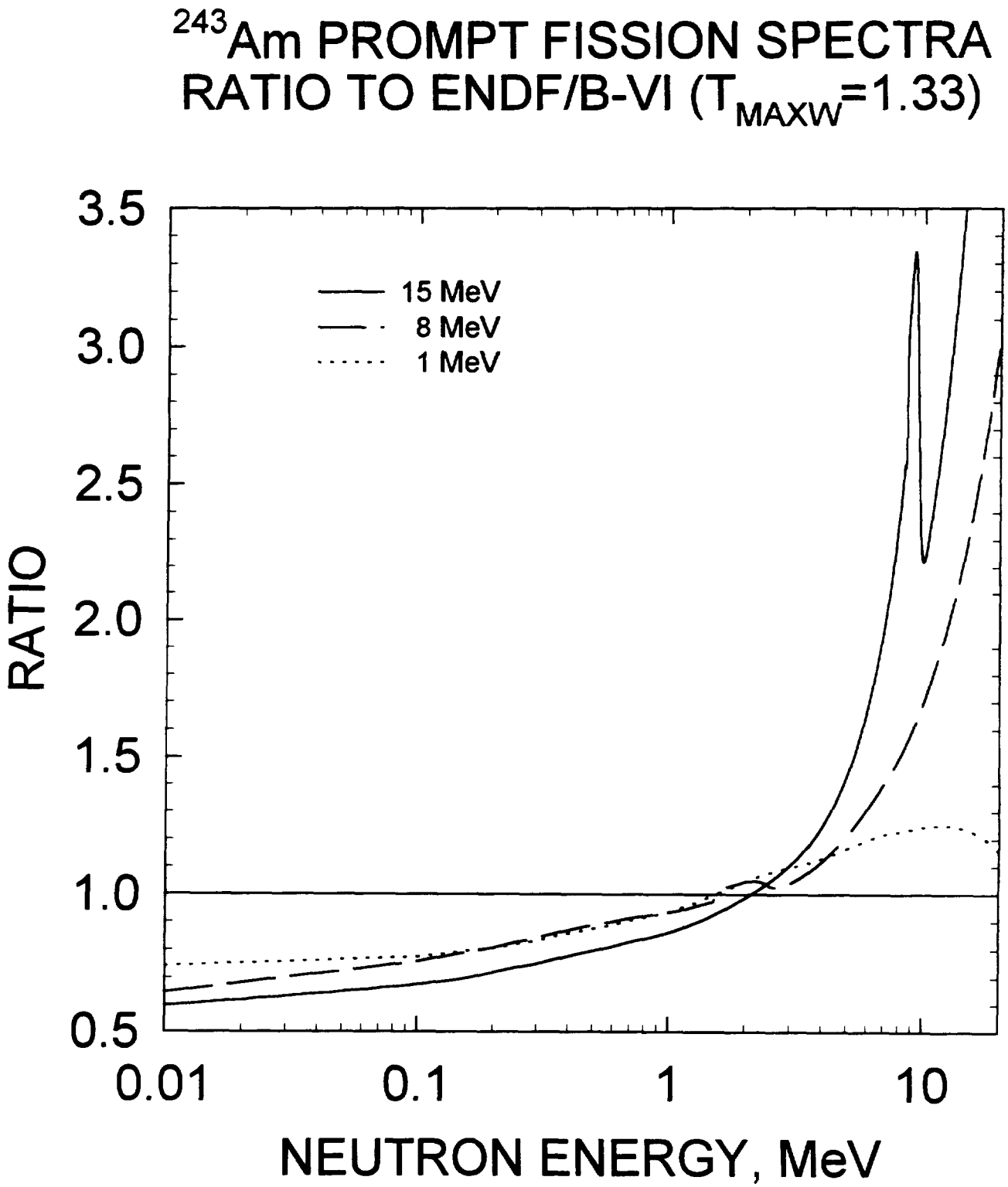
^{243}Am PROMPT FISSION SPECTRA
RATIO TO ENDF/B-VI (T_{MAXW}=1.33)
15 MeV
8 MeV
1 MeV
RATIO
3.5
3.0
2.5
2.0
1.5
1.0
0.5
0.01
0.1
1
10
NEUTRON ENERGY, MeV

FIG. 5.10

^{243}Am FISSION NEUTRON SPECTRA RATIO TO MADLAND-NIX MODEL CALCULATION

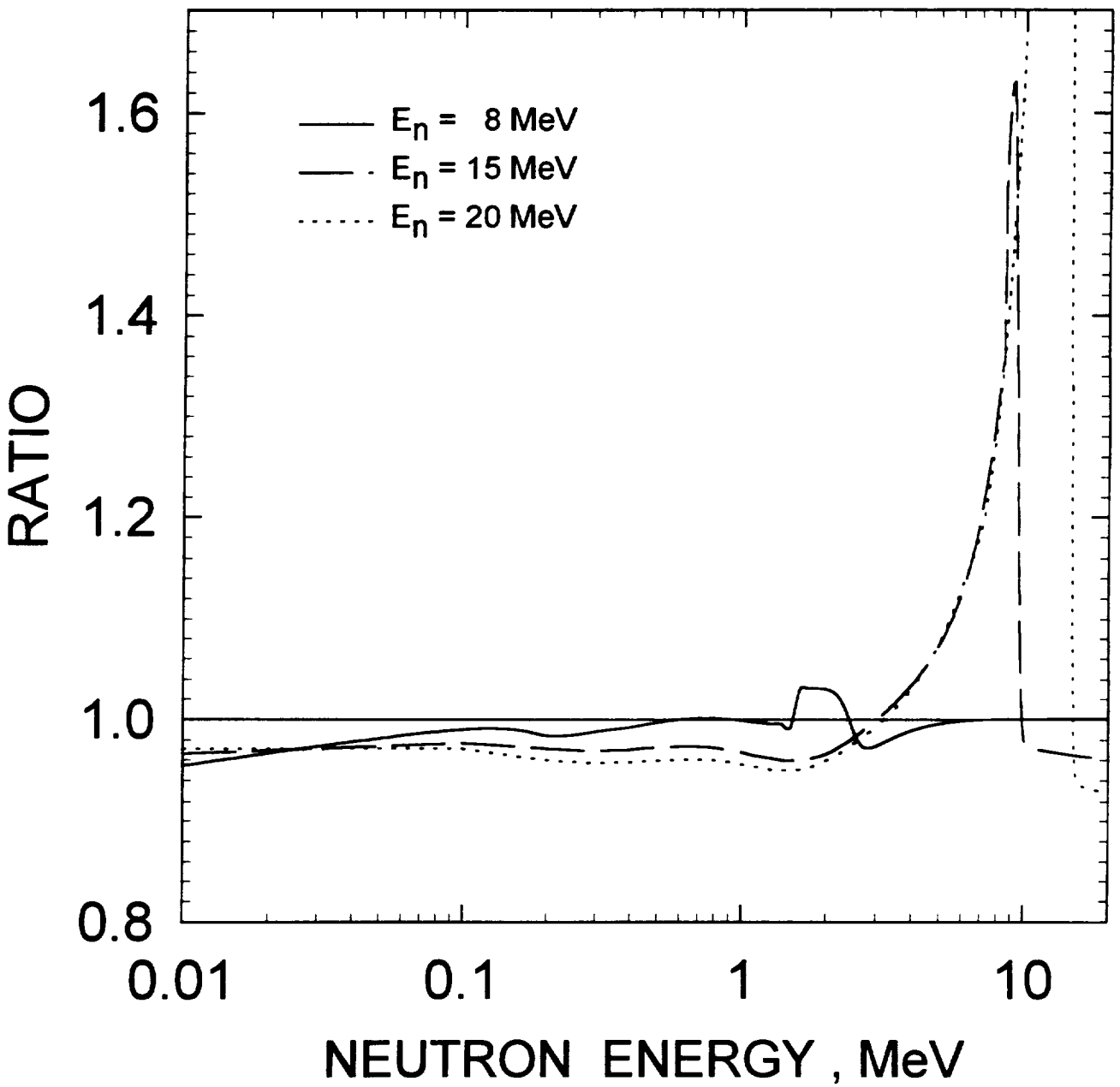

FIG.5.11

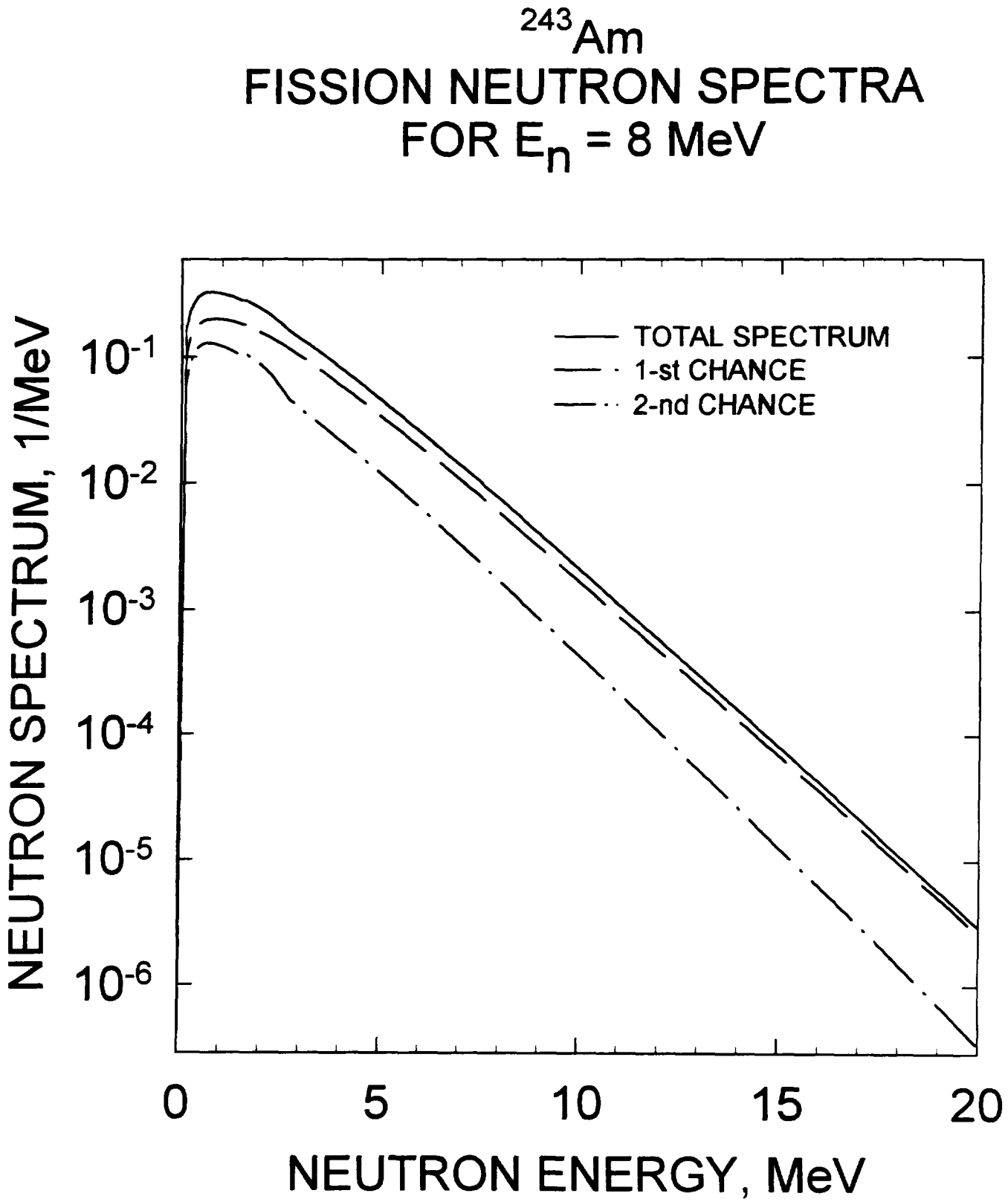
^{243}Am
FISSION NEUTRON SPECTRA
FOR E_n = 8 MeV
NEUTRON SPECTRUM, 1/MeV
10^{-1}
10^{-2}
10^{-3}
10^{-4}
10^{-5}
10^{-6}
TOTAL SPECTRUM
1-st CHANCE
2-nd CHANCE
0
5
10
15
20
NEUTRON ENERGY, MeV

FIG.5.12

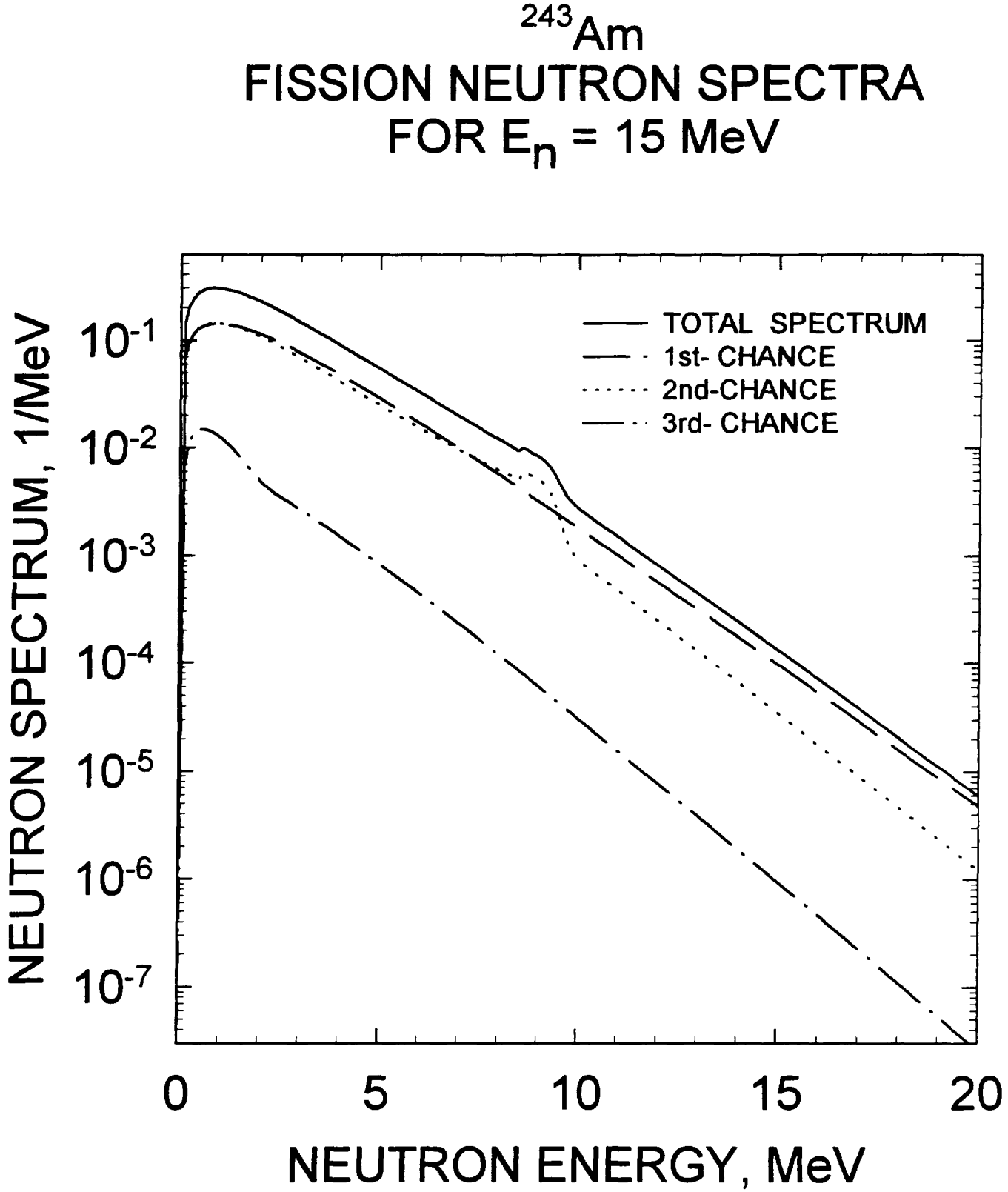
^{243}Am
FISSION NEUTRON SPECTRA
FOR E_n = 15 MeV
TOTAL SPECTRUM
1st- CHANCE
2nd-CHANCE
3rd- CHANCE
NEUTRON SPECTRUM, 1/MeV
10^{-1}
10^{-2}
10^{-3}
10^{-4}
10^{-5}
10^{-6}
10^{-7}
0
5
10
15
20
NEUTRON ENERGY, MeV

FIG.5.13

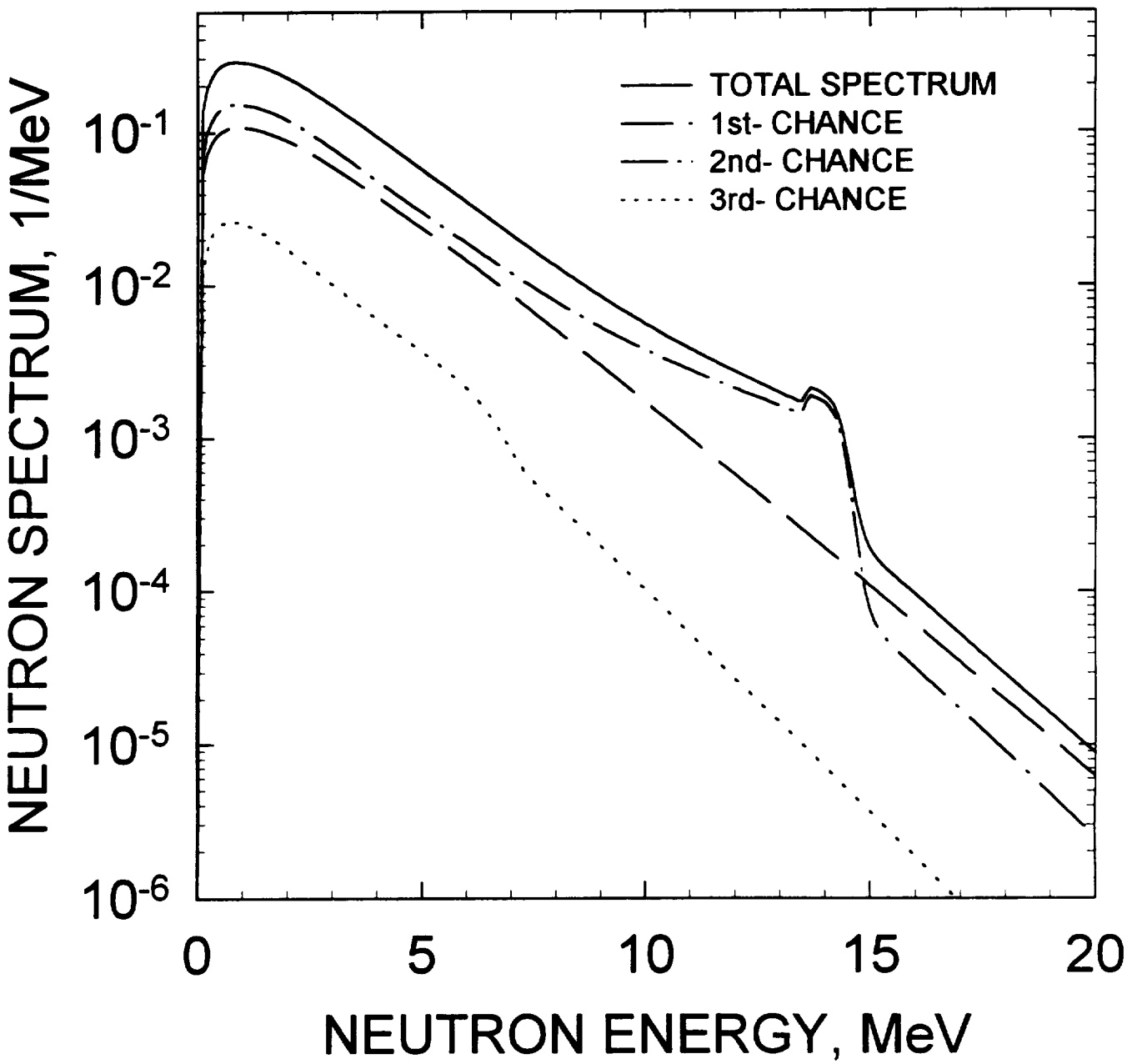
^{243}Am
FISSION NEUTRON SPECTRA
FOR E_n = 20 MeV
TOTAL SPECTRUM
1st- CHANCE
2nd- CHANCE
3rd- CHANCE
NEUTRON SPECTRUM, 1/MeV
10^{-1}
10^{-2}
10^{-3}
10^{-4}
10^{-5}
10^{-6}
0
5
10
15
20
NEUTRON ENERGY, MeV

FIG.5.14

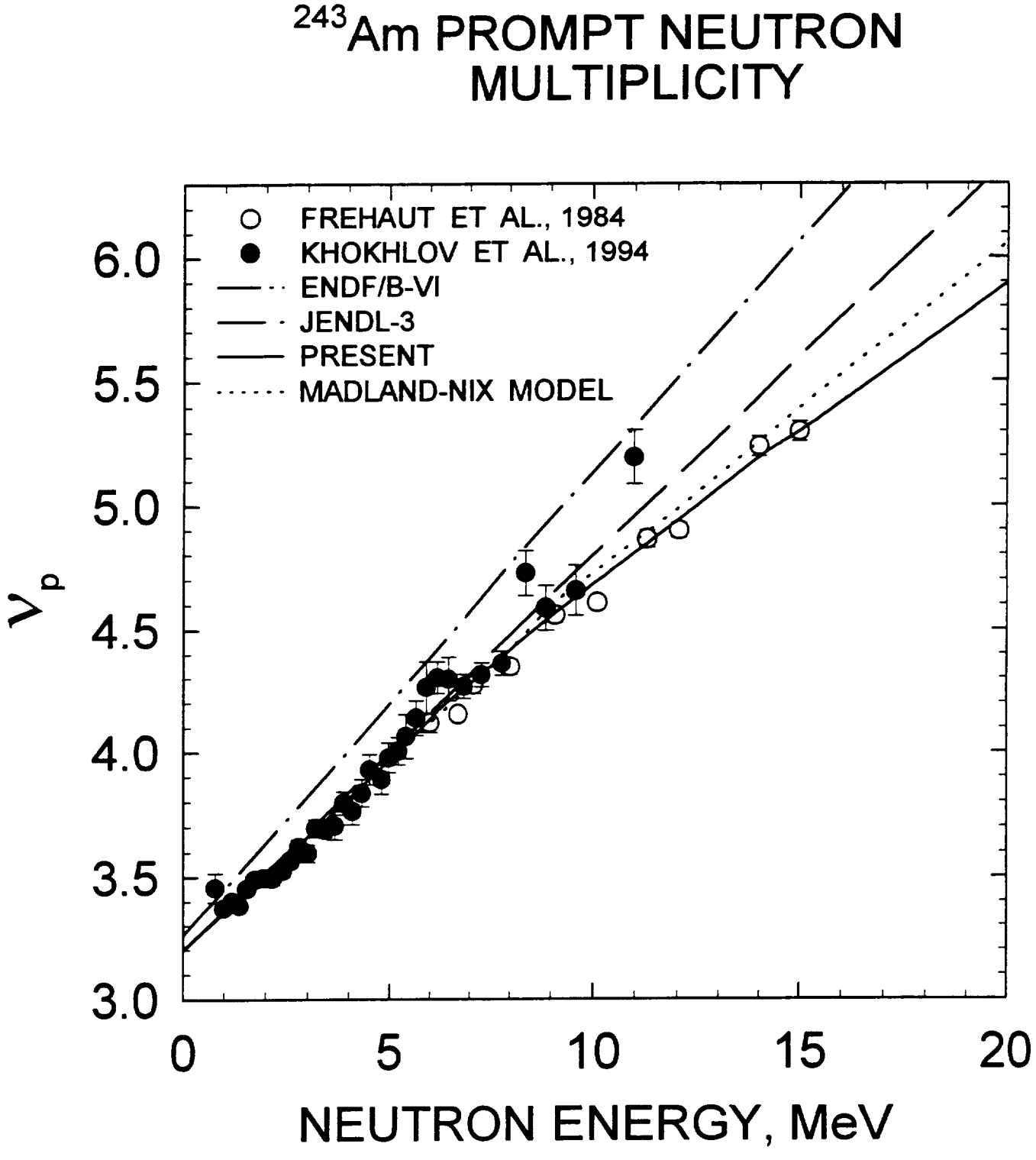
^{243}Am PROMPT NEUTRON MULTIPLICITY
FREHAUT ET AL., 1984
KHOKHLOV ET AL., 1994
ENDF/B-VI
JENDL-3
PRESENT
MADLAND-NIX MODEL
ν_p
6.0
5.5
5.0
4.5
4.0
3.5
3.0
0
5
10
15
20
NEUTRON ENERGY, MeV

FIG.6.1

Nuclear Data Section
International Atomic Energy Agency
P.O. Box 100
A-1400 Vienna
Austria

e-mail, INTERNET: SERVICES@IAEAND.IAEA.OR.AT
fax: (43-1)20607
cable: INATOM VIENNA a
telex: 1-12645 atom a
telephone: (43-1)2060-21710

online: TELNET or FTP: IAEAND.IAEA.OR.AT
username: IAEANDS for interactive Nuclear Data Information System
username: ANONYMOUS for FTP file transfer
username: FENDL for FTP file transfer of FENDL files
For users with web-browsers: http://www.iaea.or.at